NASA CR-168148

NASA

CURRENT COLLECTION FROM THE SPACE PLASMA THROUGH DEFECTS IN HIGH VOLTAGE SOLAR ARRAY INSULATION

by R. P. Stillwell

Prepared for

LEWIS RESEARCH CENTER

NATIONAL AERONAUTICS AND SPACE ADMINISTRATION

GRANT NSG 3196

January 1983

Approved by
Harold R. Kaufman and Raymond S. Robinson
Department of Physics
Colorado State University
Fort Collins, Colorado 80523

1 Report No	2 Government Accession No	3 Recipient's Catalog No
CR-168148		

4 Title and Subtitle	5 Report Date
CURRENT COLLECTION FROM THE SPACE PLASMA THROUGH DEFECTS IN HIGH VOLTAGE SOLAR ARRAY INSULATION (U)	January 1983
	6 Performing Organization Code
7 Author(s)	8 Performing Organization Report No
R. P. Stillwell	Final Report
	10 Work Unit No
9 Performing Organization Name and Address	11 Contract or Grant No
Department of Physics Colorado State University Fort Collins, Colorado 80523	NSG-3196
	13 Type of Report and Period Covered
12 Sponsoring Agency Name and Address	
NASA Lewis Research Center 21000 Brookpark Road Cleveland, OH 44135	14 Sponsoring Agency Code

15 Supplementary Notes

Grant Manager: Norman T. Grier
NASA Lewis Research Center
Cleveland, OH 44135

This report is the Ph D. thesis of R. P. Stillwell, in addition to being the final report of this grant.

16 Abstract

For spacecraft operation in the near-earth environment, solar cell arrays constitute the major source of reliable long-term power. Optimization of mass and power efficiency results in a general requirement for high voltage solar arrays. The space plasma environment, though, can result in large currents being collected by exposed solar cells. The solution of a protective covering of transparent insulation is not a complete solution, inasmuch as defects in the insulation result in anomalously large currents being collected through the defects.

Tests simulating the electron collection from small defects in an insulation have shown that there are two major collection modes. The first mode involves current enhancement by means of a surface phenomenon involving the surrounding insulator. In the second mode the current collection is enhanced by vaporization and ionization of the insulator material, in addition to the surface enhancement of the first mode. Tests have shown that roughening the sample surface decreases collection, while increasing the sample temperature decreases the electron collection for polyimide (Kapton), but not for mica. These data indicate that secondary electron emission plays an important part in the surface enhancement mode, because roughening a surface decreases the secondary yield, and increasing sample temperature decreases the secondary yield for polymers, but not for mica. Experiments have also shown that defect size greatly increases the electron collection in the surface enhancement mode, but that current collection is relatively insensitive to defect size in the vapor enhancement mode.

Tests involving ion collection indicate that, for negative potentials up to 1000 V, the collection follows electrostatic probe theory. At higher potentials arcing occurs. Data indicate that the arcing may be due to vaporization of the insulator due to ion impact.

A model for the electron collection in the surface enhanced collection mode has been developed. The model relates the secondary electron emission yield to the electron collection. It correctly predicts the qualitative effects of hole size, sample temperature and roughening of sample surface. The theory has also been shown to predict electron collection within a factor of two for the polymers teflon and polyimide.

17 Key Words (Suggested by Author(s))	18 Distribution Statement
Plasma Physics Space Plasma Solar Arrays	Unclassified - Unlimited

19. Security Classif. (of this report)	20 Security Classif. (of this page)	21. No. of Pages	22 Price*
Unclassified	Unclassified		

* For sale by the National Technical Information Service, Springfield, Virginia 22161

NASA-C-168 (Rev 10-75)

N83-31474#

TABLE OF CONTENTS

LIST OF FIGURES

LIST OF TABLES

I. INTRODUCTION

Background

For spacecraft operation in the near-earth environment, solar cell arrays constitute the major source of reliable long-term power. The minimization of total mass for such spacecraft results in the general requirement for high voltage solar arrays. Operating in the space plasma environment,[1-2] though, can result in large currents being collected by exposed solar cells,[3-5] with corresponding reductions in power output from the arrays. A protective covering of transparent insulation is not a complete solution to the current collection problem, due to the occurrence of defects, either during the manufacturing process or resulting from collisions with micrometeorites.

Early experiments by Cole, Ogawa and Sellen[6] showed that positive electrodes behind a pinhole opening in the insulating sheet could collect electron currents as much as two orders of magnitude greater than expected from electrostatic probe theory. They suggested that the electron collection could be explained by a secondary electron emission process. An incoming electron striking the insulator surface near the hole may cause the emission of a secondary electron. Such a secondary electron can then be attracted toward the hole by a potential gradient. The accelerated secondary may then again strike the insulator, at a location closer to the hole, again causing further secondary emission. In this manner, incoming electrons striking the insulator can cause electrons to be collected by the pinhole even though the original electron trajectory may not intersect the hole.

A subsequent investigation[7] found that, for potentials of 0 to 3000 volts, polyimide insulation surrounding a pinhole collected a current only a factor of several greater than expected from electrostatic probe theory. In this investigation Grier and McKinzie postulated that this higher electron collection was due to sputtered insulation being ionized and thereby increasing the current collection.

A later paper by Grier and McKinzie[8] confirmed their previous results for other insulating materials, as well as reporting that the insulation around the holes appeared charred after testing. For polyimide samples, they also reported that the electron collection increased with time.

An investigation by Domitz and Grier[9,10] confirmed the results of Cole, Ogawa and Sellen, that electron collection was orders of magnitude higher than expected. They further found that current collection was

essentially independent of hole size and of electrode material behind the pinhole, and that current collection increased with insulator area surrounding the hole up to about 30 cm^2, where the current collection becomes independent of area.

Results found by Kennerud[5] indicated that, for positive electrode potentials less than about 1000 volts, the electron current was dependent on hole size. Above about 1000 volts, the current became independent. It was also reported that current collection was independent of the adhesive used to bond the insulator to the electrode. The currents collected in this investigation were also found to be several orders of magnitude higher than expected from electrostatic probe theory. Further reports of ground test,[11-14] as well as space flight experiments[15] continue to confirm that a small hole in an insulator collects orders of magnitude higher currents than could be expected from electrostatic probe theory.

A computer simulation of electron collection has been done.[16-19] Such simulations have been accomplished both with[18,19] and without[16,17,19] secondary electron emission. The results of the simulation have been reported only for low electrode potentials ($\leq$200 volts), but they are in rough agreement with experimental results for that range.

Gabriel, Garner and Kitamura[20] have measured the plasma sheath around a pinhole. They showed that the sheath is approximately hemispherical in geometry. However, analysis of the current collection indicates that the insulator did not contribute to the current collection and that their results can be explained with electrostatic probe theory.

Negatively biased electrodes, surrounded by insulation, collect significantly less current than positively biased electrodes. Kennerud[5] reported that the current varies as $V^{3/2}$ (Child's law), while Domitz and Grier[9-10] report that the current varies as V^b, where b ranges from 1 to 1.5. Kennerud[5] also reported that ion collection was independent of hole size, which contradicts the results of Grier and Domitz.[10]

The magnitude of ion collection was verified on a flight experiment[15] to be in agreement with ground tests of the same geometry. Grier and Stevens[15] also reported that the insulation surrounding a pinhole had no significant effect on current collection.

A major problem encountered in negative bias experiments has been arcing.[9] Although Kennerud[5] did not report any arcing, it is difficult to compare test results, inasmuch as different plasma environments (including ion species) were used.

Present Investigation

This thesis represents the work of a lengthy investigation[21-24] of the current collection by an exposed conductor, which is surrounded by an insulator. The thesis includes all the important results found.

The electron densities, 5×10^4 to 10^5 cm^{-3}, used during the investigation were chosen because they approximate the environment expected for both an electrically propelled spacecraft, due to its own charge exchange plasma[25] and a spacecraft in the natural plasma environment of a near-earth orbit.[1,2]

The object of this investigation was to determine the current collection enhancement mechanism. The results reported herein indicate that there are two different electron collection modes. One mode involves current collection enhancement due to a surface mechanism. The other mode involves the surface mechanism plus additional enhancement due to vaporization of the insulation material. The electron collection for these two modes differs by more than an order of magnitude. The existence of these two collection modes explains many of the contradictions found when comparing the results of previous investigations.

It was found that the surface enhancement mechanism depends on secondary electron emission from the insulator material. A model was formulated, based on secondary electron emission from the insulator, to describe the surface enhancement mechanism.

II. APPARATUS AND PROCEDURE

Vacuum Facilities

Two vacuum facilities were used in the experiments. One was a 45 cm diameter, 72 cm long cylindrical glass vacuum system (the small vacuum facility). The other system was a 1.2 m diameter, 4.6 m long stainless steel vacuum system (the large vacuum facility) with a cryogenic liner. Some typical parameters for these systems are shown in Table 2-1.

Plasma Sources

An argon hollow cathode was used to generate the plasma in both vacuum facilities, although the cathode configurations used in the two facilities differed (see Fig. 2-1). One hollow cathode used in the small vacuum system was of conventional design. This cathode had a tungsten tip, which was electron-beam welded to a hollow tantalum tube. The tungsten tip had a 0.7 mm diameter orifice. Within the tantalum tube was a small porous-tungsten insert, which was impregnated with barium-strontium carbonates. These carbonates were reduced to oxides upon heating before use. A heater element was wrapped around the tantalum tube near the tip. During operation, argon gas flowed through the cathode, at rates of 0.1 to 0.6 A-equiv. The heater element was used to raise the insert to thermionic emission temperatures, which resulted in the creation of a plasma within the cathode. A small positively biased circular wire (keeper), close to the tip, and a 5.4 cm diameter cylindrical anode drew the electrons through the orifice into the vacuum chamber. The electrons entering the vacuum chamber collided with neutral argon atoms, generating ions, in addition to those carried out the orifice with the argon flow. A detailed discussion of the internal processes for this type of hollow cathode is given by Siegfried and Wilbur.[1]

Two positions were used for the hollow cathode in the small vacuum system, a vertical position (see Fig. 2-2(b)) and a horizontal position, both at the base of the chamber. In the vertical position a baffle capped the anode thereby preventing a direct line of sight from the cathode to the sample for either emitted or sputtered particles. The cathode configuration indicated in Fig. 2-1(b) was used in the large vacuum facility. This hollow cathode employed an oxide free rolled Ta foil as the electron-emitting insert. The W tip had a 1.0 mm diameter orifice, and was removable during operation. The tip was held to the Ta

Table 2-1. Typical parameters for the two vacuum facilities used in subject investigation.

	Small Vacuum Facility	Large Vacuum Facility
Background pressure	$7\text{-}25 \times 10^{-5}$ Torr	$2\text{-}3 \times 10^{-5}$ Torr
Electron temperature	4-9 eV	4-13 eV
Electron density	$2\text{-}10 \times 10^{5}$ cm^{-3}	$8\text{-}45 \times 10^{4}$ cm^{-3}

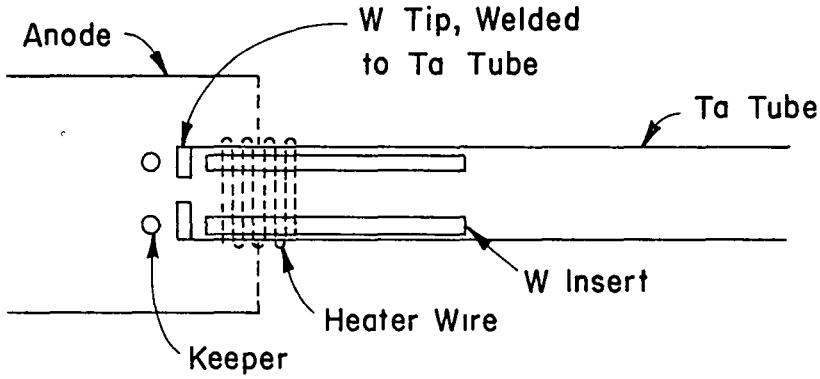

(a) Plasma Source Used in Small Vaccum Facility

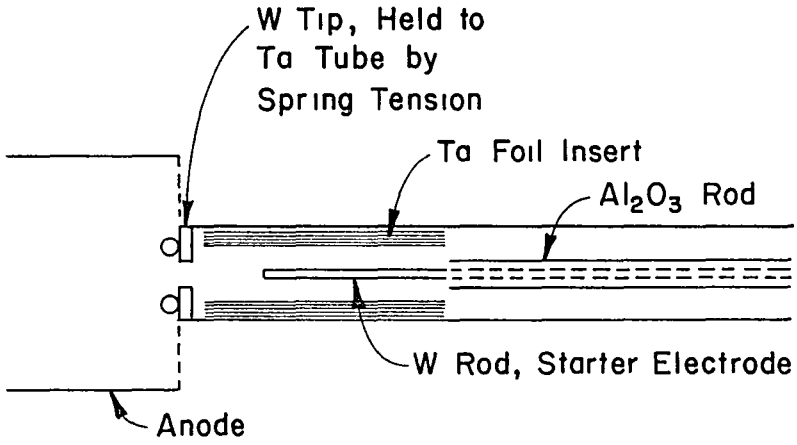

(b) Plasma Source Used in Large Vaccum Facility

Fig. 2-1. Hollow cathode configurations used in subject investigation.

tube by spring tension. No keeper or external heater was used. The cathode discharge was started by means of a bias on an internal electrode, which was turned off after emission was initiated. The use of this hollow cathode required a minimum anode current to maintain operation. This minimum current limited the density range that was achieved. The rate of argon gas flowing through the hollow cathode was typically 1.2 to 1.5 A-equiv. A more detailed description of this cathode configuration and performance is given elsewhere.[2]

The hollow cathode configuration used in the small vacuum facility was changed from that in Fig. 2-1(a) to that in Fig. 2-1(b) when the investigation was moved into the large facility, due to the frequency with which the insert needed to be treated with emissive mix following exposure to the atmosphere. The oxide-free insert used in the unconventional hollow cathode of Fig. 2-1(b) greatly improved the reliability of the cathode.

Sample Designs

The current collection by defects in the insulation covering of high voltage solar arrays was simulated by superimposing a sheet of insulating material, with a hole in it, over a conducting disc at a high potential. Two types of sample designs were used.

The first sample design was constructed from a 12 × 12 cm printed circuit board, made of fiberglass and covered with a copper film. The circuit board was etched to leave a centered 7.9 cm diameter copper disc. An electrical connector was soldered to the copper disc from the rear of the board to provide an insulated connection to the high voltage power supply. The insulating sheet was then attached by an adhesive to the sample holder. The adhesive was restricted to distances of more than 5 mm from the hole. This sample design was used only in the small vacuum facility. Its configuration and position in the chamber are indicated in Fig. 2-2.

A second sample holder was fabricated to permit measurement and control of the sample temperature. This design consisted of an aluminum frame containing a brass disc, 6 cm in diameter. The conductor was insulated from the frame, and protected from the plasma by a screen covering the aluminum frame. The sample was placed between two Al rims which were attached to the frame. The insulator was then bonded to the conductor by an adhesive, covering the entire conductor except the exposed hole in the insulation. A heater and a thermocouple were attached to the underside of the brass disc. This design was used in both vacuum facilities. Its position in the small vacuum chamber was similar to that of the first design in Fig. 2-2, except that the insulating sheet was vertical (facing the side wall). This second design is indicated in Fig. 2-3, together with its position in the large vacuum facility.

It should be noted that the different sample designs and adhesive configurations were found not to affect the experimental results.

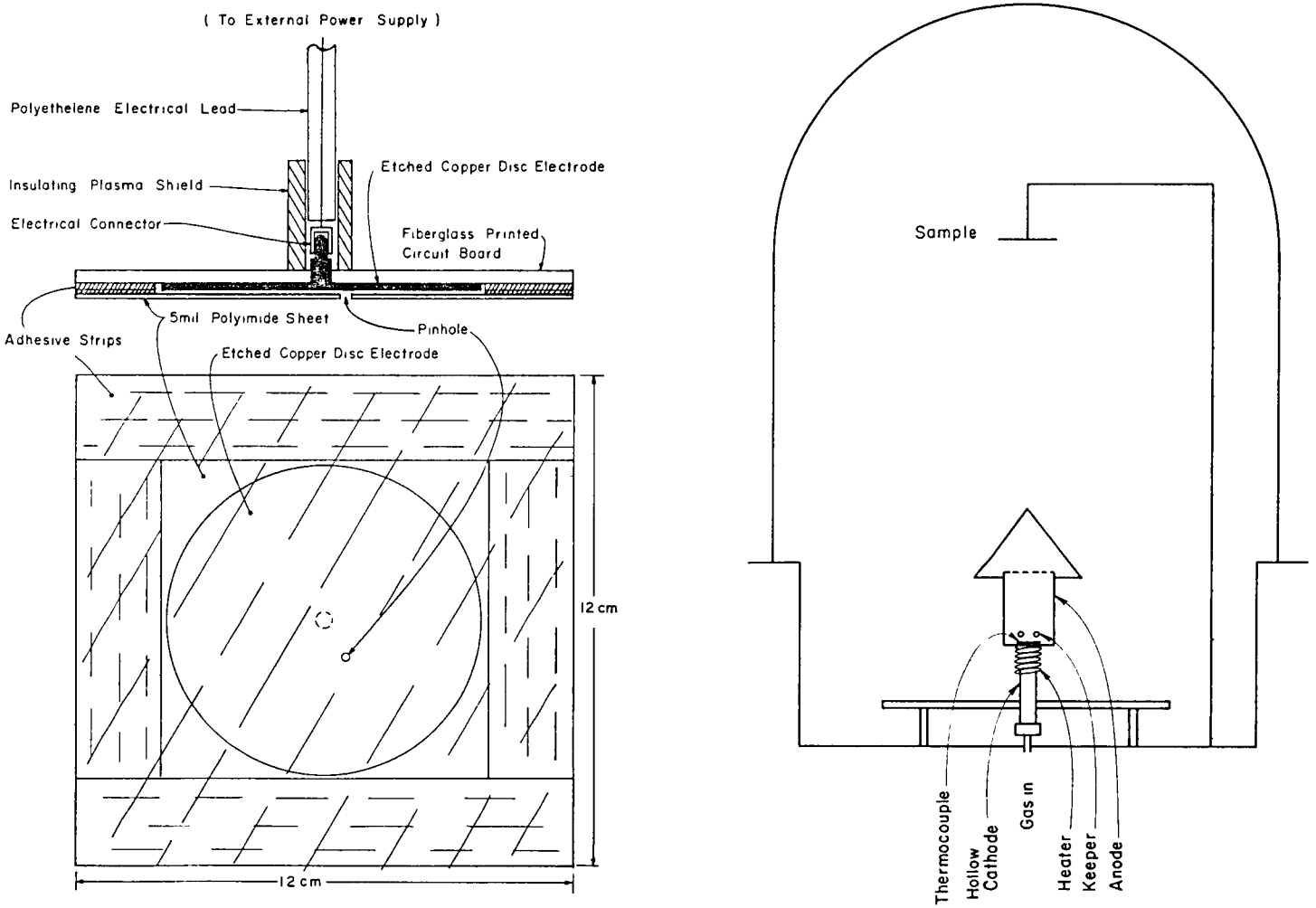

(a) Sample design. (b) Location of sample in facility.

Fig. 2-2. Nonheated sample configuration in small vacuum facility.

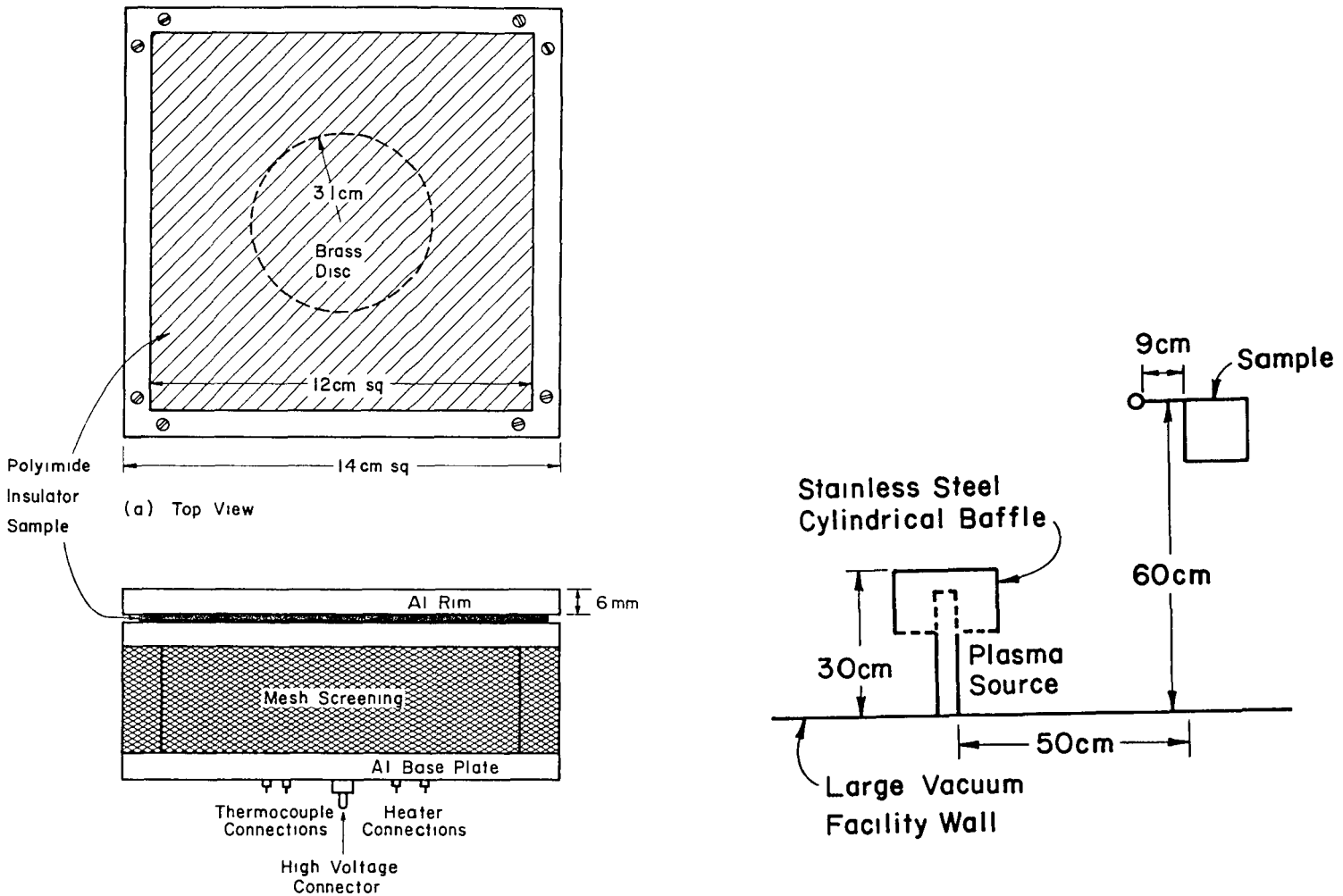

(a) Sample design. (b) Location of sample in facility.

Fig. 2-3. Heated sample configuration in large vacuum facility.

Plasma Measurements

The plasma parameters were measured with a spherical Langmuir probe, using thick-sheath analysis (see Appendix A). Two probe diameters were used, a 1.3 cm diameter probe in the small vacuum facility and a 1.75 cm diameter probe in the large vacuum facility. It was necessary to go to a larger probe for plasma measurements in the large vacuum facility due to the small random current densities that were encountered. The current collected by the probe is proportional to the random current density.

In the small vacuum system the probe was approximately 4 to 6 cm from the sample. It was moved toward the sample for plasma measurements, then moved away from the sample during current-collection tests, using a rotating mechanical linkage. In the large vacuum facility the probe was attached to an aluminum rod, 9 cm long and attached to the frame of the sample holder.

The plasma parameters measured for all tests were the electron density, electron temperature and plasma potential of the bulk plasma.

Testing Procedure

The general procedure for a test was to record the sample parameters, that is, insulator material, hole size and surface condition. The sample was then placed in the vacuum facility and the plasma parameters measured. The conductor potential was increased and the hole current as a function of conductor potential was measured.

The cleaning procedure used was to place the sample in the vacuum facility and allow it to be bombarded by the plasma (>30 min. in the small system and >15 min. in the large system) before testing. This procedure assured desorption of gases from the insulator surface.

When temperature measurements were taken, at least 30 minutes were allowed for the insulator to come to thermal equilibrium with the conductor.

The voltage sources were a Spellman current and voltage regulated, 10,000 volt, 100 mA direct-current power supply, used for experiments in the large facility; and a 150 kV, 5 mA, direct-current unregulated power supply for tests in the small vacuum facility. Meters of appropriate ranges, were used to measure the collected currents and the conductor potential.

Testing was carried out by varying the conductor potential and recording the voltage-current curve. Sample temperatures were recorded and Langmuir probe measurements taken before or after each test. Current leakage from the sample holder and connecting wires was periodically monitored by using an insulator sample with no hole.

III. EXPERIMENTAL RESULTS

Positive Bias - Electron Collection

Collection Modes. Two distinct collection modes were observed for positive-bias experiments. The two modes differed in current collection by more than an order of magnitude. The first mode involved only current collection enhanced by a surface phenomenon (herein referred to as the surface-enhanced collection mode). This mode is characterized by a roughly linear current-voltage characteristic. The second mode involves vaporization of the insulator material (herein referred to as the vapor-enhanced collection mode). It appears that the vaporized material is ionized and thereby enhances the electron collection. It has been observed in the large vacuum facility that whenever there was a jump in the current collection (sudden current increase for a constant conductor potential), the jump was visually correlated with the appearance of a bluish glow localized near the hole, or an arc seen in the hole.

All the data for the surface-enhanced collection mode were taken in the large vacuum facility. The vapor-enhanced collection modes that are presented were all taken in the small vacuum facility, unless otherwise specified. The current-voltage curve taken in the small vacuum facility were typically of the shape shown in Fig. 3-1. In Fig. 3-1, the current-voltage curve begins with a very small current collection (not always seen with smaller holes because of the meters used), the characteristic then jumped to a lower potential and higher current (jump denoted by dotted line). The upper region is the vapor-enhanced collection region. Operation in this region was usually accompanied by observation of a localized glow, or arc, at the hole. The extreme upper region where the current increases and conductor potential decreases represents the destruction of the insulator near the hole. This rapid destruction was not always reached. After each test the sample was always inspected. It was found that the insulator material was always discolored about the hole and a brownish layer of material deposited on the exposed conductor.

Normalization. During the experimental investigation, tests were performed in plasmas that varied in electron density by two orders of magnitude and in electron temperature by a factor of several. To effectively compare data taken under different plasma parameters, it was necessary to normalize the data.

It has been previously suggested that the sheath should be approximately hemispherical.[1] This suggestion is in agreement with sheath measurements of previous investigations.[2,3] The hemispherical shape of

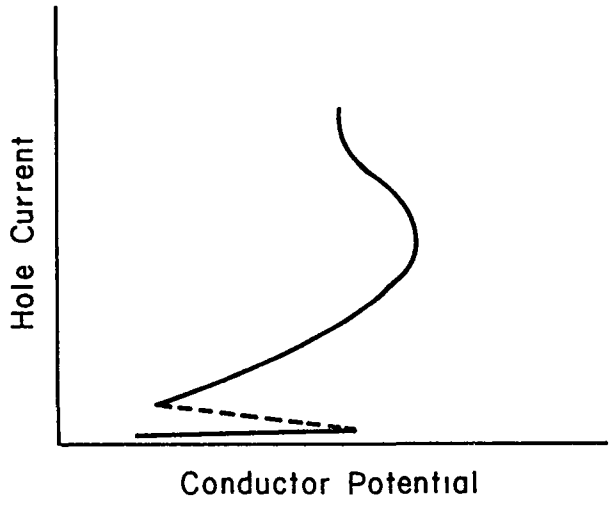

Fig. 3-1. Typical current-voltage characteristics observed in small vacuum facility.

the sheath indicates that the spherical probe approach for low density plasmas (thick sheath analysis) is appropriate for determining the normalization factor. The current collected by a spherical probe is given by (see Appendix A)

$$I \simeq j_o A_p \frac{eV_p}{kT_e} \quad \text{for} \quad eV_p >> kT_e \ , \tag{3-1}$$

where A_p is the surface area of the probe, e is the electronic charge, V_p is the probe potential, T_e is the electron temperature, k is Boltzmann's constant and j_o is the random current density. The expression for j_o is[4]

$$j_o = \frac{1}{4} en \left[8kT_e/\pi m_e\right]^{1/2} \ , \tag{3-2}$$

where n is the electron density and m_e is the electronic mass. Equation (3-1) indicates that in analyzing the data, a normalized hole current, IkT_e/j_o, should facilitate comparison of data taken under different plasma conditions to be compared. A comparison of non-normalized and normalized data is shown in Fig. 3-2 for the surface enhanced collection mode. Figure 3-2 clearly shows that, for the different plasma parameters, the current-voltage characteristics differ before normalization. But once the hole currents are normalized, the characteristics reduce essentially one line.

In the vapor-enhanced collection mode, agreement between data taken under different conditions should be poor, since the vaporization and ionization of the vaporized material should be dependent on background pressure, roughness of hole, and surface history. Figure 3-3 shows a comparison of non-normalized and normalized data in this mode. The normalized data is found to be in better agreement at the higher conductor potentials. This result is reasonable, inasmuch as lower potentials are closer to initiation conditions, and a larger variability could be expected near initiation conditions.

Variation in Current Collection. While the data collected in the surface-enhanced collection mode was reproducible, that of the vapor-enhanced collection mode was far less so. This was especially true when comparisons were made of tests taken in the two different vacuum facilities. Figure 3-4 shows this variation. The characteristics taken at the two lower neutral pressures were taken in the large facility, the test at the high neutral pressure was taken in the small facility. The tests at the two higher pressures were visually confirmed to be in the vapor-enhanced collection mode. Figure 3-4 indicates that the magnitude of normalized current collection can differ significantly with plasma parameters and neutral density. This variation emphasizes that only rough agreement can be expected in the vapor-enhanced collection mode. The difference in electron collection was probably due to the

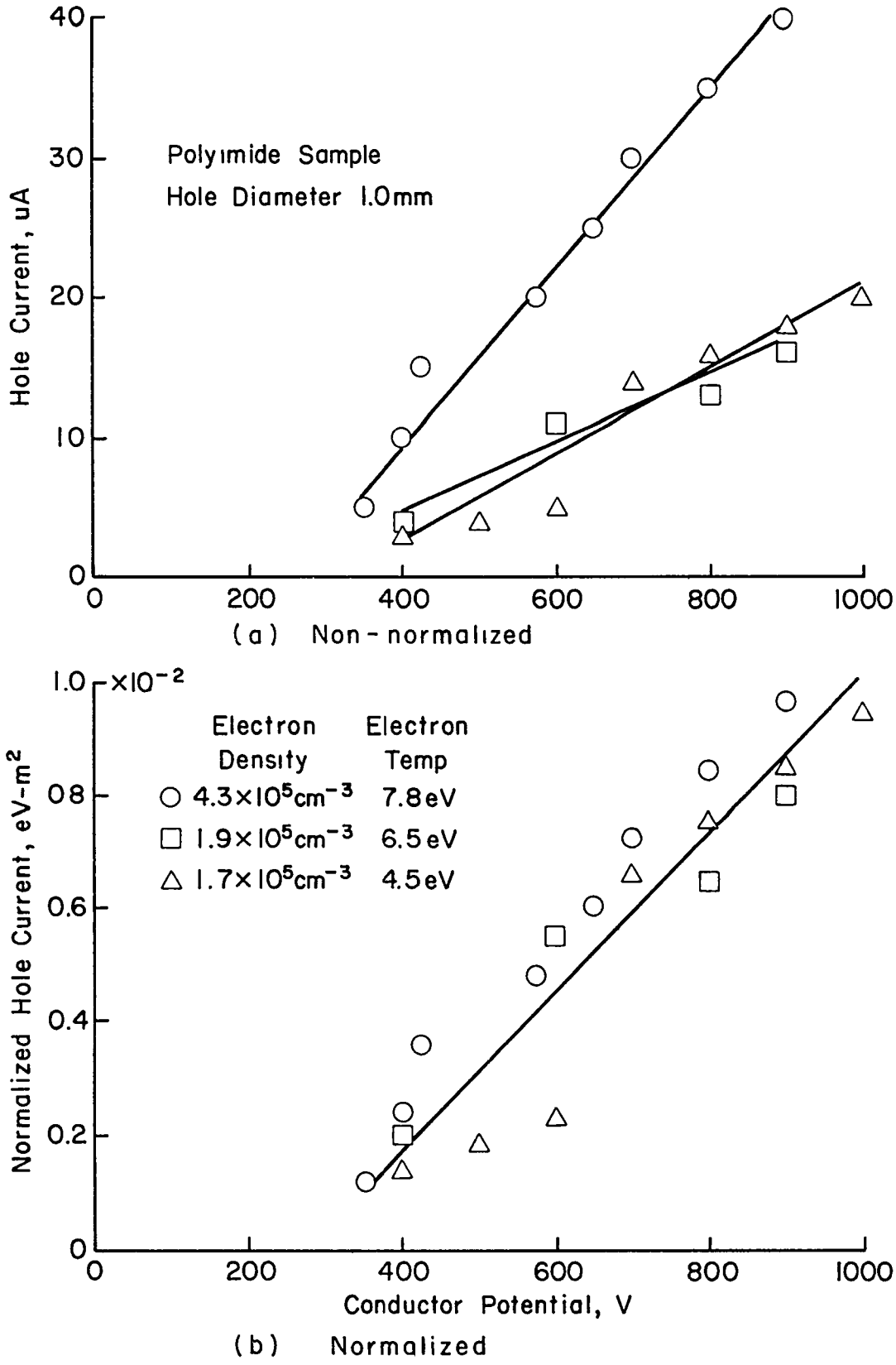

Fig. 3-2. Comparison of non-normalized and normalized current collection for the surface enhanced collection mode.

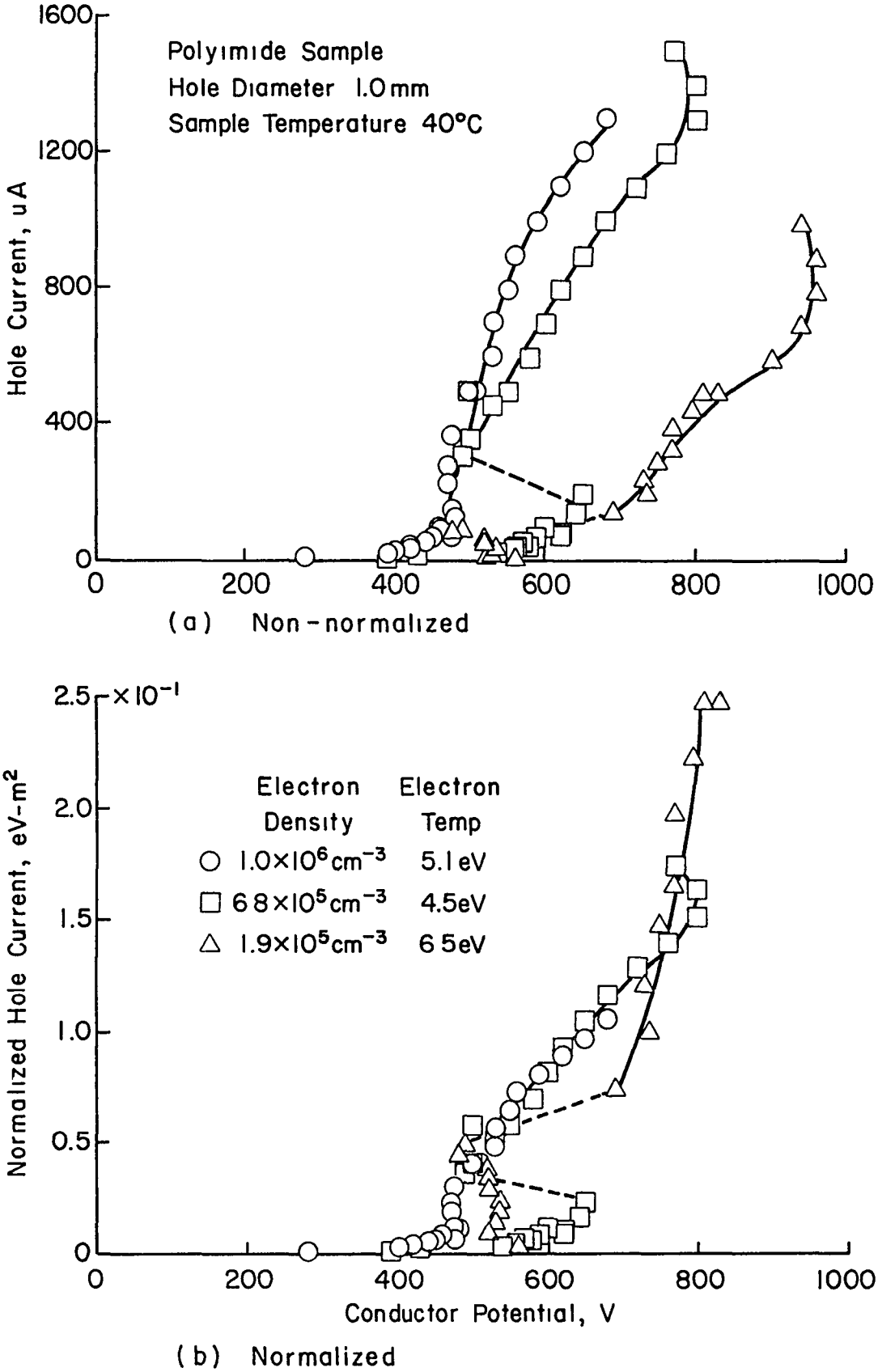

Fig. 3-3. Comparison of non-normalized and normalized current collection in the vapor enhanced collection mode.

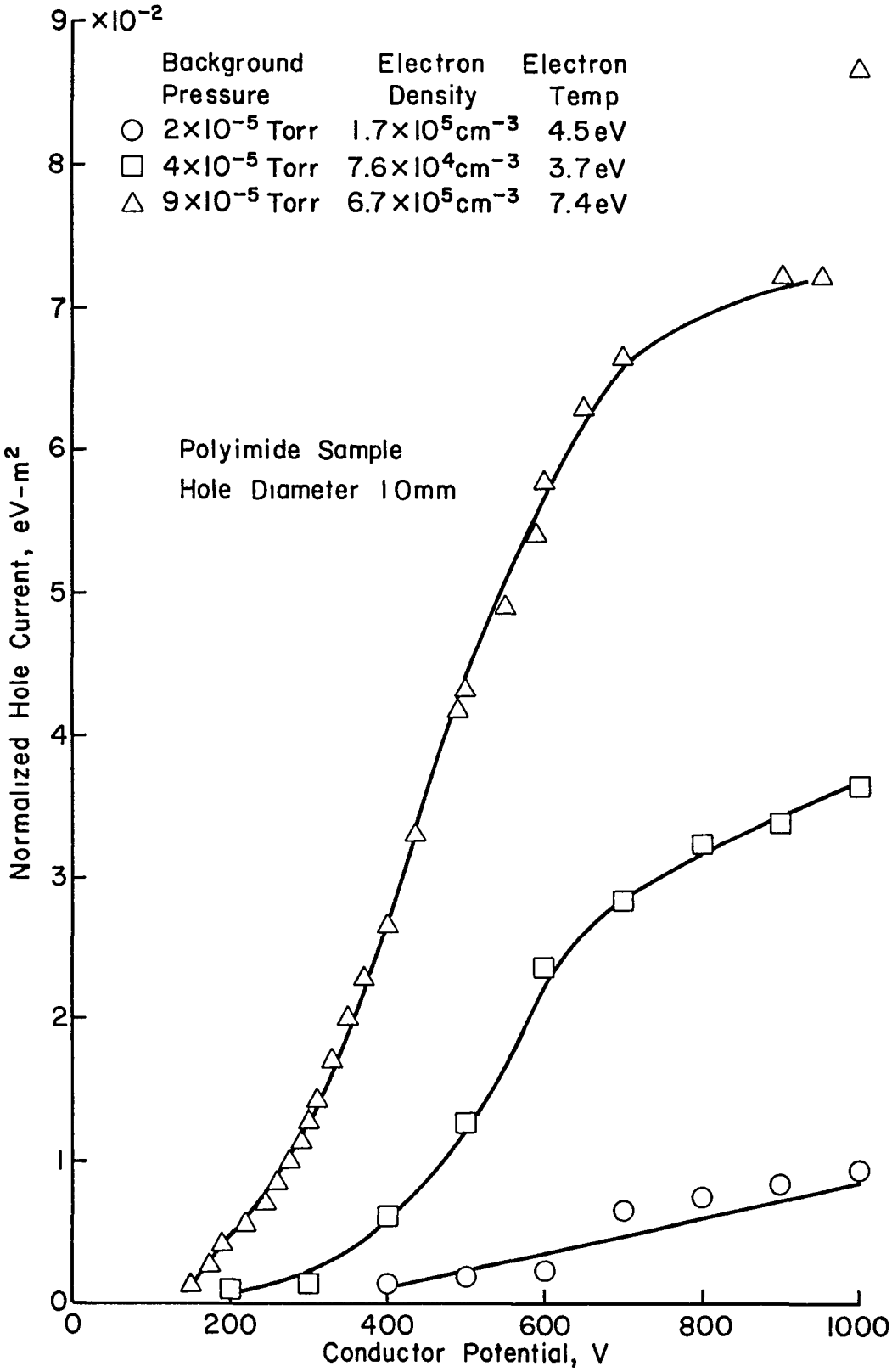

Fig. 3-4. Comparison of current collection for the various background pressures and plasma parameters.

variation in the amount of vaporization, caused by the difference in current density, and ionization, in turn caused by the difference in background pressure.

The data presented for the vapor-enhanced collection mode herein were all taken at the higher neutral pressures with electron densities in the range of 10^5-10^6 cm^{-3}. This data has also been presented previously by the author.[1,5,6]

Comparison with Electrostatic Probe Theory. In order to determine how the collected current is enhanced by the presence of the surrounding insulation, it is useful to make a comparison with electrostatic probe theory. The probe theory that appears most appropriate is the planar probe theory of Parker and Whipple (see Appendix B). In the theory, the current is given by

$$I \simeq j_o A_p \left[1 + \frac{b^2}{4} + \left(1 - \frac{b^2}{4}\right) \frac{eV_p}{kT_e}\right] , \quad \text{for} \quad eV_p >> kT_e \tag{3-3}$$

where b is a constant varying from 0 to 2. For b = 0,

$$I \frac{kT_e}{j_o} \simeq A_p V_p . \tag{3-4}$$

which is the same form as the spherical-probe equation.

Figure 3-5 shows a comparison of the two collection modes with probe theory. The surface-enhanced collection mode gives currents approximately an order of magnitude higher than probe theory, while the vapor-enhanced mode yields currents over two orders of magnitude greater. This comparison illustrates the difference between the current collection that was experimentally observed and what was originally expected. It should be noted that although the current predicted by probe theory appears independent of probe potential in Fig. 3-5, this is because of the scale used in Fig. 3-5.

Adhesives. As described in the Apparatus and Procedure section, the insulating material was held in contact with the conductor by an adhesive. Since the adhesive continued up to the hole edge, it was important to determine the effect of the adhesive on the electron collection.

Two types of double-sided pressure sensitive adhesives were tested, a low priced commercial brand (Scotch Double Stick Tape, by 3M) and a space qualified type (Y966, also by 3M). The low priced commercial adhesive was found to have modified sticking properties after testing at high temperature (<120°C), while no such change was evident for the space qualified adhesive. Such a change in properties for an organic material in a vacuum environment is almost always associated with outgassing. If the type of adhesive can affect the current collection, significantly different results should have been obtained with the two different adhesives tested.

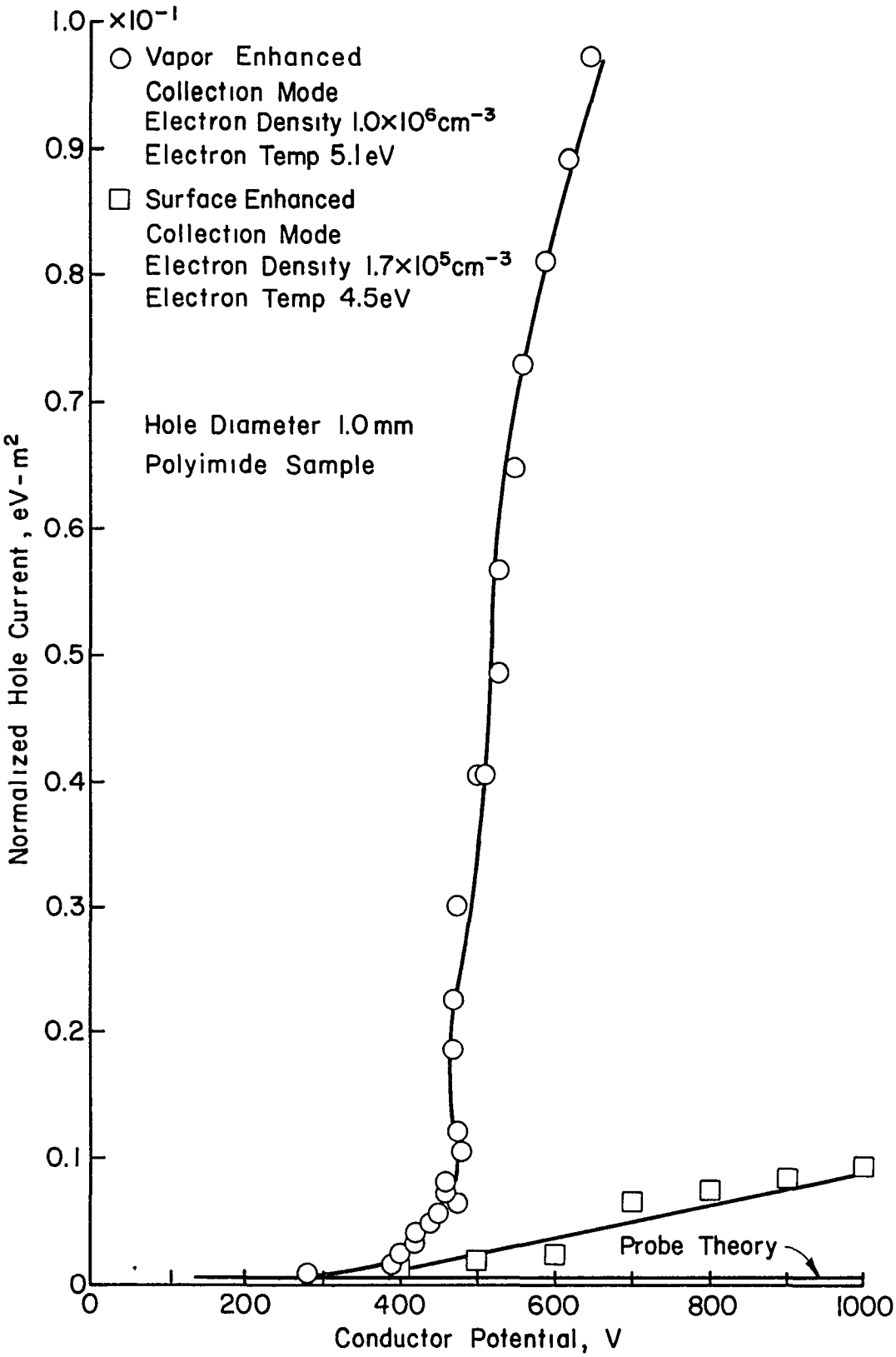

Fig. 3-5. Comparison of the two current collection modes with theory.

The results of the adhesive tests in both collection modes showed no significant difference between the two adhesive types.

Sample Material. Three insulator materials were tested, polyimide, teflon and inorganically bonded iso-mica. The insulating materials were all thin sheets, the polyimide and teflon 0.127 mm thick and the iso-mica 0.254 mm thick. All the samples, for better comparison, had hole diameters of 1.0 mm. The three materials were chosen because of widely different properties. In particular the secondary yield of the materials differ, and so different electron-collection characteristics were expected.

Figure 3-6 compares the electron collection characteristics with the three insulator materials in the surface-enhanced collection mode.

Although teflon and polyimide have different secondary yields, the current collection was found to be roughly equal. This unexpected result is discussed in Section IV.

Hole Size. Different hole diameters were tested to determine the effect of hole size on electron collection. For the surface-enhanced collection mode, five hole diameters were tested, 0.35, 1.0, 2.0, 3.0 and 5.0 mm. The results of these tests are shown in Fig. 3-7. It is indicated in Fig. 3-7 that the electron collection is strongly dependent on hole size in this collection mode. Analysis of the data shows that the current was not proportional to the exposed conductor area, although the collected current increased continuously with hole area.

Three different hole diameters were tested for the vapor-enhanced collection mode, 0.35, 1.0 and 2.0 mm. The results of these tests are shown in Fig. 3-8. The data of Fig. 3-8 show that the hole size is not important to the electron collection in this mode. This phenomenon is in agreement with the assumption that the vaporization and ionization of the insulating material is the dominant process in the vapor-enhanced collection mode.

These above results are also in agreement with the results found by Kennerud.[2] Although Kennerud did not envision two collection modes, his data indicate that below a conductor potential of roughly 1000 volts the current collection was dependent on hole size, but above this potential the current became independent of hole size.

Textured Samples. To learn more about the surface phenomenon occurring, a textured sample was tested. The insulator surface was textured by mechanically rubbing a fine grade of sandpaper over the surface facing the plasma. This was done before cleaning and punching the hole in the sample. The results of this test are shown in Fig. 3-9, for the surface-enhanced collection mode. The figure shows that the textured surface collected less current than the nontextured surface.

It has been found that roughening a surface decreases the secondary electron emission yield (see Appendix C). The collection mechanism suggested by Cole, Ogawa and Sellen[7] (see Introduction) could therefore explain this observation.

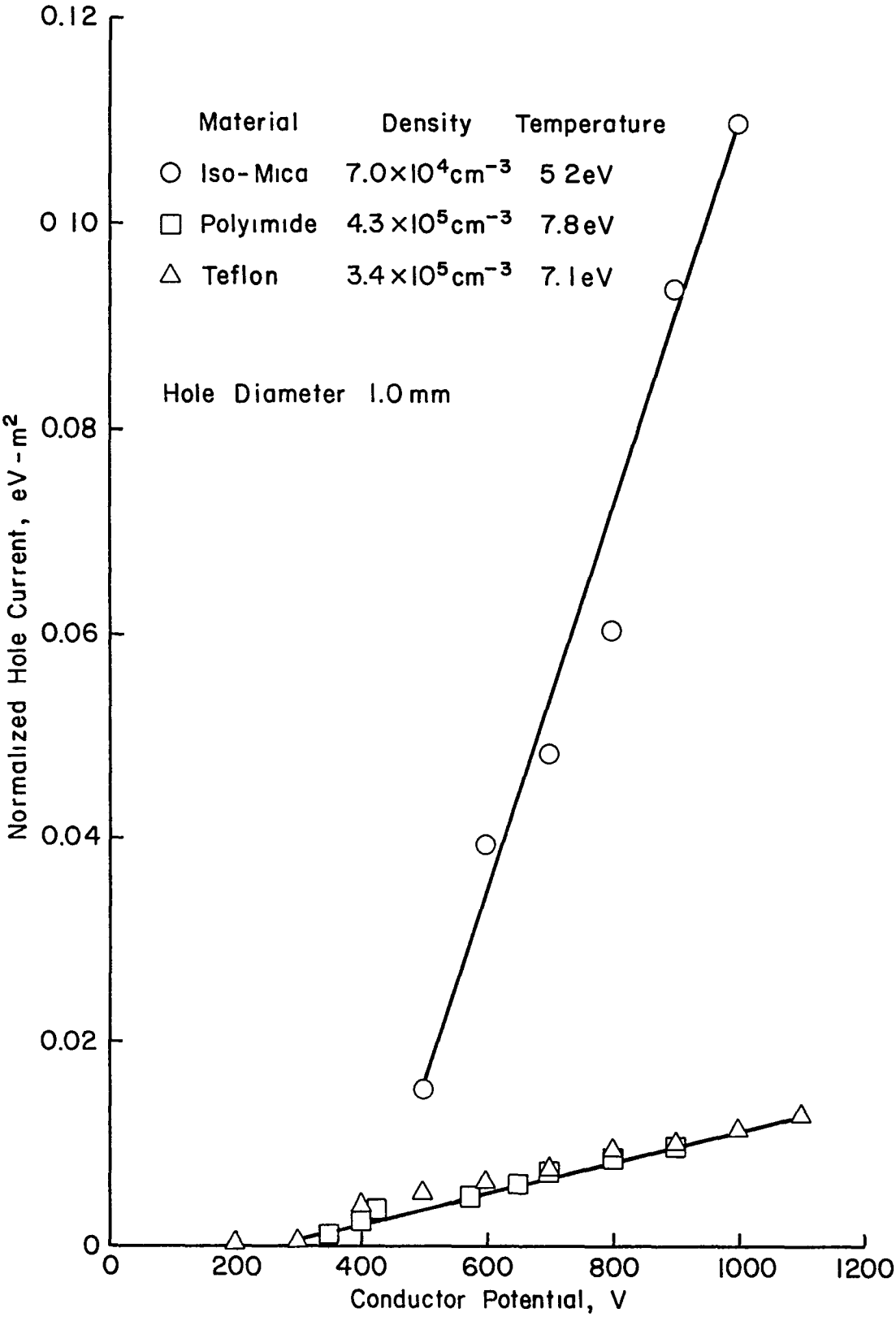

Fig. 3-6. Comparison of electron collection using polyimide, teflon and iso-mica insulators in the surface enhanced collection mode.

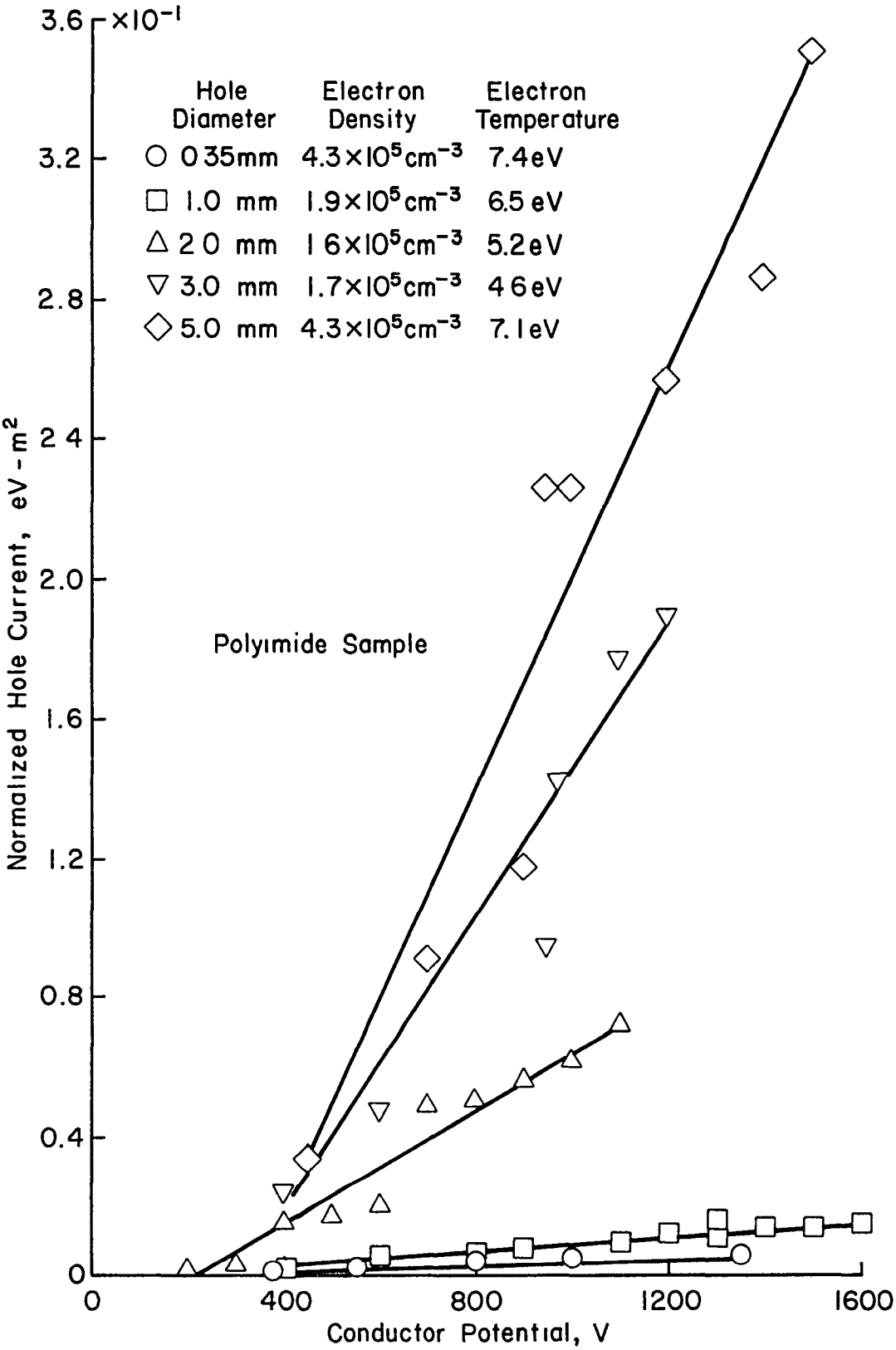

Fig. 3-7. Effect of hole size on current collection in the surface enhanced collection mode.

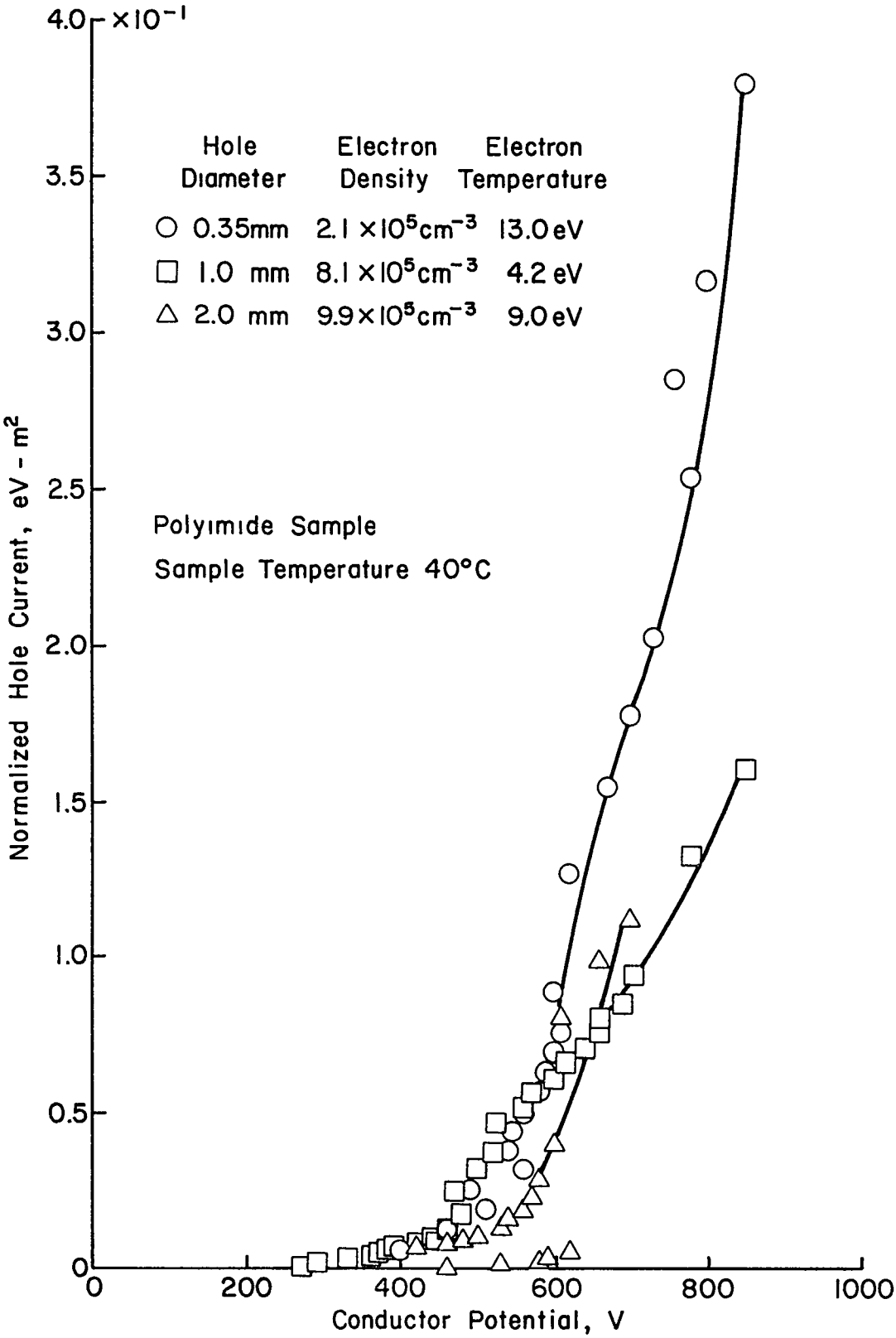

Fig. 3-8. Effect of hole size on current collection in the vapor enhanced collection mode.

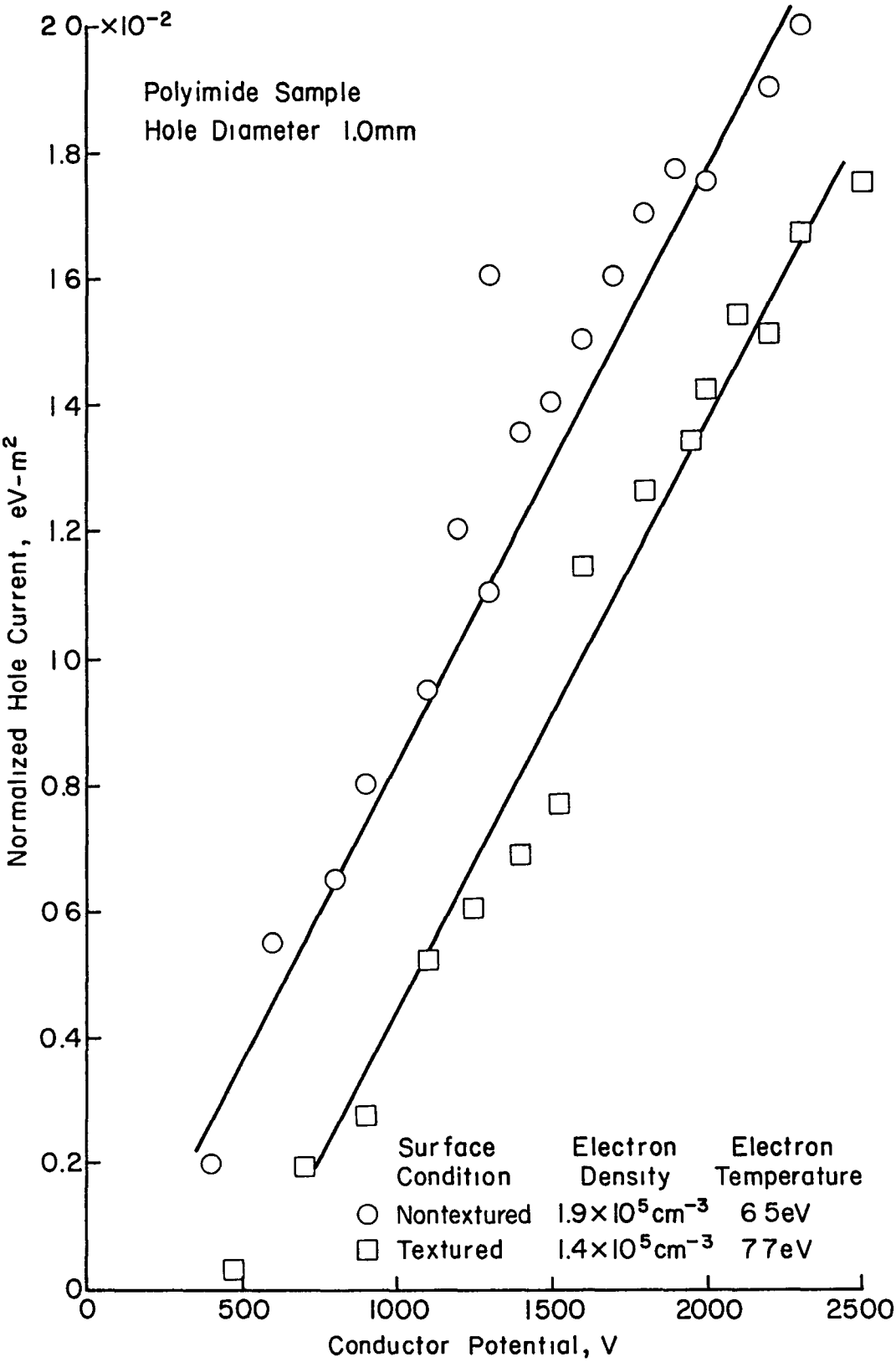

Fig. 3-9. Comparison of textured and nontextured surface on current collection in surface enhanced collection mode.

To determine if a surface phenomenon plays any part in the vapor-enhanced collection mode, textured surfaces were also tested in this mode. The samples were textured in a different manner for these tests. Radial lines and concentric circles were scribed onto the surface, radiating from the hole, with a sharp metal stylus. The results of these tests are shown in Fig. 3-10.

Figure 3-10 shows that the electron collection decreases with textured surfaces, even in the vapor-enhanced collection mode. This indicates that some of the same surface phenomena observed in the surface enhanced mode are still operating and important to the collection process in the vapor-enhanced mode.

Sample Temperature. The temperature of the sample was varied to determine the effect of this variable. It was found that increasing the temperatures caused decreased electron collection in both collection modes (see Figs. 3-11 and 3-12).

In the vapor-enhanced collection mode the increasing temperature might have been expected to increase collection by increasing vaporization. On the other hand secondary emission often decreases with increasing temperature (see Appendix C). Since the current collection actually decreased in this mode, the data of Fig. 3-12 indicate the importance of surface phenomena to this collection mode.

To determine if secondary emission is responsible for the current decrease with increasing temperature, a mica sample was also tested. This insulator selection was made because it has been found that mica does not have a significant temperature dependence for secondary yield (see Appendix C).

The iso-mica sample was tested six times at three different temperatures, 27°, 50° and 85°C (two tests per temperature). The results of the tests are shown in Fig. 3-13. From the results shown, electron collection is independent of sample temperature. This indicates that the spread observed with polyimide was indeed due to secondary electron effects.

A polyimide sample with a 5.0 mm hole diameter was tested (see Fig. 3-14). It was found that, for this hole diameter, there was no appreciable temperature effect. As the hole size is increased, a larger fraction of the electron current would be expected to be collected directly by the exposed conductor. This would have the effect of reducing any temperature effect by decreasing the fraction of the total electron current that strikes the surrounding insulator material.

Onset of Vaporization. In discussing the two types of collection modes, the conditions necessary for a mode change have been ignored. This section will discuss the observation made on the transition from one mode to another.

The onset of vaporization, as defined here, is the point at which the current-voltage curve deviated from the expected normalized data for the 1.0 mm diameter hole. In the case of the other hole sizes, the

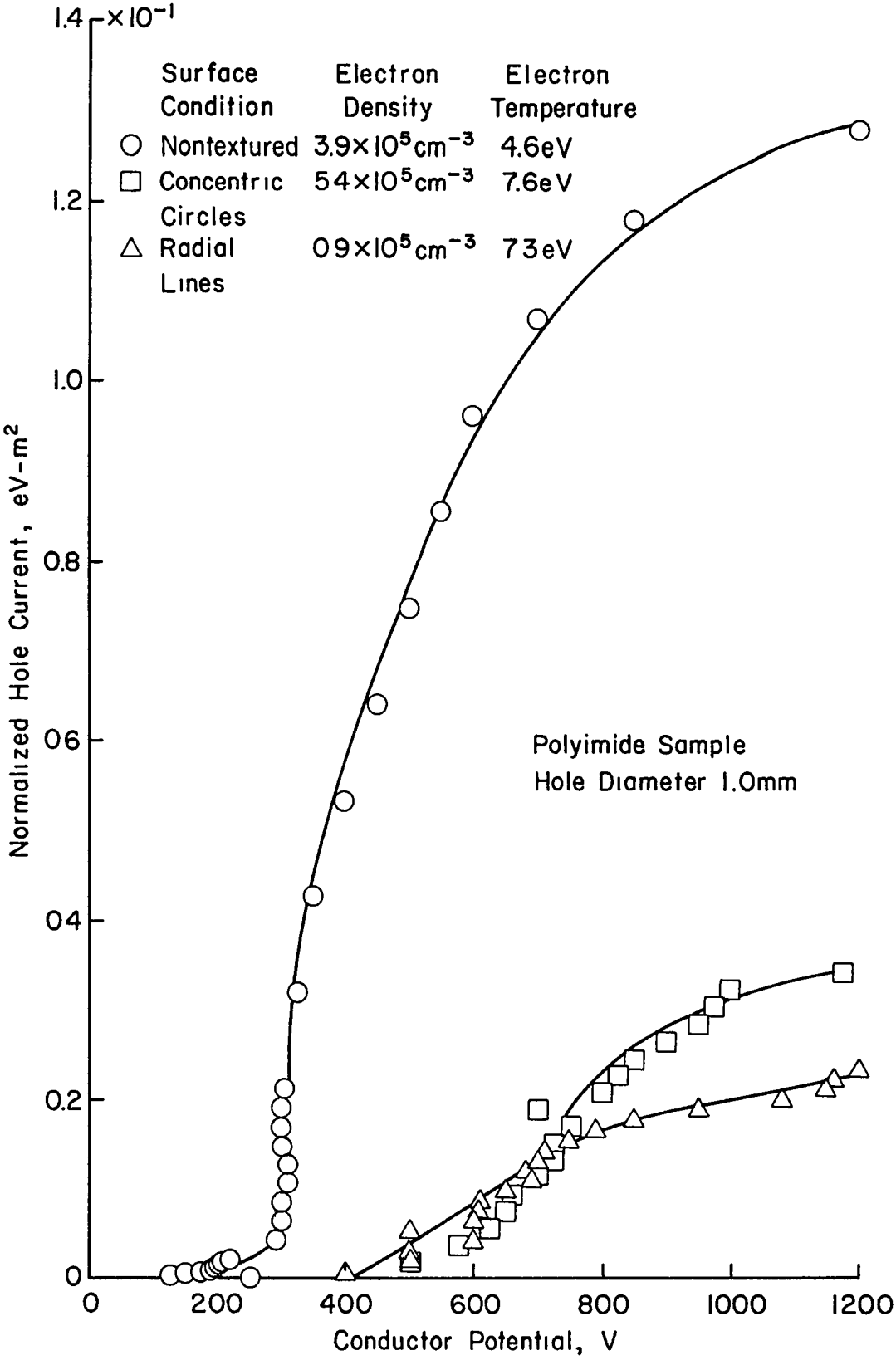

Fig. 3-10. Comparison of textured and nontextured surface on current collection in the vapor enhanced collection mode.

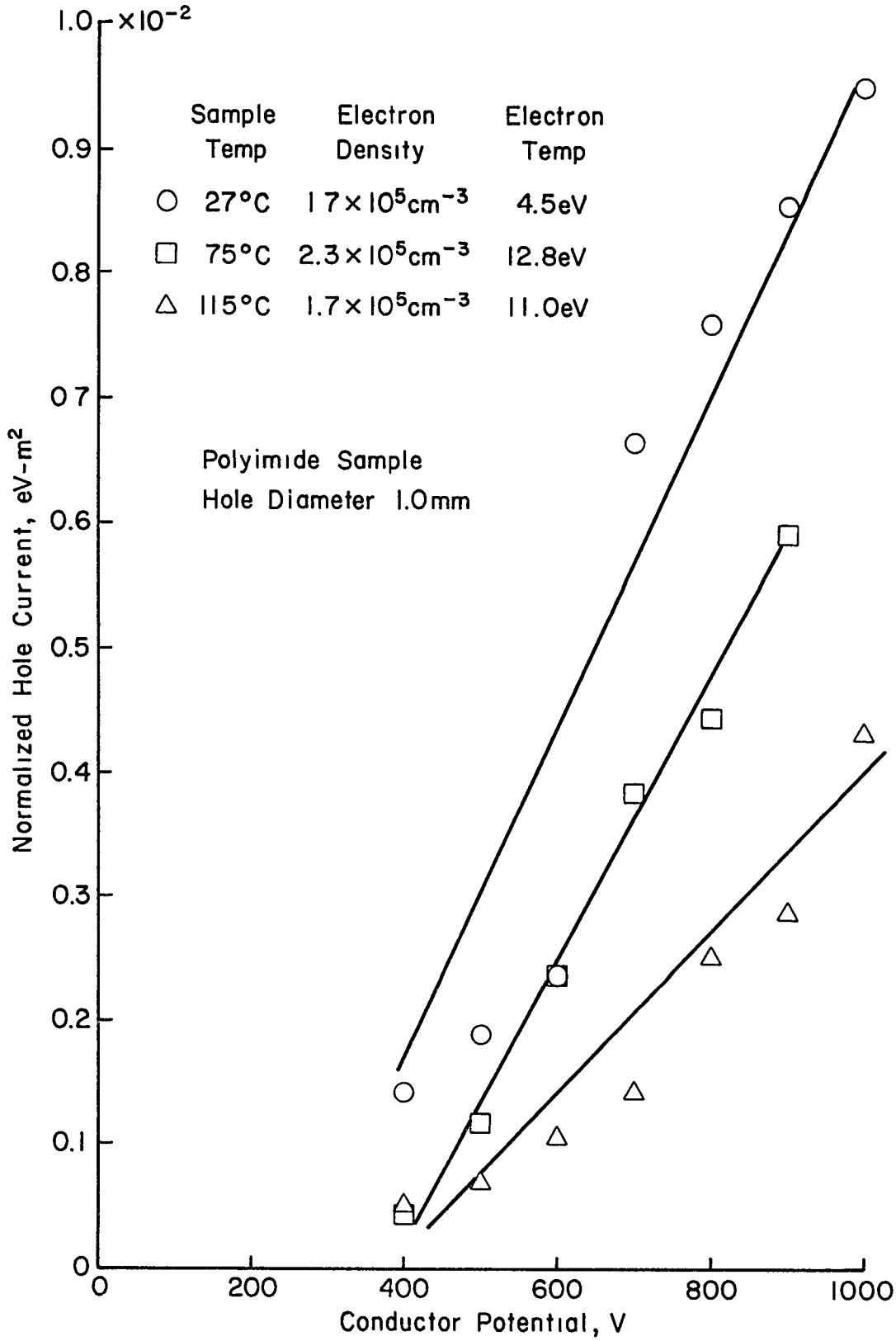

Fig. 3-11. Effect of sample temperature on the electron collection of a 1.0 mm diameter hole in the surface enhanced collection mode.

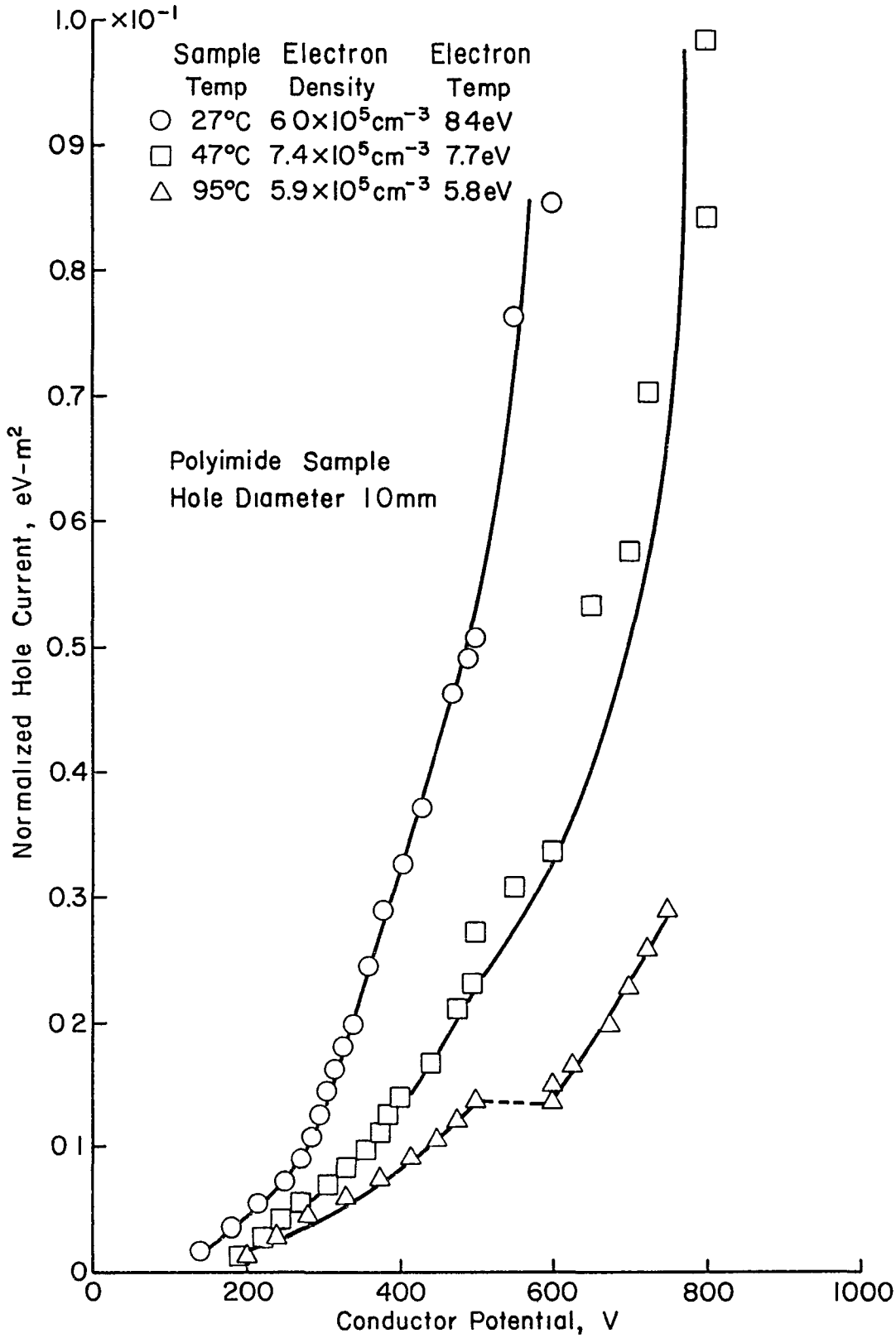

Fig. 3-12. Effect of sample temperature on the electron collection of a 1.0 mm diameter hole in the vapor enhanced collection mode.

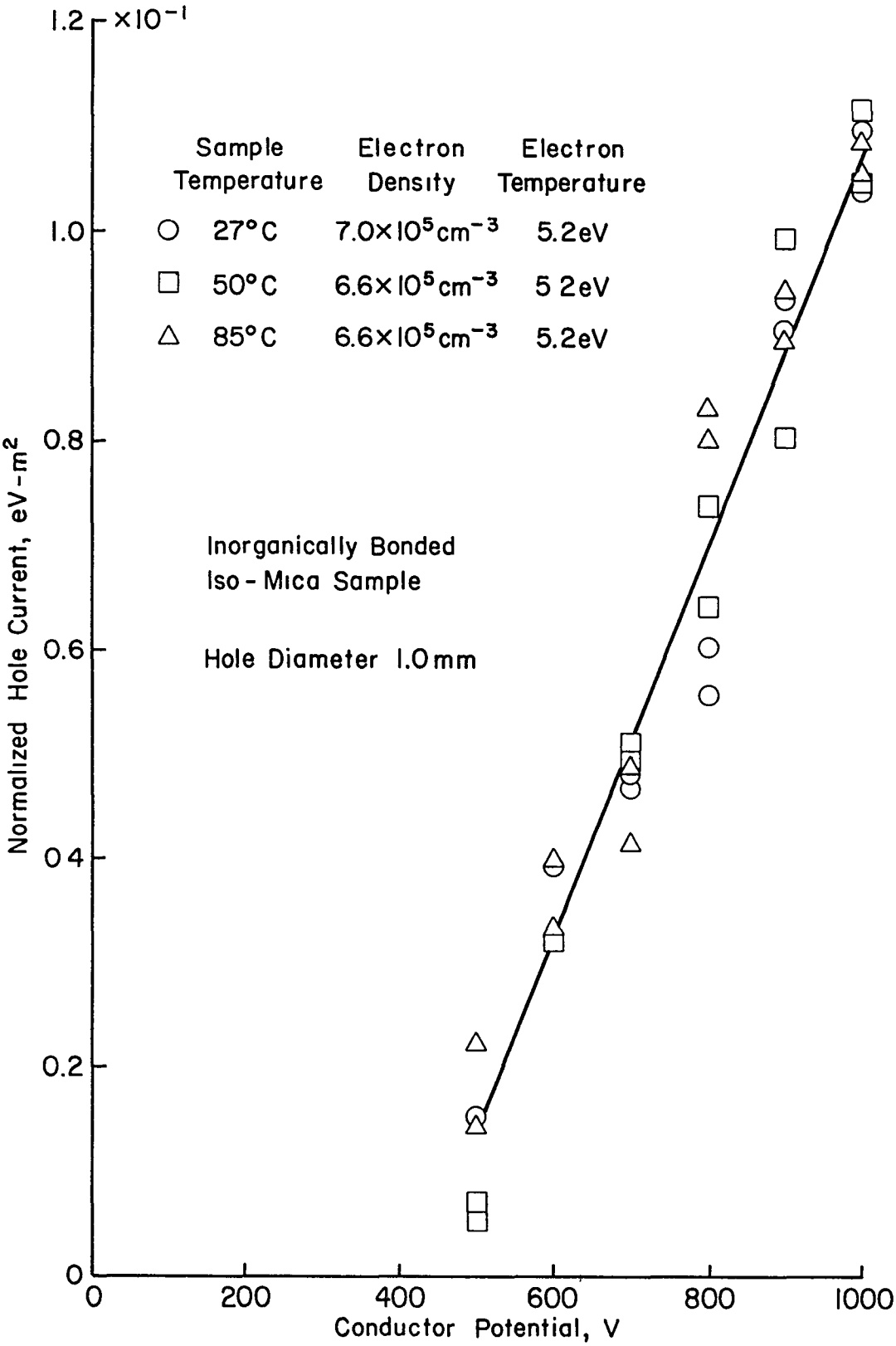

Fig. 3-13. Effect of sample temperature on the electron collection of a mica sample in the surface enhanced collection mode.

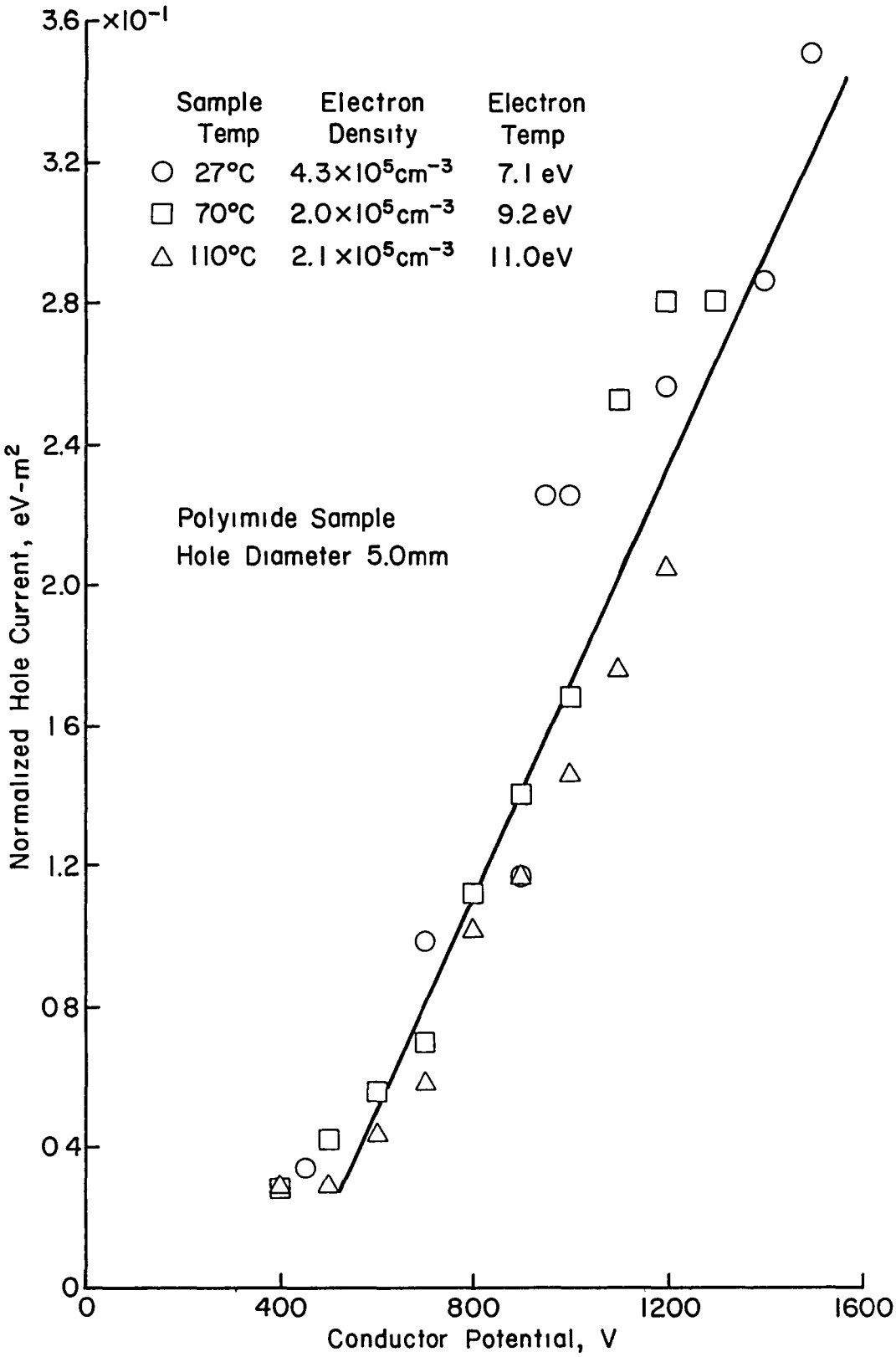

Fig. 3-14. Effect of sample temperature on the electron collection of a 5.0 mm diameter hole in the surface enhanced collection mode.

onset was defined as either the point at which the current departed significantly from a linear extrapolaton from lower voltage data, or the point at which the current jumped to a higher value.

When current jump was observed, it was accompanied by a blue glow, localized about the hole, or an arc in the hole. These visual observations are consistent with the insulator material being vaporized. The vaporized material would enhance the local neutral density about the hole so that the ionization of this material would increase both the local plasma density and collection.

For different hole sizes it was found that the trend was for larger holes (above 2 mm) to require more power before vaporization occurred, as shown in Fig. 3-15. The scatter shown in Fig. 3-15 for the 1.0 mm diameter hole was probably due to the roughness of the hole edge. If the hole edge was rough, this would allow some vaporization to occur at low power levels. If more tests had been conducted at the other hole diameters, similar scatter might have been observed elsewhere in Fig. 3-15.

Comparison of data for different sample temperatures results in a rough trend of reduced power required for the onset of vaporization with increasing temperature. However, the data were not sufficiently complete to support this conclusion with a high degree of confidence.

Subsequent Tests After Vaporization. It was found that once vaporization had occurred, the results of that test could not be repeated on the same sample. Subsequent tests on the same sample showed a substantial decrease in electron collection (see Fig. 3-16). One possible explanation was that the effect was due to adsorbed gas layers on the insulator surface. As time passes, the electron bombardment of the insulator removes the adsorbed layers, changing the surface properties. This possibility was tested by using a fresh sample, then removing the sample from the small vacuum facility, after testing, and exposed it to air for 17 hours. The sample was then replaced and tested again. The second testing showed drastically reduced current collection from the first test, indicating that removal of adsorbed gas layers were not the cause of the current reduction.

Another possibility was that, when the vaporized material deposited the brownish film over the exposed conductor, the presence of this film reduced electron collection. This possibility was tested by constructing a sample holder of the type shown in Fig. 2-2 which allowed the conducting disc beneath the insulating sheet to be rotated to a clean portion of the copper. These tests showed that the current collection still decreased with subsequent tests.

Another likely possibility appeared to be that, once vaporization of the insulator material occurs, it changes the secondary electron emission yield of the material by electron bombardment. In this regard tests on the mica sample (see Fig. 3-13) are of interest. In those

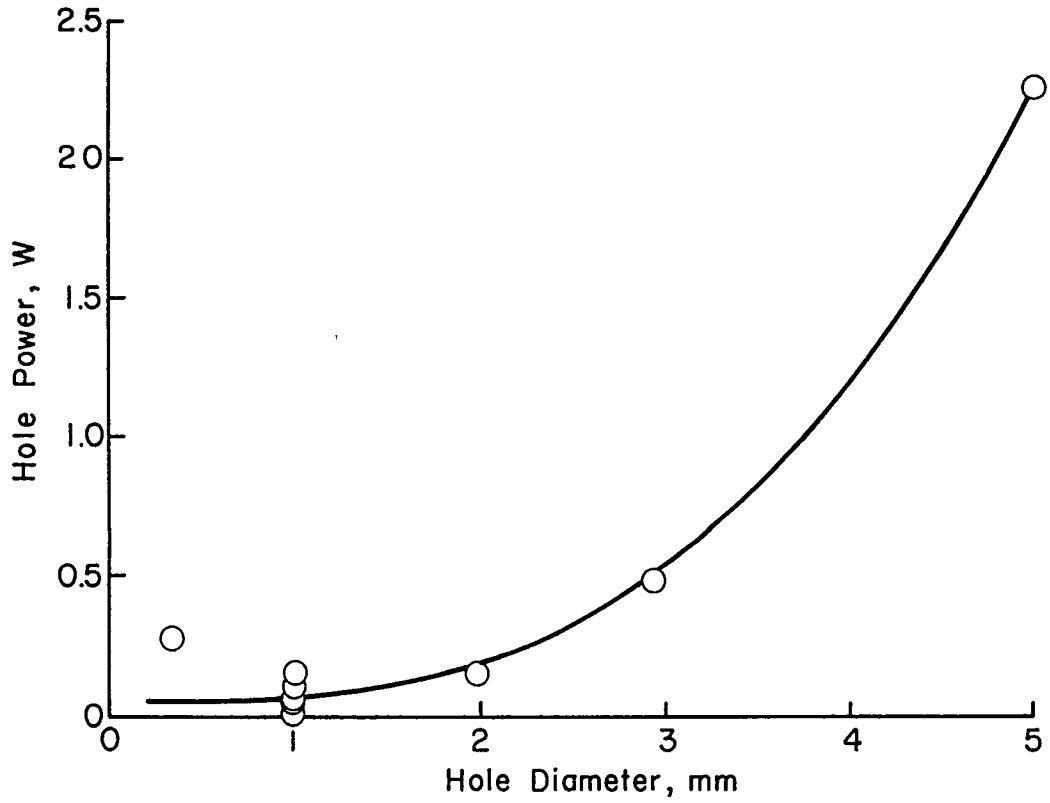

Fig. 3-15. Power required for onset of vapor enhanced mode for a polyimide sample versus hole diameter.

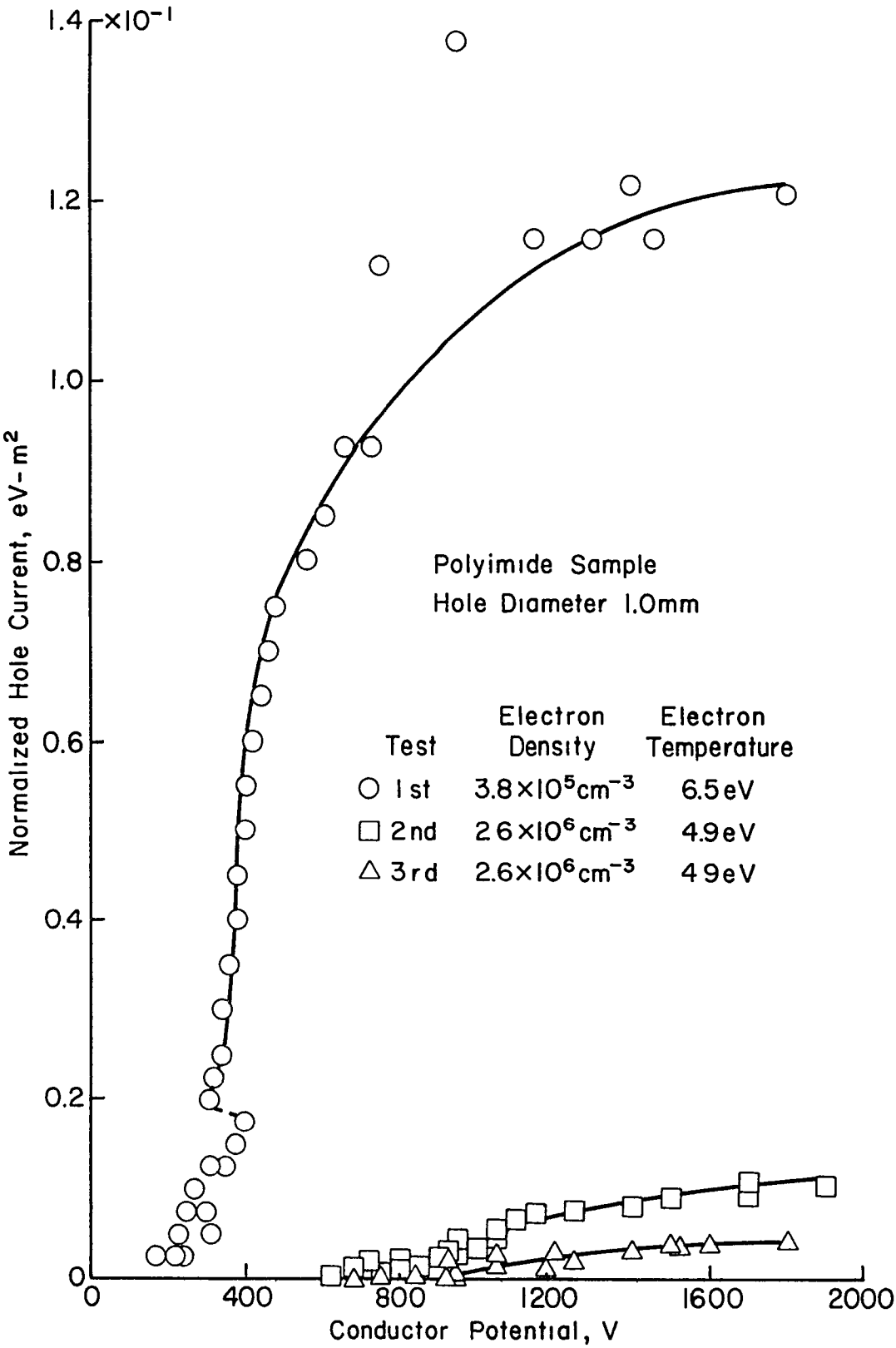

Fig. 3-16. Effect of repeating a test on a sample after vaporization had occurred.

tests, the same sample was used successively six times without a noticeable decrease in electron current, when tested in the surface-enhanced collection mode. Mica is more resistant, in general, to thermal and electrical damage than most materials, so that resistance to such damage might be expected.

Healing Effect. Occasionally during a test in the vapor-enhanced collection mode, the current began to drop. This "healing" only occurred in this mode. No correlation can be found between the power at the point of current decrease and background pressure on plasma conditions (see Table 3-2).

The probable cause of the healing is vaporized material being deposited on the conductor to an extent sufficient to reduce electron collection. Kennerud[2] reported similar behavior for teflon, indicating that this behavior may be common to many types of insulators.

Negative Bias - Ion Collection

Several tests were conducted with negative bias in the small vacuum facility. Tests were all similar in that for conductor potentials below -1000 volts, the current collection was small ($\sim 10^{-7}$ amps), while at higher potentials (between -1000 and -2000 volts) arcing was observed. Detailed data were taken up to -1000 volts. The arcing will be discussed later.

Hole Size. Four hole diameters were tested, 2.0, 3.0, 4.1, and 5.0 mm. The results of those tests are shown in Fig. 3-17. To determine if the ion collection is linearly dependent on hole area, the data were normalized in two ways, with 0.6 times the Bohm current density and 0.6 times the Bohm current (see Fig. 3-18). The Bohm current density is given by[4]

$$J_{Bohm} = ne\,[kT_e/m_i]^{1/2} \tag{3-6}$$

and the Bohm current by

$$I_{Bohm} = J_{Bohm} A_h\ , \tag{3-7}$$

where m_i is the ion mass and A_h is the hole area. The factor of 0.6 times used with the Bohm current density and the Bohm current were used to be consistent with a stable sheath.[8] The degree of correlation obtained in these two approaches indicate that the Bohm current approach is the more correct one, in that it collapses the ion characteristics to nearly a single line. The Bohm current normalization also indicates that the ion collection is nearly proportional to hole area.

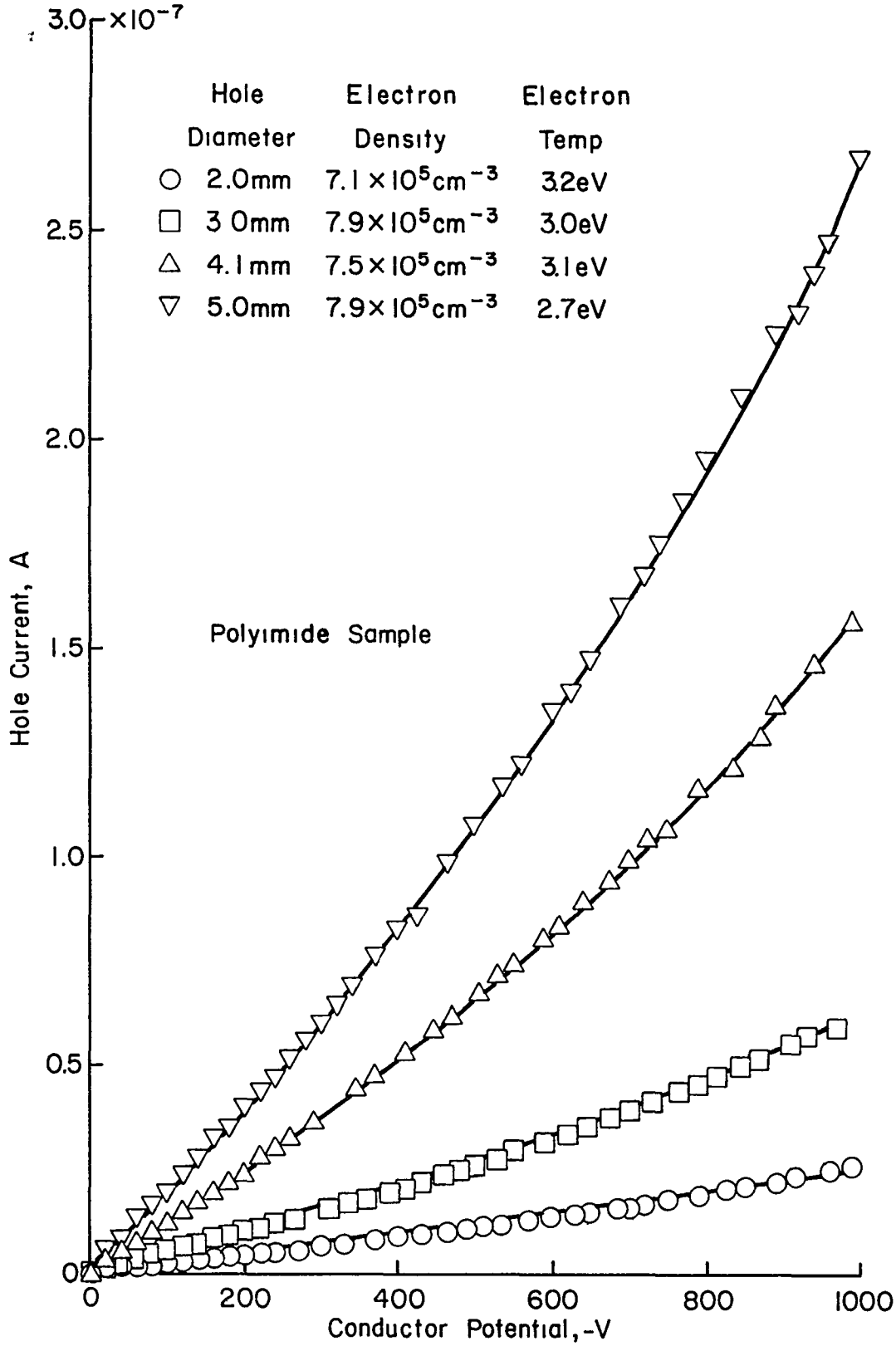

Fig. 3-17. Comparison of ion collection for four different hole sizes in polyimide.

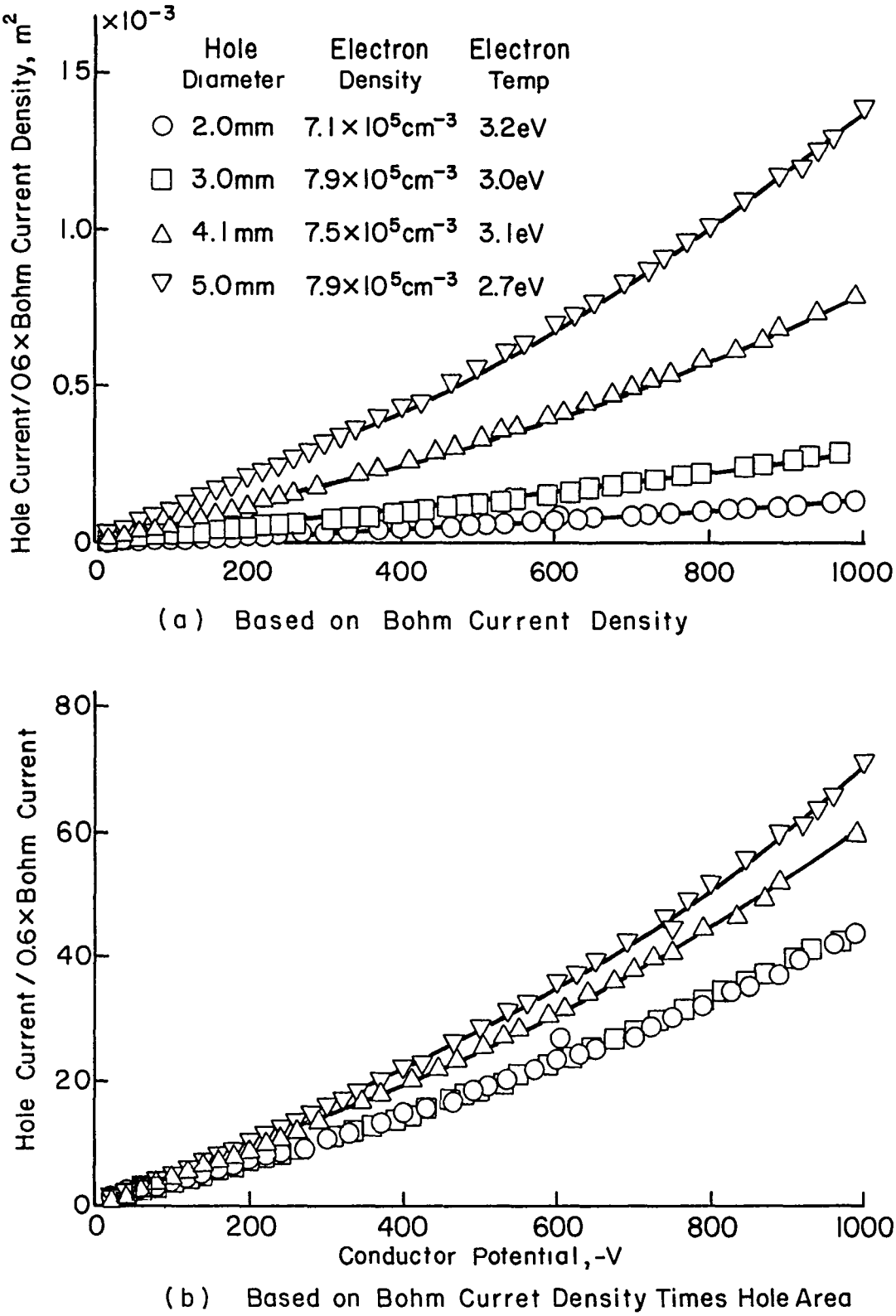

Fig. 3-18. Ion collection characteristics for four hole sizes using a polyimide sample.

Table 3-1.* Conditions for current decrease in vaporization-enhanced collection mode for a 1.0 mm diameter hole in polyimide at 27°C.

Power (watts)	Electron Density (cm^{-3})	Electron Temperature (eV)	Neutral Pressure (Torr)
0.36	4.3×10^5	7.8	2×10^{-5}
0.23	2.0×10^5	6.0	1.9×10^{-5}
0.13	1.5×10^5	8.1	2×10^{-5}
0.13	1.9×10^5	9.9	2×10^{-5}
0.10	1.7×10^5	10.9	2×10^{-5}
0.09	2.3×10^5	12.8	2×10^{-5}

*All data taken in large vacuum facility.

Comparison with Electrostatic Probe Theory. In comparing the experimental results with electrostatic probe theory, the planar probe theory of Parker and Whipple is appropriate. The expression for the ion collection from a monoenergetic distribution is (see Appendix B)

$$I = 0.6\ I_{Bohm}\ [1 + \frac{V}{E_o} - \frac{b^2}{4}\ \frac{V^2}{E_o(E_o+V)}] \qquad (3\text{-}8)$$

where V is the conductor potential, I_{Bohm} is the Bohm current and E_o is given by

$$E_o = kT_e/2\ . \qquad (3\text{-}9)$$

The results of tests with hole diameters of 2.0 and 5.0 mm are compared with the probe theory in Fig. 3-19. The value of the parameter b in Eq. (3-8) was found to be 1.93 ± 0.01 for the four curves shown in Figs. 3-17 and 3-18. The comparison with probe theory indicates that the experimental results are in good agreement with probe theory.

It should be noted that the value of b found, 1.93, is in rough agreement with the value of b, 1.80, found previously for electron collection in the small vacuum facility.[5]

Arcing. At large negative conductor potentials (between -1000 and -2000 volts) arcing was observed. A possible explanation for the arcing is vaporization. If, as in electron collection, vaporization of the insulator material can significantly increase the current collection, this vaporization could cause the arcing. The cause of the vaporization would probably have to be somewhat different from that of electron collection, inasmuch as the ion collection is so small before the arcing occurs. Vaporization could be quite localized and due to ion impacts. One indication that ion impacts could be the cause of vaporization is that the arcing appears to be gas-dependent. Kennerud,[2] who used nitrogen as the ion species, did not report any arcing. Domitz and Grier[9] also reported arcing and their ion species were oxygen, nitrogen and hydrogen. The data obtained during this investigation were not sufficient to permit further understanding of this arcing problem.

Error Analysis

In calculating the errors associated with the normalized hole current, two major sources should be considered, the accuracy of the current meters and the errors in analyzing the Langmuir probe characteristics.

The errors associated with the conductor potential are due only to the accuracy of the potential measurements.

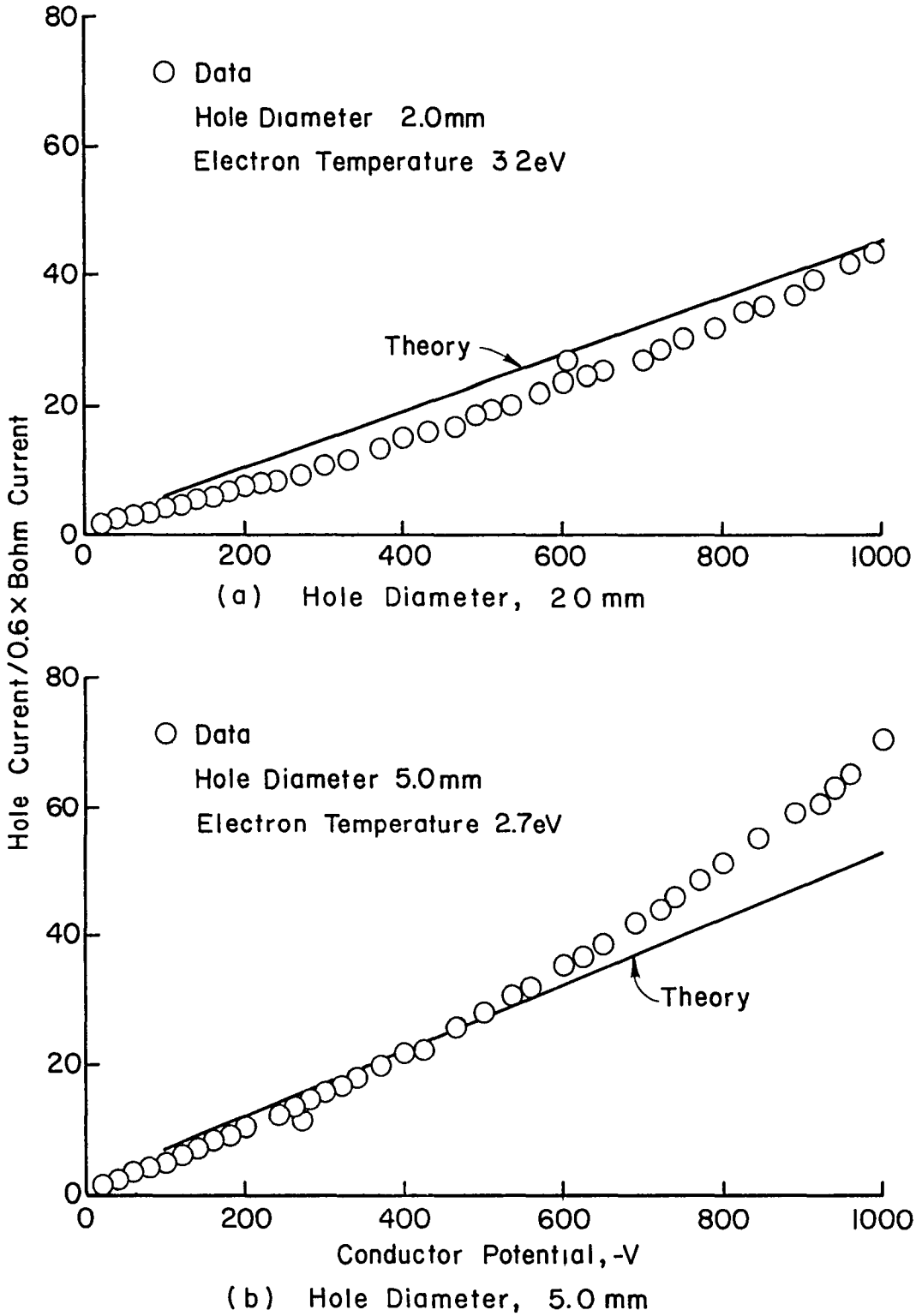

Fig. 3-19. Comparison of experimental results with planar probe theory for ion collection by a polyimide sample.

Positive Bias. In terms of the probe characteristics, the normalized hole current for positive bias is

$$IkT_e/j_o = 4Ia^2e/(dI/dV)_p \ , \tag{3-10}$$

where I is the hole current, a is the probe radius, e is the electronic charge, kT_e is the electron temperature (in eV), j_o is the random current density and $(dI/dV)_p$ is the slope of the Langmuir probe characteristic in the attracting region (see Appendix A). The error is obtained from

$$IkT_e/j_o \pm \Delta(IkT_e/j_o) = \frac{4a^2e(I\pm\Delta I)}{[(dI/dV)_p \pm \Delta(dI/dV)_p]}$$

$$\approx 4a^2e \left[I/(dI/dV)_p \pm \left(\frac{I\Delta(dI/dV)_p}{(dI/dV)_p^2} + \frac{\Delta I}{(dI/dV)_p} \right) \right] , \tag{3-11}$$

to a first-order approximation. Equation (3-11) indicates that

$$\Delta(IkT_e/j_o) \approx 4a^2e \left[\frac{I\Delta(dI/dV)_p}{(dI/dV)_p^2} + \frac{\Delta I}{(dI/dV)_p} \right] . \tag{3-12}$$

The current uncertainty, ΔI, is the meter uncertainty, and therefore depends on the meter used during a particular test. The probe characteristic slope uncertainty, $\Delta(dI/dV)_p$, is given by the standard deviation

$$\Delta(dI/dV)_p = 1/N^{1/2} \left[\sum_{i=1}^{N} [(dI/dV)_i - (dI/dV)_p]^2 \right]^{1/2} , \tag{3-13}$$

where (N+1) is the number of points in the attracting region and $(dI/dV)_i$ is the slope taken between consecutive points.

Figures 3-20 and 3-21 illustrate the uncertainty in the normalized hole current for the surface enhanced collection mode and the vapor enhanced collection mode, respectively. It should be noted that the conductor potential uncertainty is within the symbol size for the vapor enhanced collection mode.

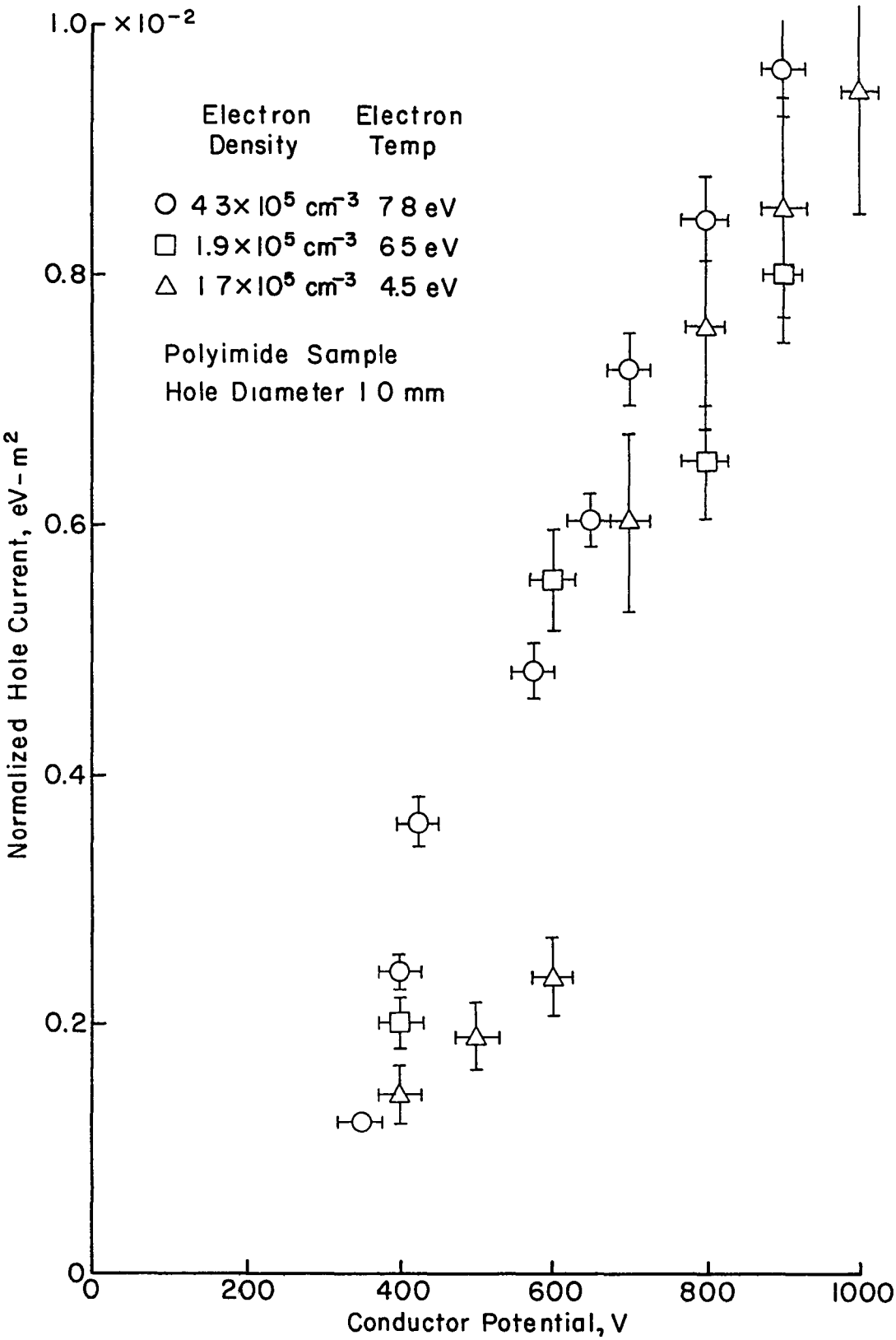

Fig. 3-20. Uncertainty in normalized hole current and conductor potential for the surface enhanced collection mode.

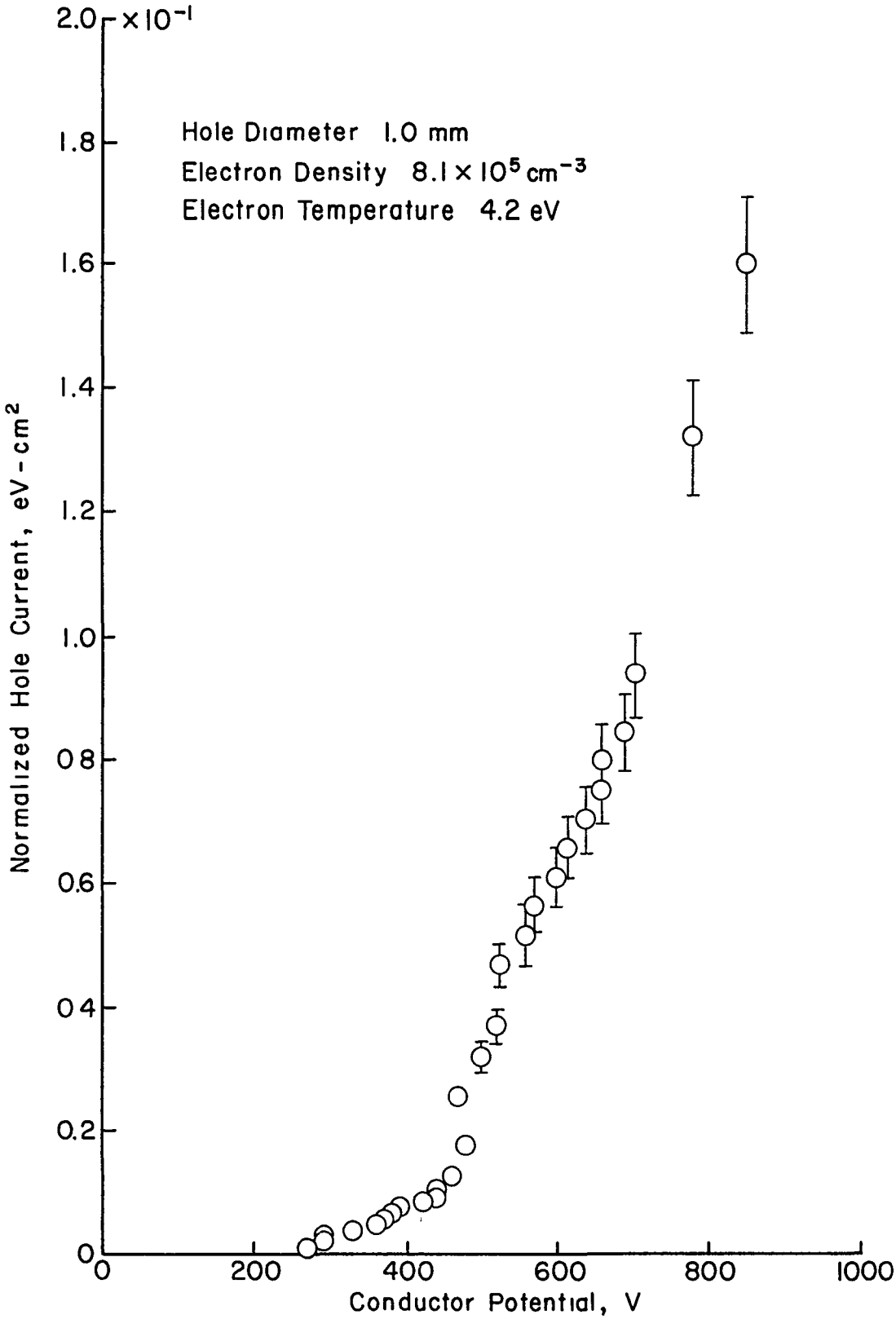

Fig. 3-21. Uncertainty in the normalized hole current for the vapor enhanced collection mode.

Negative Bias. The normalization used for negative bias is

$$I/.6I_{Bohm} = \frac{I}{.6\ A_h[m_e/8\pi m_i]^{1/2}\ 1/a^2\ kT_e(dI/dV)_p}, \tag{3-14}$$

where A_h is the area of the exposed conductor, m_e and m_i are the electronic and ionic masses, respectively. The uncertainty is found from

$$\frac{I}{.6I_{Bohm}} \pm \Delta\left(\frac{I}{.6I_{Bohm}}\right) = \left[\frac{8\pi m_i}{m_e}\right]^{1/2} \frac{a^2}{.6A_h} \times$$

$$\frac{(I\pm\Delta I)}{(kT_e\pm\Delta(kT_e))[(dI/dV)_p\pm\Delta(dI/dV)_p]}$$

$$\approx \left[\frac{8\pi m_i}{m_e}\right]^{1/2} \frac{a^2}{.6A_h}\left[\frac{I}{kT_e(dI/dV)_p}\right.$$

$$\left. \pm \left(\frac{I\Delta(dI/dV)_p/(dI/dV)_p + I(\Delta(kT_e/kT_e) + \Delta I}{kT_e(dI/dV)_p}\right)\right], \tag{3-15}$$

or

$$\Delta\left(\frac{I}{.6I_{Bohm}}\right) \approx \left(\frac{8\pi m_i}{m_e}\right)^{1/2} \frac{a^2}{.6A_h} \frac{1}{(kT_e)(dI/dV)_p} \times$$

$$\left[\frac{I\Delta(dI/dV)_p}{(dI/dV)_p} + \frac{I\Delta(kT_e)}{kT_e} + \Delta I\right], \tag{3-16}$$

to a first-order approximation.

The uncertainty in the electron temperature, $\Delta(kT_e)$ is given by the standard deviation,

$$\Delta(kT_e) = \frac{1}{N^{1/2}}\left[\sum_{i=1}^{N}[(kT_e)_i - kT_e]^2\right]^{1/2}, \tag{3-17}$$

where kT_e is the electron temperature used and $(kT_e)_i$ is the temperature calculated between consecutive points in the slope, that is

$$(kT_e)_i = \frac{1}{(d\ell nI/dV)_i} \quad , \tag{3-18}$$

in the transition region (see Appendix A).

Figure 3-22 illustrates the uncertainty in the normalized hole current for negative bias. The uncertainty in the conductor potential is within the symbol size.

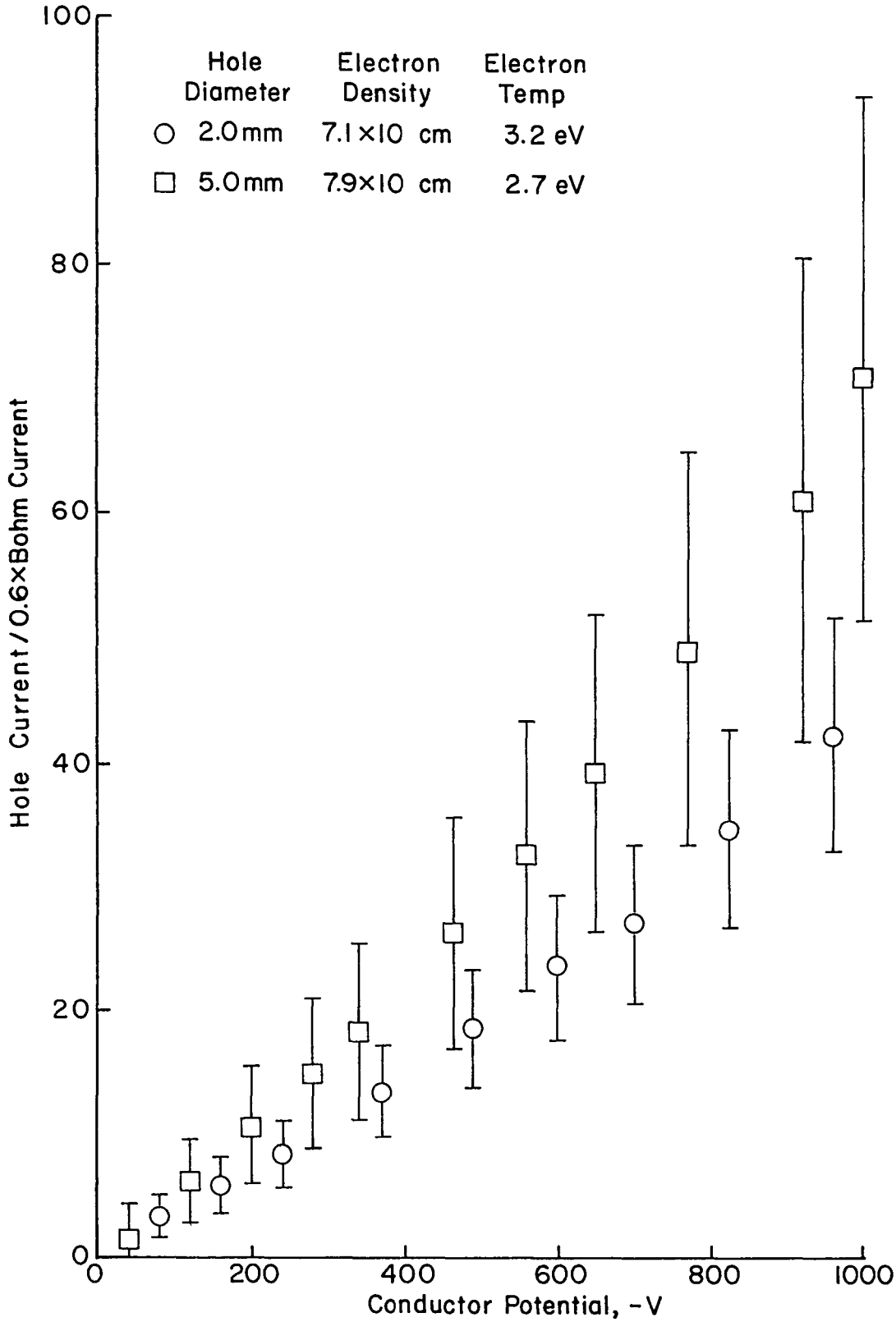

Fig. 3-22. Uncertainty in the normalized hole current for negative bias.

IV. THEORY

The electron-collection model presented herein follows a suggestion by Cole, Ogawa and Sellen,[1] and is intended only to represent the surface-enhanced collection mode. An incoming electron strikes the insulator surface near the hole, causing a secondary electron to be emitted with a certain probability. The secondary electron is then attracted toward the exposed conductor by a potential gradient. In this manner, an incoming electron striking the insulator close to the hole causes an electron to be collected by the exposed conductor.

Plasma Sheath

In order to model the electron collection process, it is helpful to know the shape of the plasma sheath. From sheath measurements made by Gabriel, Garner and Kitamura[2] near an exposed conductor surrounded by an insulator, the sheath appears approximately hemispherical. Figure 4-1 indicates the shape of the plasma sheath around a hole (from Gabriel, Garner and Kitamura[2]). The sheath is represented by equipotential lines, indicated by the numbers on the graph. Although the low current levels observed by Gabriel, Garner and Kitamura might appear to exclude an insulator contribution to the current collection, the general shape of the sheath is still of interest.

To determine if the electron flow was space charge limited, currents were calculated for space charge flow between two concentric spheres. The hole radius was used as the radius of the inner sphere and an experimentally determined sheath radius was used for the outer sphere radius. This sheath radius was found by determining the sheath size needed to collect the observed current with a 1.0 mm diameter hole. The current collection for space charge limited flow is given by[3]

$$I = 16\pi\varepsilon_o \frac{\sqrt{2}}{9} \sqrt{e/m_e}\ V^{3/2}/\alpha^2 , \qquad (4\text{-}1)$$

where ε_o is the permittivity of free space, e is the electronic charge, m_e is the electronic mass, and V is the potential difference between the spheres. α is a term that is dependent on the ratio of the radii of the two spheres. These calculations showed that the currents expected from space charge limited flow were more than two orders of magnitude larger than the observed currents for the surface-enhanced collection mode.

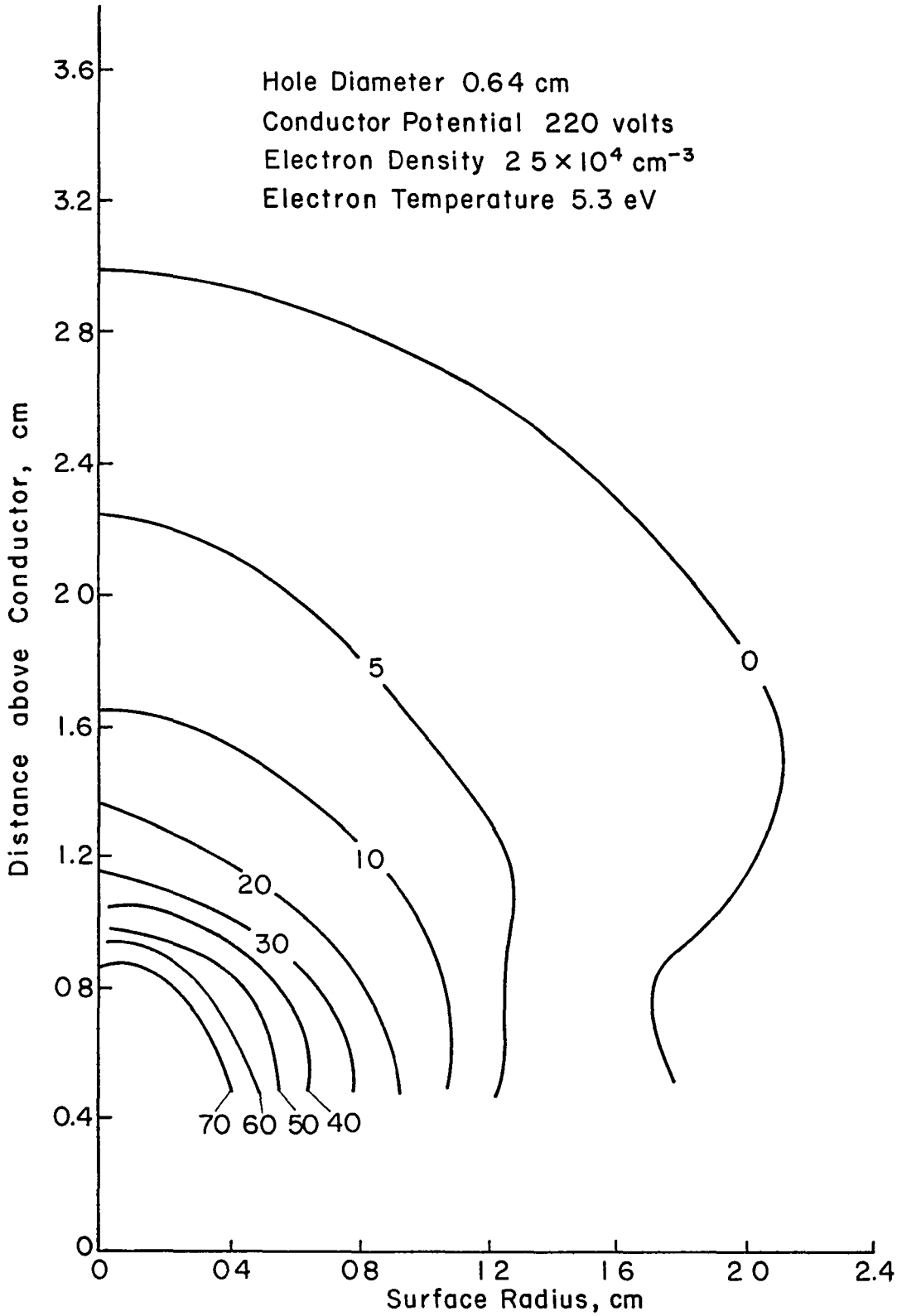

Fig. 4-1. Shape of the plasma sheath around a hole.[2]

The space charge limited flow calculations thus demonstrated that the current collection was orbit limited. That is, not all electrons that entered the plasma sheath were collected. The approach to modeling should therefore be to modify an orbit limited theory to include part of the insulator as a collector. The most likely theory to start with is the planar probe theory of Parker and Whipple (see Appendix B). The planar probe theory has the correct geometry as well as an approximately hemispherical sheath. The collected current is given by

$$I = j_o A[1 + \frac{b^2}{4} + (1 - \frac{b^2}{4}) \frac{eV}{kT_e}] , \qquad (4-2)$$

where j_o is the random current density, A is the area of the probe, V is the potential of the probe, k is Boltzmann's constant and T_e is the electron temperature. The constant b is adjustable ($0 \leq b \leq 2$), and is related to the incoming trajectories. A way to determine the meaning of b is by analogy to spherical probe analysis. The electron collection by a spherical probe in the attracting region (see Appendix A) depends on the electron density. That is, for high electron densities, the current collection is independent of probe potential. This occurs because the size of the plasma sheath is essentially independent of probe potential. This condition would be reflected in Eq. (4-2) for $b \to 2$. For the low density plasmas treated herein, the electron collection is proportional to probe potential. That is, the plasma sheath size increases with probe potential. This condition would be reflected in Eq. (4-2) for $b \to 0$. From this analogy it is clear that the parameter b reflects how the plasma sheath depends on the probe potential. For the electron densities treated herein, it is assumed that b is zero in Eq. (4-2). It should be noted that for $b = 0$, Eq. (4-2) has the same form as the equation for spherical probe theory (see Appendix A).

Collection Area

Two approaches to determining the collection area were tried. The first approach used the assumption that the entire surface area under the plasma sheath contributed to electron collection. Trajectories for the secondary electrons moving across the insulator surface were calculated. For a radial electric field, as might be expected, all the secondary electrons produced struck the exposed conductor. For polyimide and conductor potentials between 50 and 1000 V, the insulator charged to potentials greater than the conductor potential, inasmuch as the secondary yield was greater than one in this range. For an insulator surface with a potential greater than the conductor potential, a potential gradient would be formed that would repel electrons from the hole, except for those secondaries produced at the hole edge. This approach did not appear promising.

In the second approach, only a small annular ring of insulator near the hole contributed to the electron collection. For simplicity, it was assumed that this annular ring was at a constant potential. In this approach, the condition for continuity of charge is given by

$$(A_a + A_h)/A_h = \delta \ , \tag{4-3}$$

where A_a is the area of the annular ring, A_h is the area of the exposed conductor, and δ is the secondary electron emission yield. The implicit assumption in Eq. (4-3) is that the fraction of the secondary yield that is collected by the conductor is proportional to the fraction of hole area to the total collection area, $(A_a + A_h)$.

To demonstrate that Eq. (4-3) is a condition for continuity of charge, consider a secondary electron yield of four. From Eq. (4-3), the annular ring area is three times that of the hole area, consequently, an incoming electron striking within the collection radius, r_c, causes four secondary electrons to be emitted. Of the four electrons, three again strike within the annular ring and one is collected by the conductor. In this manner, one electron is collected by the conductor for each electron striking the insulator, and the charge on the annular ring is maintained constant during steady state conditions.

Using Eq. (4-3) as a basis for a model, the planar probe theory can easily be modified. The probe potential in Eq. (4-2) should be an effective potential over the collection region. The value used was the average potential over the collection area, that is

$$V_{eff} = \frac{V_c A_h + V_a A_a}{A_h + A_a} \tag{4-4}$$

where V_c is the conductor potential and V_a is the potential of the annular ring.

This model was compared to experimental data to determine if it had any physically realizable solutions. The data used in this comparison was for a 1.0 mm diameter hole with an electron density of 1.6×10^5 cm^{-3} and electron temperature of 4.5 eV. These data are shown in Fig. 3-2. The calculation procedure used for a given collector voltage, V_c, was as follows:

(i) Pick a value of r_c (collection radius of insulator).

(ii) Calculate V_{eff} from probe theory to match the experimentally observed current.

(iii) Calculate V_a needed for the assumed values V_{eff} and r_c.

(iv) Calculate δ from the value of V_a and Eq. (4-3).

(v) Repeat above steps for different values of r_c and plot the physical values of V_a (i.e., $V_a \leq V_c$) against the corresponding values of δ from step (iv). These results are compared with values from the values of δ from expression

$$\delta(E,\theta) = e^{\beta E^{1/2}(1-\cos\theta)} \; \delta_m \frac{E}{E_m} e^2 e^{-\beta E^{1/2}} \tag{4-5}$$

where β is a material dependent absorption term, E is the primary electron energy (annular area potential, V_a, expressed in eV), θ is the incident electron angle, E_m and δ_m are material constants (from Appendix C). The results of this procedure are shown in Fig. 4-2, where the possible physical solutions for this model are shown to vary over a large range of mean incidence angle. The results of the calculcation procedure (steps (i) through (v)) are indicated by the lines with different assumed values of V_a, while the permissible values of secondary electron emission (from Eq. (4-5)) are indicated by the incidence angles (<90°).

Model

The first task in formulating the model is to determine an effective angle for the incoming electrons striking the insulator. Since the flow is orbit-limited, the path of the electron is not radial. With this in mind, a reasonable approximation for the angle is the value that gives the same secondary electron emission as the average of the angular dependence term of the secondary yield over the surface of a hemispherical sheath. This is given by

$$\langle e^{\beta E^{1/2}(1-\cos\theta)} \rangle = \int_0^{2\pi} d\psi \int_0^{\pi/2} e^{\beta E^{1/2}(1-\cos\theta)} \sin\theta d\theta \Big/ \int_0^{2\pi} d\psi \int_0^{\pi/2} \sin\theta d\theta$$

$$= 1/\beta E^{1/2} \; \{e^{\beta E^{1/2}} - 1\} \tag{4-6}$$

Over a range of 1400 eV, the angle corresponding to an averaged angular dependence of δ varied from 65° to 72°, increasing with increasing energy. The calculations presented in Fig. 4-2 indicate that solutions with angles in this range require annular ring potentials close to the conductor potential. The potential of the annular ring can then be taken to be the same as the conductor potential, that is, $V_a \approx V_c$.

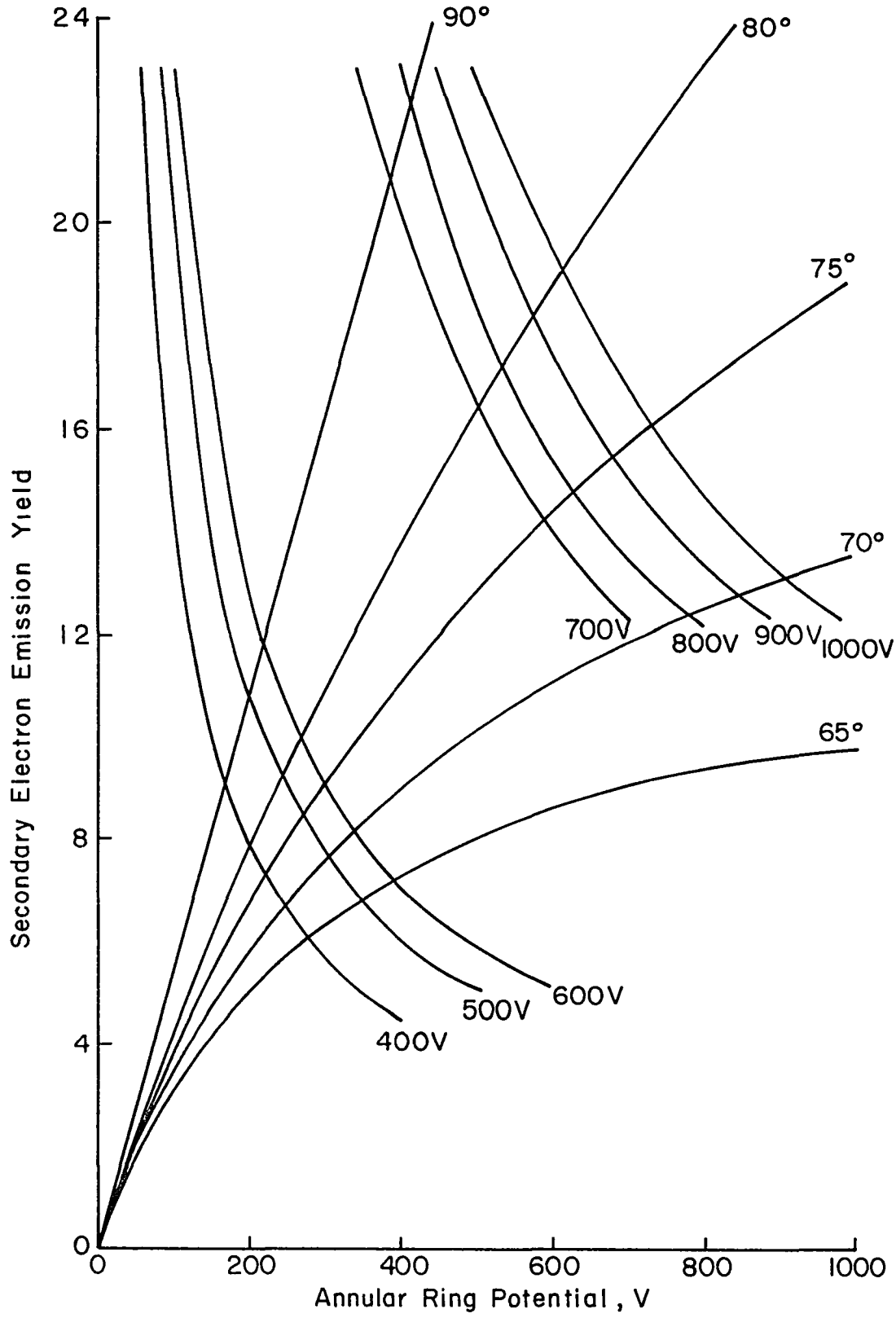

Fig. 4-2. Range of possible solutions for an experimental data set.

Having determined the potential and incident angle requirements on the annular insulator ring, the model can be used to predict electron collection for the surface enhanced collection mode. The procedure for predicting current collection is as follows:

(i) Calculate the effective incident angle for the secondary electron emission yield at a given conductor potential (Eq. (4-6)).

(ii) Calculate the secondary yield from the conductor potential using this angle and

$$\delta(E) = \langle e^{\beta E^{1/2}(1-\cos\theta)} \rangle \frac{\delta_m E}{E_m} e^2 e^{-\beta E^{1/2}} \quad . \tag{4-7}$$

(iii) Calculate the annular ring area from Eq. (4-3).

(iv) Calculate the collection radius for the desired hole diameter from

$$\pi r_c^2 = (A_h + A_a) \quad . \tag{4-8}$$

(v) Calculate the electron current for the given plasma conditions using

$$I \simeq j_o \pi r_c^2 \, eV/kT_e \tag{4-9}$$

from planar probe theory (Appendix B).

For the model as presented, the collection radius is a critical parameter in determining the collected current. The collection radius is shown in Fig. 4-3 as a function of conductor potential for three hole diameters, 1.0, 3.0 and 5.0 mm, for polyimide insulator. The calculations shown in Fig. 4-3 indicate that, after an initial sharp increase, the collection radius increases slowly with increasing conductor potential. This behavior leads to current-voltage characteristics that are roughly linear for high conductor potentials.

Comparison with Experimental Data

To determine how well the model predicts the current-voltage characteristics, the model can be compared to experimental data. The comparisons are shown in plots of normalized hole current, $I\ kT_e/j_o$,

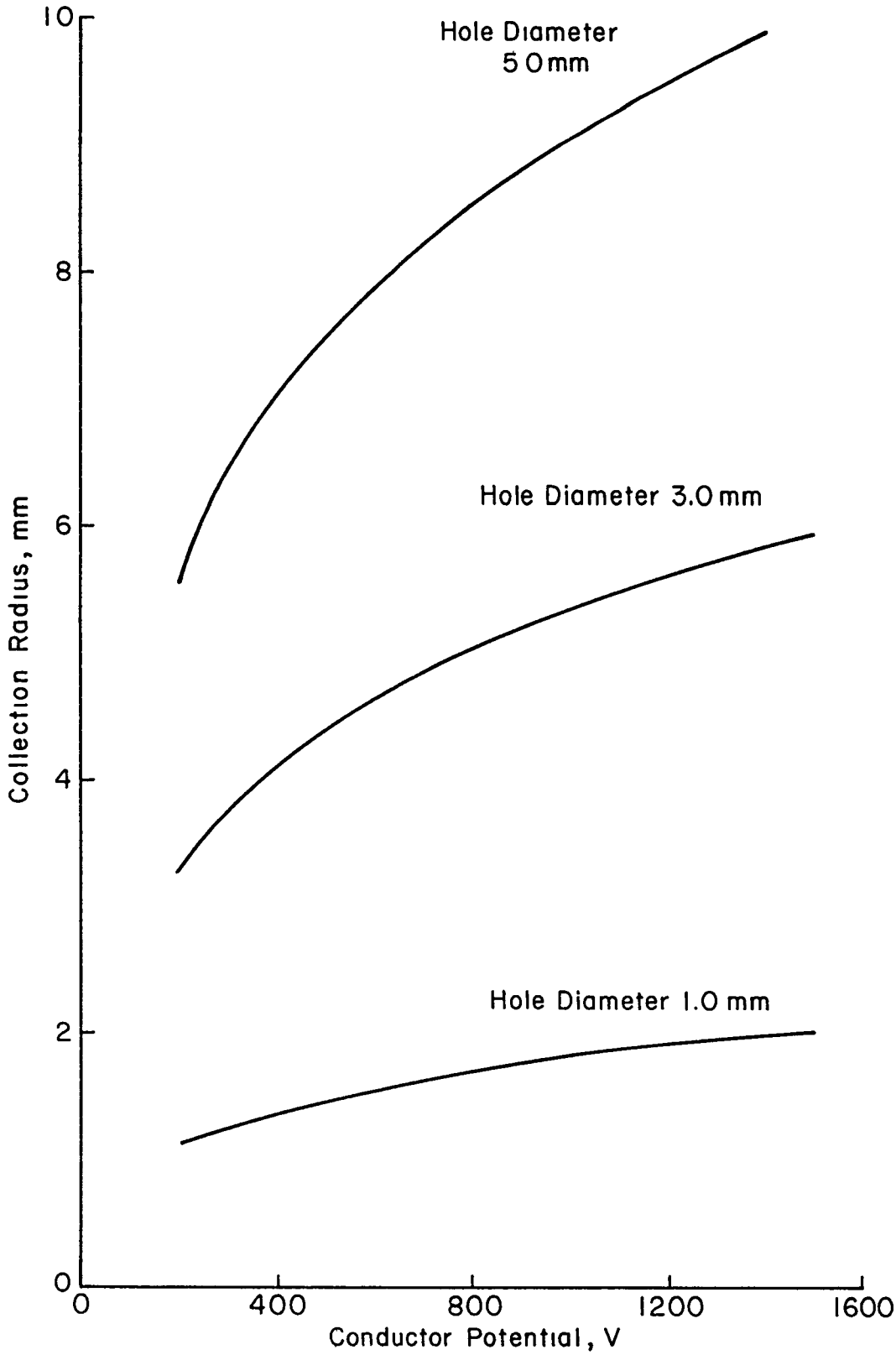

Fig. 4-3. Collection radius as a function of conductor potential and hole diameter

versus conductor potential. The use of Eq. (4-9) has been justified from theoretical considerations. The form of this equation confirms the normalization used in Section III. In order to be more precise in the comparisons, the conductor potential is referenced with respect to plasma potential. It should be noted that this differs slightly from the conductor potential in Section III, which was referenced with respect to facility ground. The difference between the two reference potentials is typically 20 volts.

The calculated current collection is compared to the experimental data in Fig. 4-4 for a 1.0 mm diameter hole at three different plasma conditions. The predicted and experimental values are in excellent agreement.

Hole Size. The model is compared to experimental data for three different hole diameters, 1.0, 3.0 and 5.0 mm, in Fig. 4-5. The model predicts the effect of hole size quite well, with experiment and theory agreeing within a factor of two.

The model indicates that the correct normalization factor should be IkT_e/A_hJ_o. That is,

$$\frac{IkT_e}{J_oA_h} = \delta V_p \quad . \tag{4-10}$$

The current-voltage curves for the different hole sizes should collapse onto one line, using this normalization. The fact that they do not is an indication of the limits of the theory.

Sample Temperature. It was found that, for a 1.0 mm diameter hole in polyimide, increasing sample temperature resulted in a decrease in current collection. A comparison of the theory with experiment (see Fig. 4-6) shows that the model also predicts a decrease in current with increasing sample temperature (see Appendix C), but not of the magnitude the data indicates. This will be discussed later in this paper.

In testing a 5.0 mm diameter hole in polyimide, no sample temperature effect was observed (see Fig. 3-14). However, the model still predicts a temperature effect. In fact, the temperature effect is proportionally the same as for the 1.0 mm diameter hole. That is, for a similar temperature increase, the predicted current drops by the same ratio. This disagreement with observed behavior cannot be explained at this time.

While testing iso-mica, it was found that there was no sample temperature effect. The literature reports that the secondary yield for mica is temperature independent. From Eq. (4-3), it can be readily seen that the theory predicts no temperature effect if the secondary yield is independent of temperature. The absence of a temperature effect is thus correctly predicted for mica.

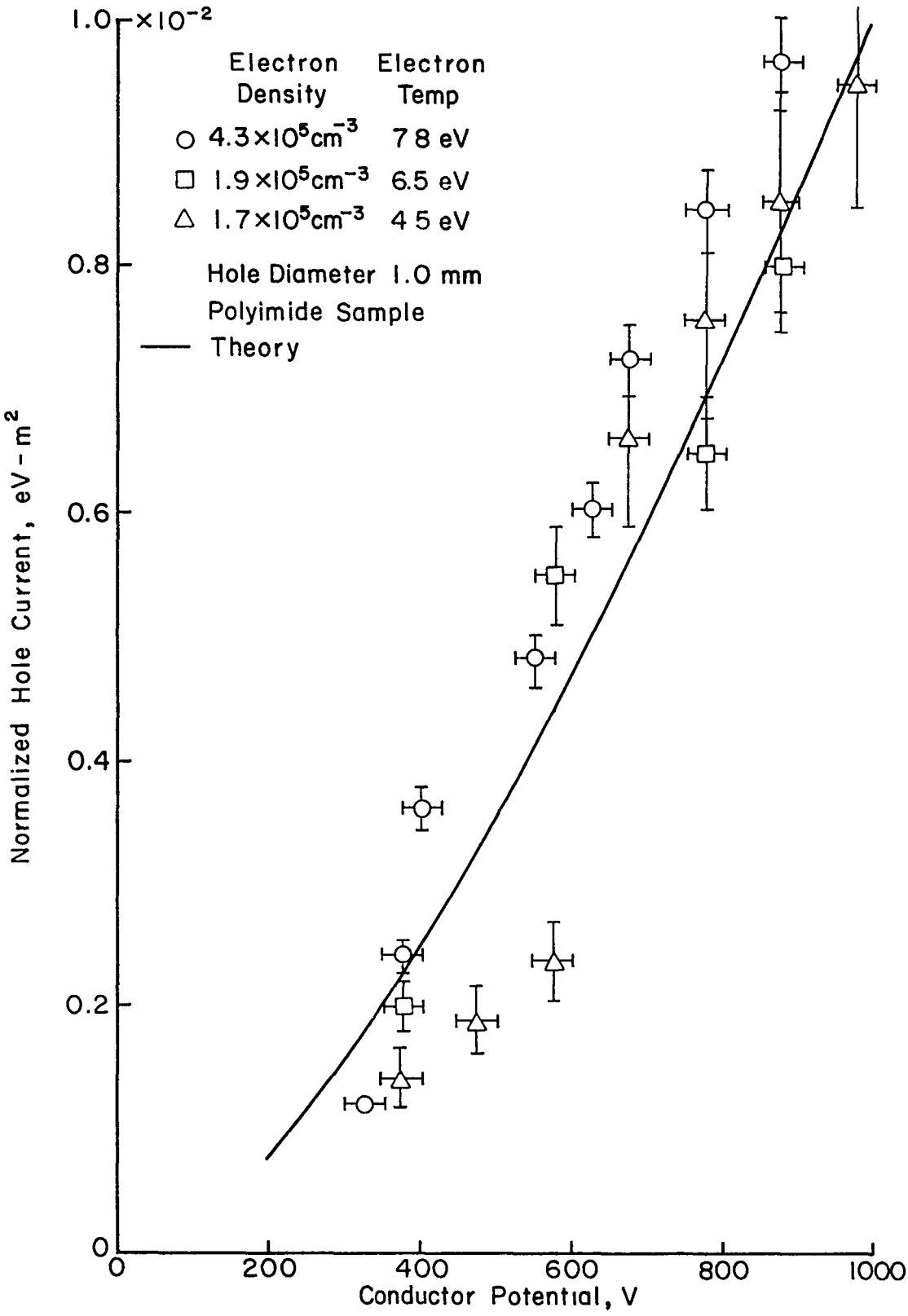

Fig. 4-4. Comparison of theory and experiment for different plasma conditions.

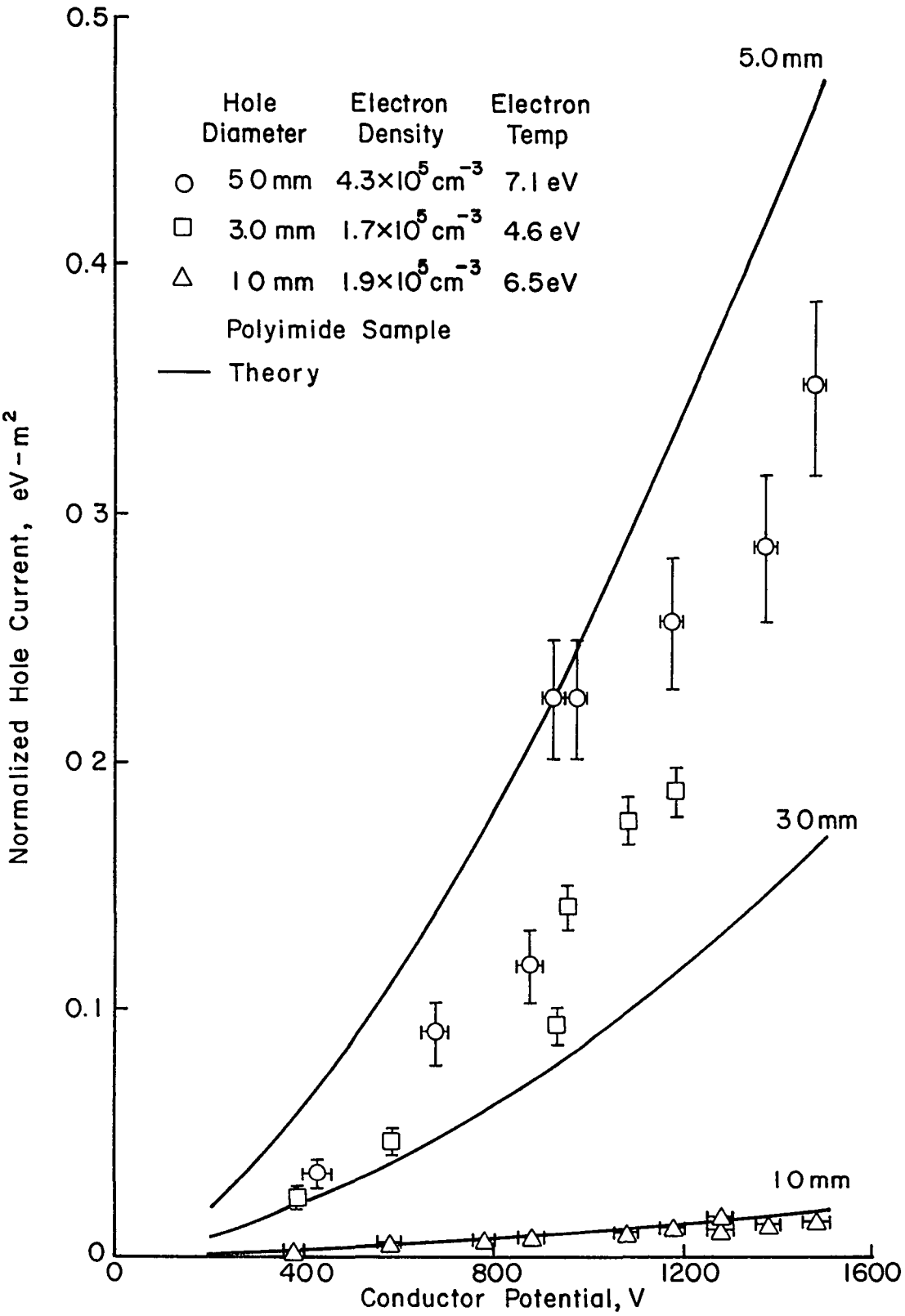

Fig. 4-5. Comparison of theory and experiment for different hole diameters.

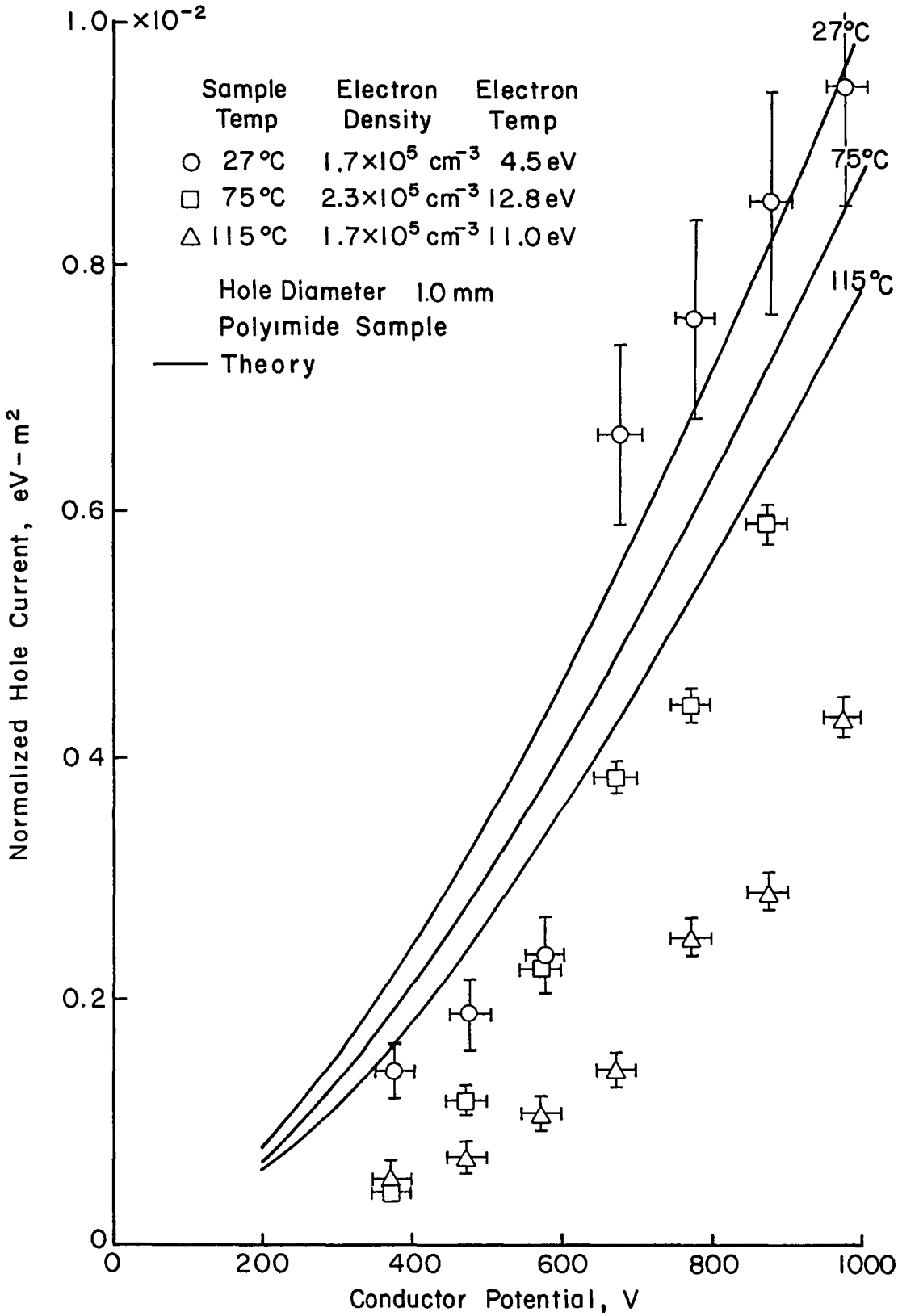

Fig. 4-6. Comparison of theory and experiment for different sample temperatures.

In demonstrating that increasing sample temperature decreases current collection for polyimide, it has been shown that any parameter that decreases the secondary yield decreases electron collection. This was illustrated in the observed effect of sample roughness. Roughening a surface decreases the secondary yield and, as such, the model predicts that the current collection should decrease. This is in agreement with observed experimental data (see Section III).

Insulator Material. Two sample materials, whose secondary yields are known, were tested, polyimide and teflon. On first inspection, their secondary electron emission yields appear sufficiently different to cause different electron collection (the primary reason for choosing the two materials). After testing, when the averaged angular dependence, Eq. (4-6), was selected for the secondary yield, the coefficients were found to be very similar. This similarity in the average secondary yields explains why two apparently dissimilar materials produced very similar electron collection (see Fig. 4-7).

Discussion of the Model

The fundamental parameter upon which the model depends is the secondary electron emission yield, and, as such, it is appropriate to discuss the state of the theory for the secondary emission process. There are at present several theories for secondary electron emission. All of these theories are unsatisfactory in one respect or another. The theory of Lye and Dekker (see Appendix C) appears to be the most prominent in the literature. It correctly predicts a temperature effect for some insulators but not for metals, which is correct in both cases. However, Lye and Dekker's theory also predicts an angular dependence which deviates sharply from experimental observation. The form of Dekker's universal curve for secondary emission is general enough that it can be fitted to almost any data.

Another theory has been proposed by Sternglass. Although it is not nearly as prominent in the literature as Lye and Dekker's theory, it has been used successfully by several people in modeling secondary emission in polymers. Sternglass' theory correctly predicts the angular dependence of the secondary yield, but also predicts a temperature dependence for metals, which has not been observed.

These comments clearly indicate that, as yet, there is no comprehensive theory for secondary electron emission. It is therefore necessary to rely to a large extent on experimental data. Unfortunately, the data on polymers is quite limited. It is only recently that such studies were started in the U.S. (early 1970's), and from the late 1950's in the U.S.S.R. Furthermore, only one study (to the author's knowledge) has been carried out on the temperature and angular dependence for polymers (see Appendix C) in the energy regime of interest here, and that study did not include polyimide.

From these observations, the reader should be aware that the accuracy of the model is strongly dependent on the accuracy of the

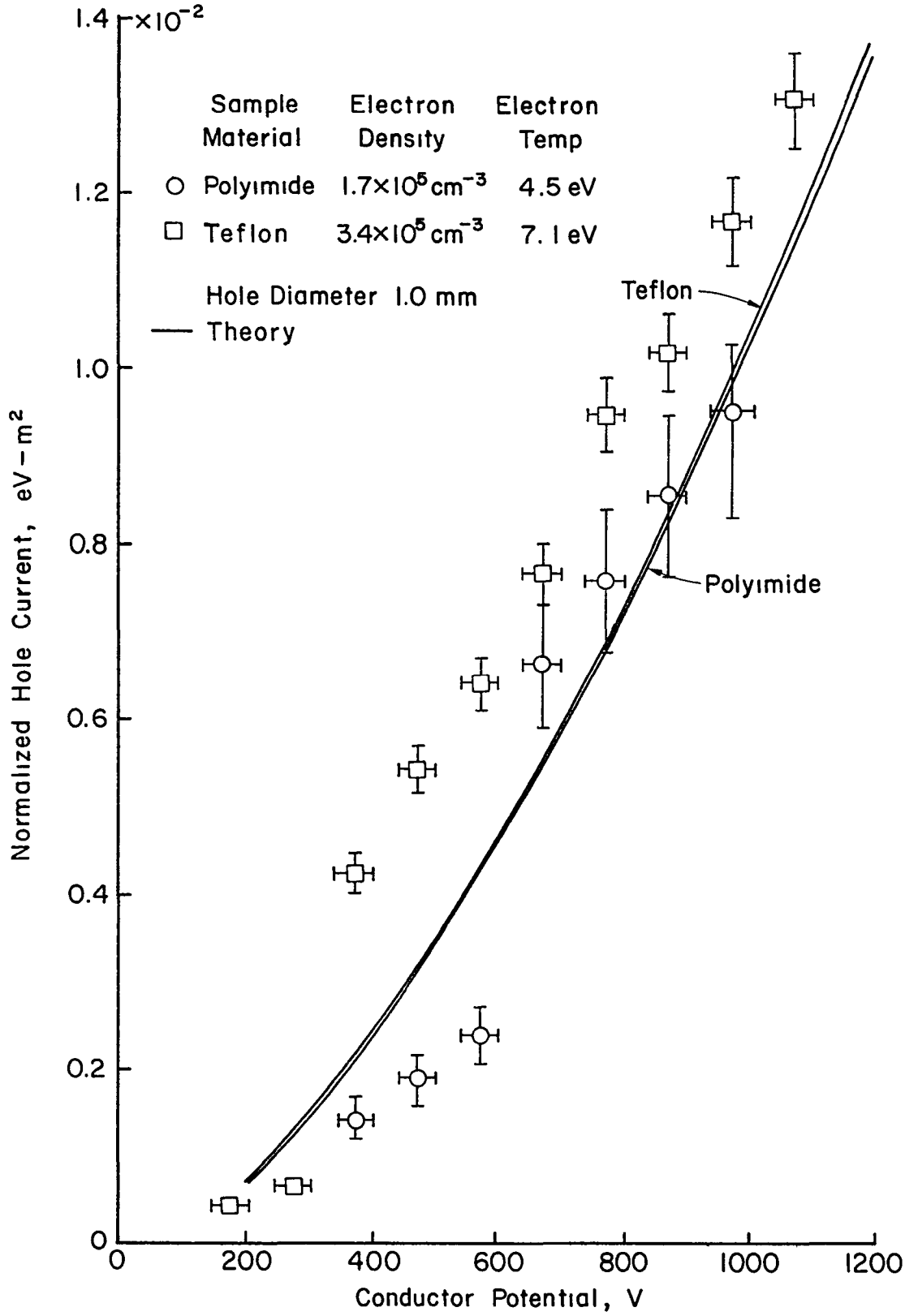

Fig. 4-7. Comparison of theory and experiment for different insulator materials.

secondary electron emission yield. This is particularly true with regard to the temperature dependence of the model. One secondary emission theory that is used herein predicts a temperature dependence that increases with energy and angle, although the experimental evidence generally does not support this. On the other hand, the temperature dependence used in the model comes from a different theory (see Appendix C for details) and is generally supported by experiment. The contradiction can be illustrated with the one experimental study done on the temperature effect for a polymer (polystrene). In this study (see Appendix C), it was found that the temperature dependence differed from Dekker's theory and was somewhat dependent on angle. This result indicates that the temperature dependence of the secondary yield for polymers must be considered questionable, and more studies need to be done before the temperature dependence can be defined.

The assumption was made that the electrons arrived at the surface with an equal probability from all solid angles within the permissible hemisphere. This assumption appears reasonable, but since the electron flow is orbit limited, an argument can be made that the electrons should strike more frequently at grazing angles. If the mean effective angle was increased by 10%, the predicted current would be higher. It would, for example, still be within a factor of two of the presently predicted currents over the conductor potential range from 200 to 1500 volts, for a 1.0 mm diameter hole. As indicated by this example, the assumption of angular distribution for electrons is believed to result in at least qualitatively correct predictions.

It was also assumed that the exposed conductor collects secondary electrons proportional to its fraction of the total collection area. If, because of electric fields, the exposed conductor collected twice the number of secondary electrons indicated by exposed area, the collection radius would be reduced. The predicted currents would then be 6 to 20% lower than presently predicted values for a 1.0 mm diameter hole in polyimide and a conductor potential of 200 to 1500 volts. The possible adverse effects of this area-proportional collection assumption are therefore believed to be small.

A few summary comments should be made about the model. Many authors who have studied the phenomenon of electron collection through a defect in insulation over a high voltage solar array have proposed that secondary electron emission somehow plays an important role in the collection mechanism, but none have evaluated details of this role. In the model presented herein, a self-consistent description of the role of secondary electron emission is given. Using this model, simple calculations yield realistic predictions that include all the major features found in experimental investigations. Nevertheless, the theory presented is only a first approximation to a description of the collection mechanism. The next step in improving the model would be a calculation of the primary electron (i.e., electrons originating from the plasma) trajectories. A calculation of this type would allow the electron collection due to primary electrons and due to secondary electrons to be distinguished from each other. Furthermore, knowing the primary electron trajectories would allow for a better treatment of the angular dependence for the secondary electron emission yield.

Another improvement to the model would be calculations of the secondary electron trajectories. Knowledge of these trajectories would yield the range of movement of the secondary electrons. This would indicate if the entire hole area should be included in the calculation of the collection area. This information would be more important as the size of the hole increases.

These suggestions are meant to point out possible ways to imrpove the model herein, although both the suggestions involve considerable work. It is hoped that they may prove useful.

V. CONCLUSION

This investigation has identified two electron collection modes. One mode involves only the surface of the surrounding insulator, thereby enhancing the current collection. The second mode involves the same surface enhancement plus an additional enhancement due to the vaporization and ionization of the surrounding insulator. The occurrence of the second mode depends on the enhanced current collection of the first mode.

The surface enhancement has been found to be a function of the secondary electron emission yield of the surrounding insulator. As such, parameters which decrease the secondary yield also decrease electron collection.

The vapor-enhanced collection mode exhibits all the same properties as the surface enhanced mode except the dependence on hole size. It was found that the electron collection in this mode appears to be essentially independent of this hole size for the size range tested of up to 2.0 mm.

A model has been developed for the process of the surface enhancement. The model depends strongly on knowledge of the secondary electron yield, and as such, is extremely sensitive to uncertainties in this knowledge. The model has been shown to correctly predict all qualitative trends. Further, the predicted current collection is generally within a factor of two experimental values for the same conditions. This theory is easily followed in its formulation and can be used in a straightforward and convenient manner.

REFERENCES

Section I

1. R. S. White, Space Physics, New York, Gordon and Breach, Science Publishers, Inc., 1970.

2. R. L. F. Boyd, Space Physics - The Study of Plasmas in Space, Oxford, England, Clarendon Press, 1974.

3. W. Knauer, J. R. Bayless, G. T. Todd and J. W. Ward, "High Voltage Solar Array Study," NASA Contr. Rep. CR-72675, May 1970.

4. W. F. Springgate, "High Voltage Solar Array Study," NASA Contr. Rep. CR-72674, 1970.

5. K. L. Kennerud, "High Voltage Solar Array Experiments," NASA Contr. Rep. CR-121280, March 1974.

6. R. K. Cole, H. S. Ogawa and J. M. Sellen, Jr., "Operation of Solar Cell Arrays in Dilute Streaming Plasmas," AIAA Paper No. 69-262, 1969.

7. N. T. Grier and D. J. McKinzie, Jr., "Current Drainage to a High Voltage Probe in a Dilute Plasma," NASA Tech. Memo. TMX-67890, January 1972.

8. N. T. Grier and D. J. McKinzie, "Measured Current Drainage through Holes in Various Dielectrics up to 2 Kilovolts in a Dilute Plasma," NASA Tech. Note TND-6663, February 1972.

9. S. Domitz and N. T. Grier, "The Interaction of Spacecraft High Voltage Power Systems with the Space Plasma Environment," NASA Tech. Memo. TMX-71554, June 1974.

10. N. T. Grier and S. Domitz, "Current from a Dilute Plasma Measured through Holes in Insulators," NASA Tech. Note TND-8111, December 1975.

11. N. T. Grier, "Experimental Results on Plasma Interactions with Large Surfaces at High Voltages," NASA Tech. Memo. TM-81423, January 1980.

12. N. J. Stevens, F. D. Berkopec and C. K. Purvis, "Investigation of High Voltage Spacecraft Systems Interactions with Plasma Environments," NASA Tech. Memo. TM-78831, April 1978.

13. N. J. Stevens, "Interactions Between Spacecraft and the Charged-Particle Environment," NASA Conference Publication 2071, AFGL-TR-79-0082, pp. 268-284, 1978.

14. B. G. Herron, J. R. Bayless and D. J. Worden, "High-Voltage Solar Array Technology," J. Space. and Rockets 10, pp. 457-462, 1973.

15. N. T. Grier and N. J. Stevens, "Plasma Interaction Experiment (PIX) Flight Results," NASA Conference Publication 2071, AFGL-TR-79-0082, pp. 295-314, 1978.

16. T. P. Armstrong, R. C. Chaky, J. Enock, J. H. Nonnast and G. G. Wiseman, "Self-Consistent Numerical Simulation of Plasma-Insulator Interaction," NASA Research Grant NSG-3290, University of Kansas, August 1980.

17. J. H. Nonnast, R. C. Chaky, T. P. Armstrong, J. Enoch and G. G. Wiseman, "Numerical Simulation of Plasma-Insulator Interactions in Space. Part I: The Self-Consistent Calculation," NASA Conference Publication 2182, AFGL-TR-81-0270, pp. 932-945, 1981.

18. R. C. Chaky, J. H. Nonnast, T. P. Armstrong, J. Enoch and G. G. Wiseman, "Numerical Simulation of Plasma-Insulator Interactions in Space. Part II: Dielectric Effects," NASA Conference Publication 2182, AFGL-TR-81-0270, pp. 946-956, 1981.

19. R. C. Chaky, J. H. Nonnast and J. Enoch, "Numerical Simulation of Sheath Structure and Current Voltage Characteristics of a Conductor-Dielectric Dish in a Plasma," J. Appl. Phys. 52, pp. 7092-7098, 1981.

20. S. B. Gabriel, C. E. Garner and S. Kitamura, "Experimental Measurements of the Plasma Sheath Around Pinhole Defects in a Simulated High Voltage Solar Array," AIAA Paper No. 83-8311, January 1983.

21. H. R. Kaufman and R. S. Robinson, "Interaction of High Voltage Surface with the Space Plasma," NASA Contr. Rep. CR-159731, May 1979.

22. H. R. Kaufman and R. S. Robinson, "Interaction of High Voltage Surface with the Space Plasma," NASA Contr. Rep. CR-165131, May 1980.

23. R. P. Stillwell, H. R. Kaufman and R. S. Robinson, "Experimental Simulation of Space Plasma Interactions with High Voltage Solar Array," AIAA Paper No. 81-0741, 1981.

24. H. R. Kaufman and R. S. Robinson, "Experimental Simulation of the Interaction of Biased Solar Arrays with the Space Plasma," NASA Contr. Rep. CR-165485, May 1981.

25. H. R. Kaufman and G. C. Isaacson, "The Interaction of Solar Arrays with Electric Thrusters," AIAA Paper No. 76-1051, 1976.

Section II

1. D. Siegfried and P. J. Wilbur, "A Model for Orificed Hollow Cathodes: Theory and Experiment," AIAA Paper No. 82-1889, 1982.

2. R. P. Stillwell, R. S. Robinson, H. R. Kaufman and R. K. Cupp, "Experimental Investigation of an Argon Hollow Cathode," AIAA Paper No. 82-1890, 1982.

Section III

1. H. R. Kaufman and R. S. Robinson, "Experimental Simulation of the Interaction of Biased Solar Arrays with the Space Plasma," NASA Contr. Rep. CR-165485, May 1981.

2. K. L. Kennerud, "High Voltage Solar Array Experiments," NASA Contr. Rep. CR-121280, March 1974.

3. S. B. Gabriel, C. E. Garner and S. Kitamura, "Experimental Measurements of the Plasma Sheath Around Pinhole Defects in a Simulated High Voltage Solar Array," AIAA Paper No. 83-0311, January 1983.

4. F. F. Chen, Introduction to Plasma Physics, Plenum Press, New York, 1977.

5. H. R. Kaufman and R. S. Robinson, "Interaction of High Voltage Surface with the Space Plasma," NASA Contr. Rep. CR-159731, May 1979.

6. H. R. Kaufman and R. S. Robinson, "Interaction of High Voltage Surfaces with the Space Plasma," NASA Contr. Rep. CR-165131, May 1980.

7. R. K. Cole, H. S. Ogawa and J. M. Sellen, Jr., "Operation of Solar Cell Arrays in Dilute Streaming Plasmas," AIAA Paper No. 69-262, 1969.

8. J. D. Swift and M. J. R. Schwar, Electrical Probes for Plasma Diagnostics, American Elsevier Publishing Company, Inc., New York, 1969.

9. S. Domitz and N. T. Grier, "The Interaction of Spacecraft High Voltage Power Systems with the Space Plasma Environment," NASA Tech. Memo. TMX-71554, June 1974.

Section IV

1. R. K. Cole, H. S. Ogawa and J. M. Sellen, Jr., "Operation of Solar Cell Arrays in Dilute Streaming Plasmas," AIAA Paper No. 69-626, 1969.

2. S. B. Gabriel, C. E. Garner and S. Kitamura, "Experimental Measurements of the Plasma Sheath Around Pinhole Defects in a Simulated High Voltage Solar Array," AIAA Paper No. 83-0311, January 1983.

3. I. Langmuir and K. B. Blodgett, "Currents Limited by Space Charge Between Concentric Spheres," Phys. Rev. 23, 1924. Also in The Collected Works of Irving Langmuir, Vol. 3, Thermionic Phenomena, (C. G. Suits and H. E. Way, eds.), Pergamon Press, New York, pp. 125-135, 1961.

APPENDIX A

THICK SHEATH SPHERICAL PROBE ANALYSIS

Thick sheath spherical probe analysis was used to determine the plasma parameters. A knowledge of this probe theory is necessary for understanding the experimental procedure used to evaluate plasma parameters.

The current-voltage characteristic of a Langmuir probe has two different current collection regions of interest, the transition and attracting regimes. These regions are separated by the plasma potential, and are dealt with separately herein.

Transition Region[1]

In the transition region, the probe potential is less than plasma potential. This causes electrons to be repelled and ions to be attracted. Due to the much greater mobility of the electrons, the current collected by the probe consists mostly of electrons and the ion current can be ignored. The electron density in this transition region is given by the Boltzmann equation

$$n(V) = n_e \exp[-e(V_p - V)/kT_e] \quad , \tag{A-1}$$

where n_e is the electron density of the bulk plasma, V_p is the plasma potential, V is the probe potential, e is the electronic charge, T_e is the electron temperature, and k is the Boltzmann constant.

The current striking the probe is given by the random current density of the region around the probe multiplied by the surface area of the probe. That is,

$$I = \frac{1}{4}\, n(V) e [8kT_e/\pi m_e]^{1/2} A_p \quad , \tag{A-2}$$

or

$$I = \frac{A_p}{4} en_e[8kT_e/\pi m_e]\exp[-e(V_p-V)/kT_e] \ , \qquad (A-3)$$

where m_e is the electronic mass and A_p the surface area of the probe.

Using the logarithm of Eq. (A-3),

$$\ell nI = \ell n \frac{1}{4} n_e e A_p [8kT_e/\pi m_e]^{1/2} - eV_p/kT_e + eV/kT_e \ , \qquad (A-4)$$

and then differentiating with respect to probe potential,

$$d/dV \ (\ell nI) = e/kT_e \ , \qquad (A-5)$$

the electron temperature can be determined. The slope of a semi-log plot of electron current versus probe potential, in the transition region, therefore yields the electron temperature of the plasma.

This analysis for the transition region is applicable to any probe geometry.

Attracting Region

In the attracting region the probe potential is greater than the plasma potential; electrons are attracted and ions repelled (ion current will again be neglected). Since electrons are attracted, the current density at the probe sheath is the random current density of the bulk plasma,

$$j_r = \frac{1}{4} en_e[8kT_e/\pi m_e]^{1/2} \ . \qquad (A-6)$$

The current collected by the probe is then determined by the size of the sheath around the probe.

The size of the sheath is dependent on the ratio a/λ_D, where a is the probe radius (for spherical probe) and λ_D is the Debye length

$$\lambda_D = [\varepsilon_o kT_e/n_e]^{1/2} \ , \qquad (A-7)$$

where ε_o is the permittivity of free space. When $a/\lambda_D >> 1$, the sheath area is approximately that of the probe area (thin sheath). If $a/\lambda_D << 1$, the sheath will expand with probe potential and a thick sheath analysis must be used.[1]

The formulation for the current collection in the attracting region by a sphere presented here is that given by Medicus.[2] The results are also consistent with the original analysis of Langmuir and Smith.[3]

Beginning with conservation of both energy and angular momentum,

$$\frac{1}{2} m_e[v_{rp}^2+v_{tp}^2] = \frac{1}{2} m_e[v_{rs}^2+v_{ts}^2] + e(V-V_p) \tag{A-8}$$

and

$$av_{tp} = r_s v_{ts} = pv_s \ , \tag{A-9}$$

where v_{rp} and v_{rs} are the radial velocities at the probe and sheath, respectively, and v_{tp} and v_{ts} are the tangential velocities at the probe and sheath, respectively. The variable p is the impact parameter and v_s is given by

$$v_s^2 = v_{rs}^2 + v_{ts}^2 \ . \tag{A-10}$$

It is assumed that $v_{rp} = 0$. A grazing impact parameter is defined as the impact parameter where an incoming electron grazes the probe, as shown in Fig. A-1. The condition for grazing impact is

$$a \leq p_g \leq r_s \ . \tag{A-11}$$

At $p_g = r_s$ the current collection is limited by the sheath, while for $p_g < r_s$ the current collection is limited by the impact parameter.

From Eqs. (A-8) through (A-10), p_g can be found to be

$$p_g^2 = a^2[1 + e(V-V_p)/\tfrac{1}{2} m_e v_s^2] \ , \tag{A-12}$$

or

$$p_g^2 = a^2[1 + e(V-V_p)/u] \ , \quad \text{where } u = \tfrac{1}{2} m_e v^2 \ , \tag{A-13}$$

and the subscript s refers to the sheath.

The condition that separates the sheath limited and impact parameter limited case is

$$p_g^2 = a^2[1 + e(V-V_p)/u_k] \tag{A-14}$$

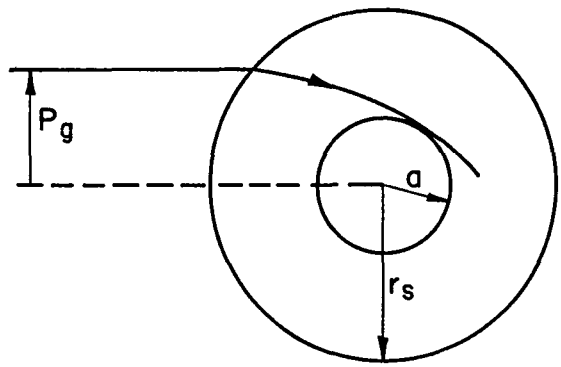

Fig. A-1. Sketch of grazing impact.

or

$$u_k^{-1} = [r_s^2/a^2-1]/e(V-V_p) \tag{A-15}$$

then for

$$u < u_k \qquad \text{sheath limited} \tag{A-16}$$

$$u > u_k \qquad \text{impact parameter limited .} \tag{A-17}$$

The current is given by

$$dI = 4\pi p_g \frac{1}{4} vdn \tag{A-18}$$

where

$$dn = n_e F(v)dv \ , \tag{A-19}$$

F(v) is the Maxwellian velocity distribution

$$F(v)dv = [m_e/2\ kT_e]^{3/2} 4\pi N^2 \exp[-m_e v^2/2kT_e]dv \ . \tag{A-20}$$

For $(V-V_p) > 0$, the integration is over two parts, $v = 0$ to v_k for the sheath limited case, and from $v = v_k$ to ∞ for the impact parameter limited case.

$$I = \pi e n_e [r_s^2 \int_0^{v_k} vF(v)dv + a^2 \int_{v_k}^{\infty} (1 + \frac{eV}{u}) vF(v)dv] \tag{A-21}$$

This yields

$$I = 4\pi^{1/2}\ e n_e \left[\frac{m_e}{2kT_e}\right] 3/2 \left[\frac{2kT_e}{m_e}\right] 2 \exp \frac{-e(V-V_p)}{\gamma kT_e} \left[\frac{a^2}{2} \frac{e(V-V_p)}{kT_e} + 1 \right.$$

$$\left. + \frac{e(V-V_p)}{\gamma kT_e} + \frac{r_s^2}{2} \left(1 - \left[1 + \frac{e(V-V_p)}{\gamma kT_e}\right]\right)\right] \ , \tag{A-22}$$

where

$$\gamma \equiv (r_s^2/a^2 - 1) \ . \tag{A-23}$$

For $r_s^2/a^2 >> 1$, Eq. (A-22) reduces to

$$I = j_r 4\pi a^2 [1 + e(V-V_p)/kT_e] \ . \tag{A-24}$$

The final expression for the electron collection for a spherical probe shows that the current is proportional to the probe potential.

From Eq. (A-24), the electron density can be found by taking the derivative of the current with respect to probe potential,

$$dI/dV = \pi a^2 e \ [8kT_e/\pi m_e]^{1/2} n_e \ , \tag{A-25}$$

the electron density is given by

$$n_e = [\pi m_e/8kT_e]^{1/2} \ 1/\pi e a^2 \ dI/dV \ . \tag{A-26}$$

Plasma Potential

Plasma potential is determined from data in both the transition and attracting regions. In the transition region, the current is given by

$$I_1 = I_r \exp[e(V_1-V_p)/kT_e] \tag{A-27}$$

where I_1 and V_1 are the current and probe potential, respectively, from the transition region, and I_r is the random current

$$I_r = 4\pi a^2 j_r \ . \tag{A-28}$$

The electron density for I_r is determined from the attracting region (see Eq. (A-26)). The plasma potential is then given by

$$V_p = V_1 + kT_e/e \ \ln \ I_r/I_1 \ . \tag{A-29}$$

Examples of Probe Analysis

As an example of probe analysis, consider the probe current-voltage characteristics taken in the small vacuum facility with a 1.0 cm diameter probe shown in Fig. A-2. The figure shows both the transition and attracting regions. The electron temperature is determined from the transition region (see Fig. A-3(a)). The electron density is determined from the slope of the characteristic in the attracting region (see Fig. A-3(b)), together with the electron temperature. The plasma potential is then determined using Eq. (A-29), and is found to be 24.0 volts.

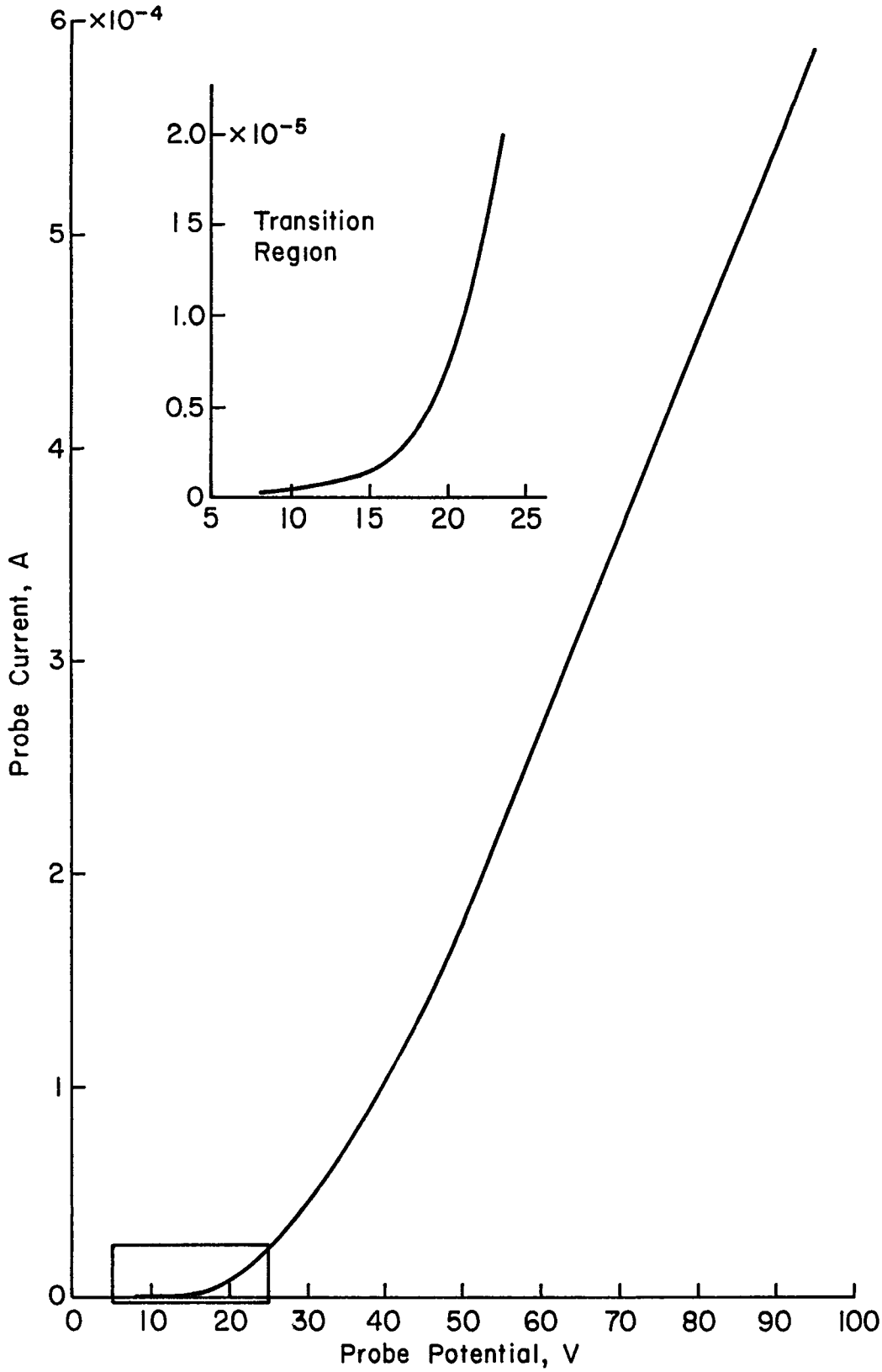

Fig. A-2. Example of a spherical Langmuir probe characteristic.

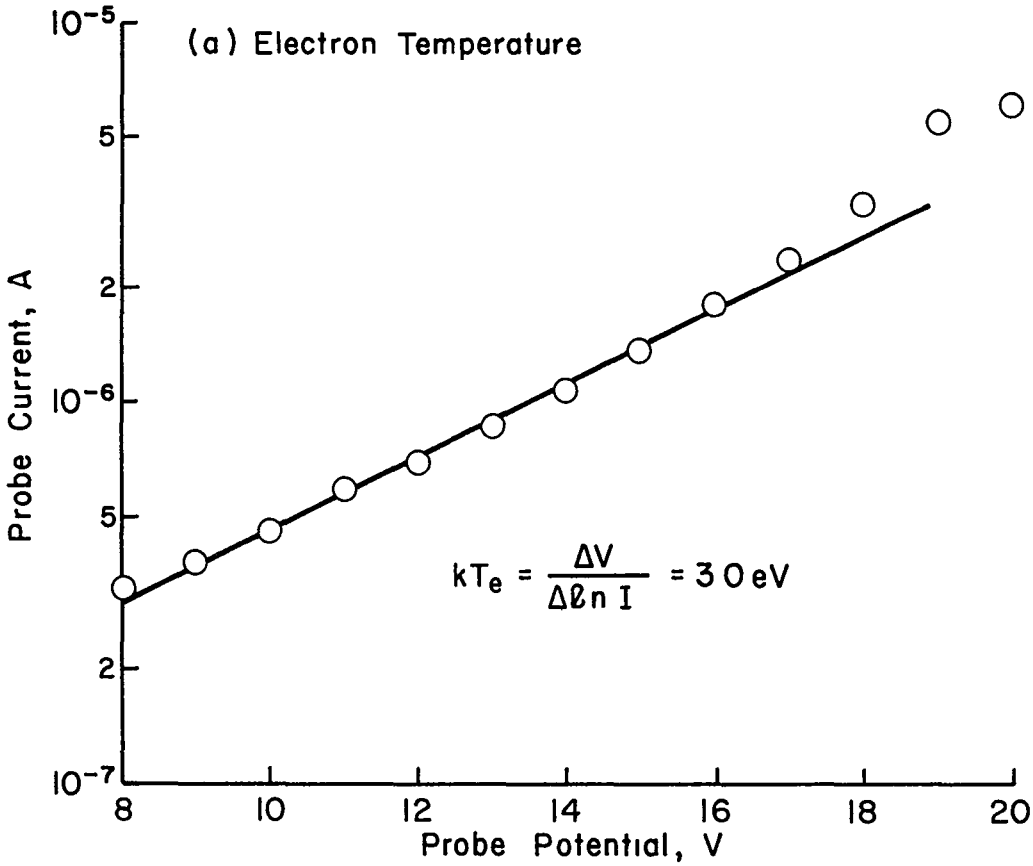

(a) Electron temperature.

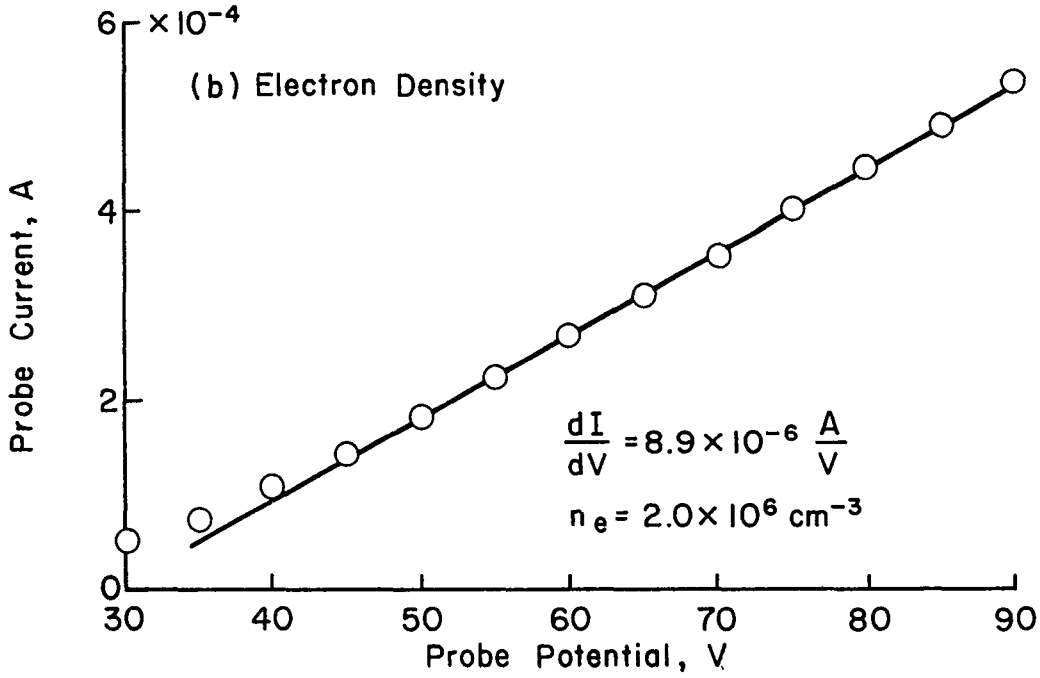

(b) Electron density.

Fig. A-3. Plasma parameters as determined from the probe characteristic.

APPENDIX B

PLANAR PROBE THEORY

The planar probe theory[1,2] of Parker and Whipple has been used to compare electron and ion collection to the expected magnitude of current collection for electrostatic probe theory, as well as in the theory. Since this theory has been used, it is important to understand its formulation. The geometry of the probe is indicated in Fig. B-1.

The current density collected by a probe may be expressed by the integral

$$J = \iiint f_\infty \vec{v} d^3\vec{v} \ , \tag{B-1}$$

where $\vec{v}$ is the velocity vector and f_∞ is the distribution function far from the probe. The difficult portion of the solution for j is determination of the limits of integration. The formulation can be initiated by writing the total energy,

$$E = \frac{1}{2} m \left[v_r^2 + v_z^2\right] + \phi(r) \ , \tag{B-2}$$

where v_r and v_z are the cylindrical components of the velocity, m is the particle mass and $\phi(r)$ is the potential energy. Introducing the probe potential, -V (for an attracting potential, V > 0) and the notation

$$X \equiv \frac{1}{2} m v_r^2 \tag{B-3}$$

$$Z \equiv \frac{1}{2} m v_z^2 \ , \tag{B-4}$$

Eqs. (B-1) and (B-2) can be written as

$$E = X + Z - V \tag{B-5}$$

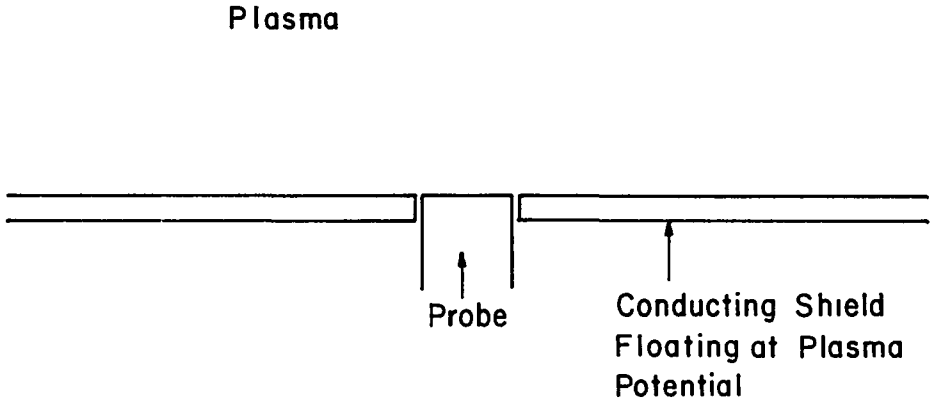

Fig. B-1. Geometry of planar probe.

$$J = \frac{2\pi}{m^2} \int_0^\infty f_\infty(E)X(E)dE \ , \tag{B-6}$$

where X(E) represents the boundary condition for current collection.

Using an impulse approximation theory, an expression for X(E) is determined to be

$$X(E) = E + V - \frac{b^2}{4}\frac{V^2}{[E+V]} \ , \tag{B-7}$$

where b is a constant that can vary from 0 to 2. The parameter b depends on the effect of the electric field on the incoming trajectories.

In the approach used by Parker and Whipple,[1] it is necessary to define some more variables,

$$\langle E \rangle = \int_0^\infty f_\infty(E)EdE / \int_0^\infty f_\infty(E)dE \tag{B-8}$$

$$J_o = 2\pi/m^2 \int_0^\infty f_\infty(E)EdE \tag{B-9}$$

where $\langle E \rangle$ is the average energy and j_o is the current density at infinity.

The normalized current density can then be written as

$$J/j_o = 1 + V/\langle E \rangle - b^2V^2/4 \frac{\int_0^\infty \frac{f_\infty(E)dE}{[E+V]}}{\int_0^\infty f_\infty(E)EdE} \tag{B-10}$$

Maxwellian Distribution

For the Maxwellian distribution

$$f_\infty(E) = n_o[n/2\pi kT]^{3/2}\exp(-E/kT) \tag{B-11}$$

the normalized current collection is

$$j/j_o = 1 + V/kT - b^2/4\ [V/kT]^2 \exp(V/kT) E_1(V/T)\ , \qquad (B\text{-}12)$$

where T is the particle temperature, n_o the ambient density, and $E_1(x)$ is

$$E_1(x) = \int_x^\infty e^{-t}\ dt/t\ . \qquad (B\text{-}13)$$

For V >> <E>, Eq. (B-12) reduces to

$$j/j_o \simeq 1 + b^2/4 + [1 - b^2/4]\ eV/kT\ . \qquad (B\text{-}14)$$

It should be noted that for b = 0, Eq. (B-14) has the same form for current collection as for a spherical probe.

Monoenergetic Distribution

For a momoenergetic distribution

$$f_\infty(E) = n_o/2\pi\ [m/2E_o]^{3/2}\ \delta(1 - E/E_o) \qquad (B\text{-}15)$$

where E_o is the singular energy and $\delta(x)$ is the Dirac delta-function, the normalized current density is

$$j/j_o = 1 + V/E_o - b^2/4\ V^2/E_o(E_o+V)\ . \qquad (B\text{-}16)$$

For ion collection, j_o is 0.6 times the Bohm current density[4] and E_o is found from the Bohm velocity,

$$v_{Bohm} = [kT_e/m_i]^{1/2} = [2E_o/m_i]^{1/2}\ , \qquad (B\text{-}17)$$

$$E_o = kT_e/2\ , \qquad (B\text{-}18)$$

where m_i is the ion mass and T_e the electron temperature.

APPENDIX C

SECONDARY ELECTRON EMISSION

Secondary electron emission consists of two components, true secondary electrons and backscattered primary electrons. The true secondary electrons are considered to be those that have an energy of less than 50 eV. This distinction between true secondaries and backscattered electrons is arbitrary, but one that is accepted as standard.[1-5] The secondary electron emission yield (total yield) is given by

$$\sigma = \frac{\text{number of emitted electrons}}{\text{number of incident electrons}} \tag{C-1}$$

or

$$\sigma = \delta + \eta \tag{C-2}$$

where δ is the true secondary yield,

$$\delta = \frac{\text{number of true secondary electrons emitted}}{\text{number of incident electrons}} \tag{C-3}$$

and η is the backscattered yield,

$$\eta = \frac{\text{number of backscattered electrons}}{\text{number of incident electrons}} . \tag{C-4}$$

The total yield is dependent on the incident electron energy, but δ and η exhibit different dependencies. This requires that η and δ be discussed independently. Since only the true secondary electron yield, δ, is considered in the model of Section IV, only δ will be discussed. Although the backscattered yield is not discussed, it is generally accepted as negligible compared to the secondary yield in the range of interest herein.

Theory

Inasmuch as the secondary coefficient, δ, is very important for the model of current collection through a defect in insulation covering a high voltage solar array, it is helpful to understand the mechanism for secondary emission. To date, there is no theory that completely explains secondary electron emission. The two theories discussed here are typical of the differences encountered in various theories. The two theories[6,7] both begin with the expression for the secondary coefficient

$$\delta = \int n(E,x)f(x)dx \tag{C-5}$$

where $n(E,x)dx$ is the number of secondaries produced per incident primary of energy E in a layer of thickness dx at a depth x below the surface, and $f(x)$ is the probability that a secondary produced at depth x escapes to the surface. Both theories assume that $n(E,x)$ is proportional to the energy loss of the primary beam per unit path length, and that $f(x)$ is given by an exponential absorption law.

The first theory discussed, that of Lye and Dekker,[6] proposed that the energy loss for primaries has a power law form

$$dE/dx = -A/E^{n}(x) \tag{C-6}$$

where A and n are constants. This form of energy loss is based on the experimental results of Young.[8,9]

Integration of the power law yields

$$E^{n+1}(x) = E^{n+1} - A(n+1)x \ . \tag{C-7}$$

By equating $E^{n+1}(x)$ to zero, the range for the primary electrons can be found to be

$$R = E^{n+1}/A(n+1) = CE^{n+1} \ . \tag{C-8}$$

This theory approximates the energy loss through the material with a constant. Using this assumption, the energy loss of primary beam per unit path length can be written as

$$dE/dx = E/R \ , \tag{C-9}$$

or

$$n(E,x) = KE/R \ , \tag{C-10}$$

where K is a material constant. The secondary coefficient is then given by

$$\delta(E) = \int_{o}^{R} KE/R \ e^{-\alpha x} dx \tag{C-11}$$

or

$$\delta(E) = K[1-\exp(-\alpha CE^{n+1})]/\alpha CE^{n} \ , \tag{C-12}$$

where α is a material constant. This expression can be reduced to a universal yield curve, as suggested by Baroody,[10] by introducing the function

$$g_n(z) = \frac{1-\exp(-z^{n+1})}{z^n} \ . \tag{C-13}$$

The reduced universal yield curve is then given by

$$\delta(E)/\delta_m = g_n(z_m E/E_m)/g_n(z_m) \tag{C-14}$$

where δ_m is the maximum value of δ at an incident energy of E_m, and z_m is the value of z where $g_n(z)$ is a maximum. This universal curve can be fit to almost any data by choosing the correct value for n.

The second theory to be discussed is that of Sternglass.[7] The first difference encountered between the theories is that Sternglass assumed that all the secondaries are produced at a mean depth, λ_m. This allows the probability of secondary escape term, f(x), to be taken out of the integral,

$$\delta(E) = Be^{-\alpha\lambda_m} \int n(E,x)dx \ , \tag{C-15}$$

where B is the proportionally constant associated with the absorption term. The probability of secondary electrons being produced is

$$n(x,E) = -1/\bar{\varepsilon}\ dE/dx\ , \tag{C-16}$$

where $\bar{\varepsilon}$ is the average energy required to produce a secondary electron inside the solid.

The energy loss is evaluated by taking into account the backscattered electrons through the introduction of the mean fraction energy of the backscattered electron, k. The total energy loss is then

$$\int dE = -E(1-k\eta)\ . \tag{C-17}$$

This differs significantly from Lye and Dekker's theory in that k and η are dependent on the atomic number of the material. Because of these dependencies, Sternglass' theory is often referred to as an atomic shell model.

The secondary yield is given by

$$\delta(E) = \frac{Be^{-\alpha\lambda_m}}{\bar{\varepsilon}} \int \frac{dE}{dx}\, dx \tag{C-18}$$

or

$$\delta(E) = B/\bar{\varepsilon}\ \exp(-\alpha\lambda_m)E(1-kn)\ . \tag{C-19}$$

Using a diffusion argument, it can be shown that the mean depth is proportional to $E^{1/2}$ or

$$\alpha\lambda_m = \beta E^{1/2}\ , \tag{C-20}$$

where β is a material constant. The constant β is related to the energy which gives the maximum yield, that is

$$\beta = 2/E_m^{1/2}\ . \tag{C-21}$$

The final expression for the secondary coefficient is

$$\delta(E) = B/\bar{\varepsilon}\ E(1-k\eta)\exp[-2\ E^{1/2}/E_m^{1/2}]\ . \tag{C-22}$$

This form yields a universal yield curve of the form

$$\delta(E)/\delta_m = E/E_m \, e^2 e^{-2(E/E_m)^{1/2}} \tag{C-23}$$

Dependence on Incident Angle

In the previous section, the two theories were developed for normal incidence. It has been shown that the secondary electron emission coefficient, δ, is strongly dependent on the angle of incidence.[11,12] To include the angle of incidence in the theories, the term x becomes $x\cos\theta$ in the absorption terms, where θ is measured from the normal to the surface. Carrying this term through the integrations yields

$$\delta(E,\theta) = \frac{KE[1-\exp(-\alpha CE^{n+1}\cos\theta)]}{\alpha CE^{n+1}\cos\theta} \tag{C-24}$$

for Lye and Dekker's theory,[13] and

$$\delta(E,\theta) = \frac{B}{\varepsilon} E(1-k\eta)\exp(-\beta E^{1/2}\cos\theta) \tag{C-25}$$

for Sternglass' theory.

For Sternglass' theory, the relationship

$$\delta(\theta^o) = \delta(0^o)\exp[2\, E^{1/2}/E_m^{1/2}\, (1-\cos\theta)] \tag{C-26}$$

can be derived. This expression compares favorably with the angular dependence found by Bruining,[12] that is

$$\delta(\theta^o) = \delta(0^o)\exp[p(1-\cos\theta)] \, , \tag{C-27}$$

where p is a constant that depends on energy.

Dependence on Temperature

It is generally agreed that there is no temperature dependence for metals,[1-3,5] however, a temperature dependence for δ has been observed in insulators.[14-16] The explanation for this difference is the energy loss mechanism of the secondary electrons produced in the material. In metals, the secondaries can collide with free and bound electrons involving large and small amounts of energy transfer. In insulators, because of the large gap between the valence and conduction bands, any energy loss mechanism of the secondaries must depend on electron collisions with lattice defects and/or electron-phonon interactions for energies less than the band gap.[5]

From electron-phonon interactions, Dekker has developed a temperature dependence for δ.[17,18] This formulation was done before the emission theory of Lye and Dekker so some of the assumptions differ. A brief outline of the theory is presented.

The theory starts with the expression

$$-\lambda \frac{d\varepsilon}{dx} = \frac{h\nu}{(2n_\nu+1)} \equiv \alpha(T) \qquad \text{(C-28)}$$

where λ is the mean free path, ε is the secondary electron energy, h is Planck's constant, and x is the depth in the material. The term n_ν is given by

$$n_\nu = 1/[\exp(h\nu/kT)-1] \ , \qquad \text{(C-29)}$$

the phonon statistics, where ν is the frequency of longitudinal optical vibration mode for an ionic crystal, and k is Boltzmann's constant. The expression $\lambda d\varepsilon/dx$ represents the energy loss per collision and is based on the works of Frohlick[19] and Seitz.[20]

Assuming that all secondaries are produced with the same energy, ε_o, the energy of a secondary after N collisions is

$$\varepsilon(N) = \varepsilon_o - N\alpha(T) \ . \qquad \text{(C-30)}$$

The mean free path of the secondaries is written as

$$\lambda = \lambda_o \varepsilon/\varepsilon_o(2n_\nu+1) \ , \qquad \text{(C-31)}$$

where λ_o is a constant.

A further assumption is that if the secondaries lose an energy ε_o', they no longer take part in the secondary emission process. This limits the maximum number of collisions to N_m, given by

$$N_m\alpha = \varepsilon_o' \ . \qquad \text{(C-32)}$$

Now, if the secondaries carry out a one-dimensional random walk normal to the surface, the range of secondaries is given by

$$x_s = [N_m\langle\lambda^2\rangle]^{1/2} \qquad \text{(C-33)}$$

or

$$x_s = [N_m \frac{\lambda_o^2}{\varepsilon_o^2(2n_\nu+1)^2} (\varepsilon_o^2+\alpha^2\langle N^2\rangle-2\varepsilon_o\alpha\langle N\rangle)]^{1/2} . \quad (C-34)$$

Then for

$$\langle N\rangle = N_m/2 \quad (C-35)$$

$$\langle N^2\rangle = N_m^2/3 , \quad (C-36)$$

and substituting Eqs. (C-32), (C-33) and (C-34) into Eq. (C-35) yields

$$x_s = \text{constant}/[2n_\nu+1] . \quad (C-37)$$

Assuming Whiddington's law,

$$dE/dx = -A/E , \quad (C-38)$$

$$E(x) = (E_o^2-2Ax)^{1/2} , \quad (C-39)$$

this gives an expression for n(E,x) of

$$n(x) = -1/\bar{\varepsilon}\ A/[E^2-2Ax]^{1/2} , \quad (C-40)$$

or for small x

$$n(Ex) \underset{\sim}{\sim} A/\bar{\varepsilon}E . \quad (C-41)$$

Then, since $\delta\alpha n(x)x_s$

$$\delta_1/\delta_2 = [2n_{\nu_2}+1/2n_{\nu_1}+1] . \quad (C-42)$$

For nonpolar insulators, the temperature dependence is

$$\delta_1/\delta_2 = \left[\int_0^{\nu_m} (2n_{\nu_2}+1)\nu^2 d\nu / \int_0^{\nu_m} (2n_{\nu_1}+1)\nu^2 d\nu\right] , \qquad \text{(C-43)}$$

where ν_m is the upper limit of ν.

For $kT >> h\nu$, both expressions (Eqs. (C-42) and (C-43)) reduce to

$$\delta_1/\delta_2 = [T_2/T_1] , \qquad \text{(C-44)}$$

which is in rough agreement with the results of Johnson and McKay.[15,16]

This formulation depends on the domination of electron-photon interaction. If the lattice defects dominate the energy loss mechanism, no temperature dependence of δ is expected, and no temperature dependence has been found in glass or mica.[21,22]

In contradiction to general findings, Sternglass[23] reports a temperature dependence for metals. Sternglass proposes that this effect can be explained by a linear temperature dependence of the absorption coefficient, α. However, it has been suggested that the temperature dependence found was due to surface contamination of the samples, and not any true temperature dependence for δ of the metals.[1]

Surface Condition

It has been observed that when a material's surface is roughened, its secondary emission yield decreases.[24] The explanation for this effect is that when a surface is roughened, microscopic Faraday spaces (spaces without fields and from which no secondary electrons can be emitted) are formed. This effectively decreases the total area from which emission may occur.

Angular Distribution of Secondary Electrons

Secondary electrons have been found to have a roughly cosine distribution.[25-27] This distribution can be understood by the following formulation.[2] The current density in the material is given by

$$j_s^{(1)}(x,\varepsilon,\Omega)d\varepsilon d\Omega = N(x,\varepsilon,\Omega)v\cos\beta d\varepsilon d\Omega , \qquad \text{(C-45)}$$

where ε is the secondary electron energy, x the electron its depth, Ω is the solid angle, N is the secondary distribution in the material, v is the electron speed, and β is the angle the electron velocity makes with the normal to the surface. The conservation of energy and momentum yield

$$\varepsilon = \varepsilon' + W \tag{C-46}$$

$$v\sin\beta = v'\sin\phi \tag{C-47}$$

where the primed values are those outside the material, ϕ is the angle of the secondary (outside the material) measured from the surface normal, and W is the potential step at the surface. The current density at the surface (x = 0) is

$$j_s(\varepsilon',\Omega')d\varepsilon' d\Omega' = j_s^{(1)}(\varepsilon,\Omega)d\varepsilon d\Omega \ , \tag{C-48}$$

which can be written as (using Eqs. (C-45) through (C-48)) as

$$J_s(\varepsilon',\Omega') = N(0,\varepsilon,\beta)\ (\varepsilon'/\varepsilon)\ v\cos\phi \tag{C-49}$$

or

$$J_s(\varepsilon',\phi)/j_s(\varepsilon',0^o) = N(\varepsilon,\beta)/N(\varepsilon,0^o)\ \cos\phi \ . \tag{C-50}$$

For an isotropic distribution,

$$j_s(\varepsilon',\phi)\alpha\cos\phi \ ,$$

which is in rough agreement with results.

Energy Distribution of Secondary Electrons

The energy distribution of true secondaries has been observed to be independent of primary electron energy.[5] This can be understood by integrating Eq. (C-49)

$$j_s(\varepsilon') = v \int \varepsilon'/\varepsilon\ N(0,\varepsilon,\beta)\cos\phi d\Omega' \ . \tag{C-51}$$

Using Eq. (C-47) and definition of $d\Omega'$ yields

$$J_s(\varepsilon') = v \int N(0,\varepsilon,\beta)\cos\beta\sin\beta d\beta \ . \tag{C-52}$$

While the magnitude of the distribution, $N(0,\varepsilon,\beta)$ should be affected by the incident electron energy, its form should be nearly independent. This would have the effect of making the relative energy distribution,

$$J_{s,Rel}(\varepsilon') = j_s(\varepsilon')/\int j_s(\varepsilon')d\varepsilon' \ , \qquad (C-53)$$

independent of incident electron energy.

It should be noted from Eq. (C-52) that as $\beta \to 0$, $E' \to 0$ and $j_s(E') \to 0$. Thus the energy distribution curve will always start at zero energy.[2]

An example of an energy distribution is given in Fig. C-1. Although this distribution is for a metal, many insulators have been found to have similar distributions.

Secondary Electron Emission from Polymers

The polymers suitable for insulation over high voltage solar arrays are primarily polyimide and teflon. Therefore, this section will be aimed at characterizing those materials.

Work done on polyimide and teflon is scarce, and all the available literature found will be mentioned. Leung, Tueling and Schnauss[29] have measured the secondary yield, δ, of polyimide at normal incidence. Matskevick[14] has measured the secondary yield of several polymers, including teflon, at normal and non-normal incidence, as well as measuring δ at several temperatures for polystyene. Gair[11] has measured both the backscattering yield, η, and the secondary yield of polyimide at several angles of incidence for primary energies of 10 to 80 keV. Willis and Skinner[30] have measured the total yield, σ, of both polyimide and teflon.

Lueng, Tueling and Schnauss[29] found that their measurements of δ fit well to the model of Sternglass.[7]

The data for teflon from Matskevick,[14] for normal incidence at 20°C, was found to be modeled well by Sternglass' expression, Eq. (C-23). It should be noted that these data were previously fitted to Lye and Dekker's[6] expression for a universal yield curve by Wall, Burke and Frederickson.[31] This fit was found to be inferior to the fit obtained using Sternglass' theory. The secondary yield for teflon and polyimide are shown in Fig. C-2.

The angular dependence for teflon and polyimide was found from Sternglass' theory, Eq. (C-26). The values of β, as well as other parameters for teflon and polyimide are given in Table C-1.

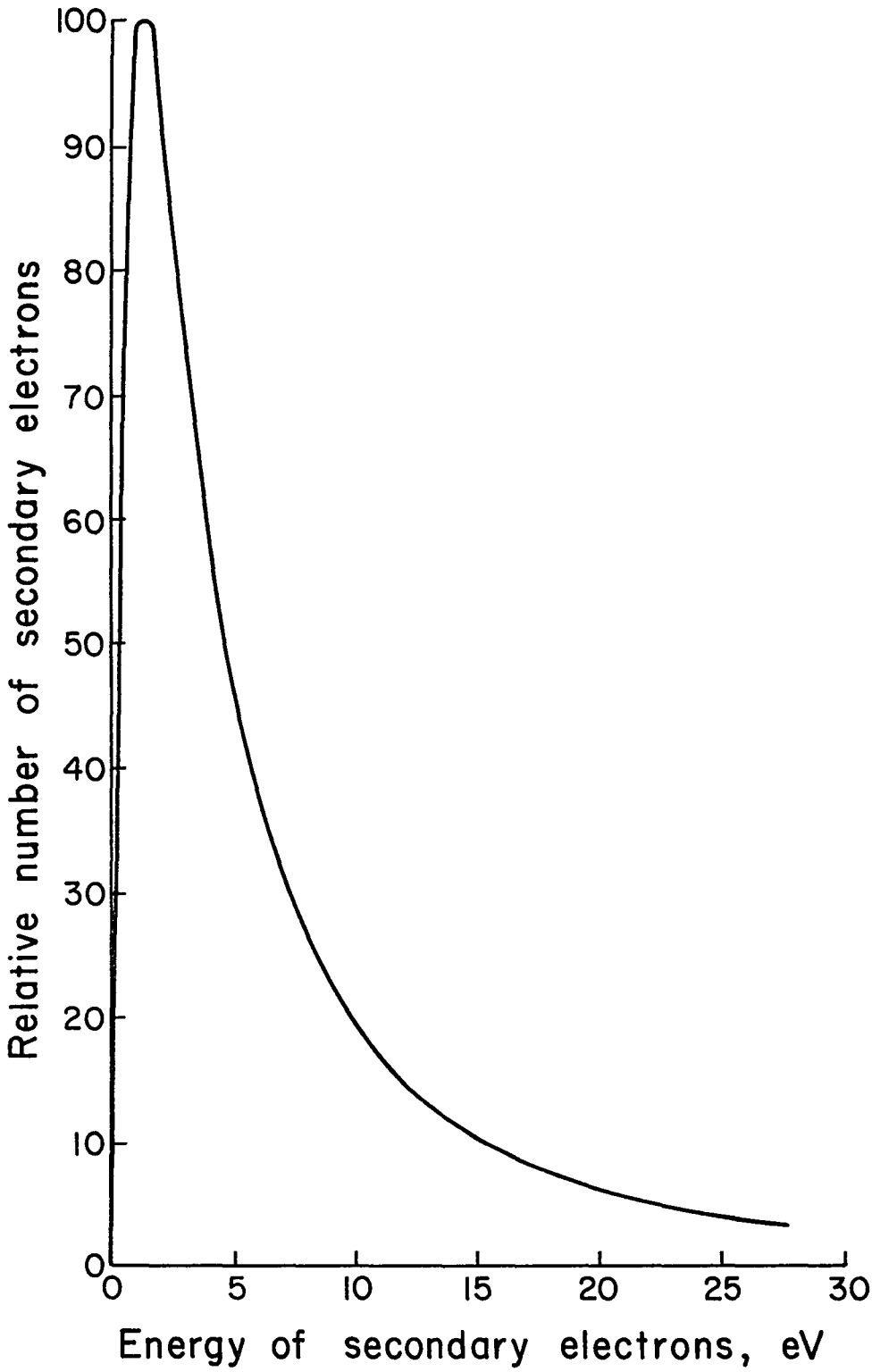

Fig. C-1. Energy distribution of secondary electrons for tantalum.[28]

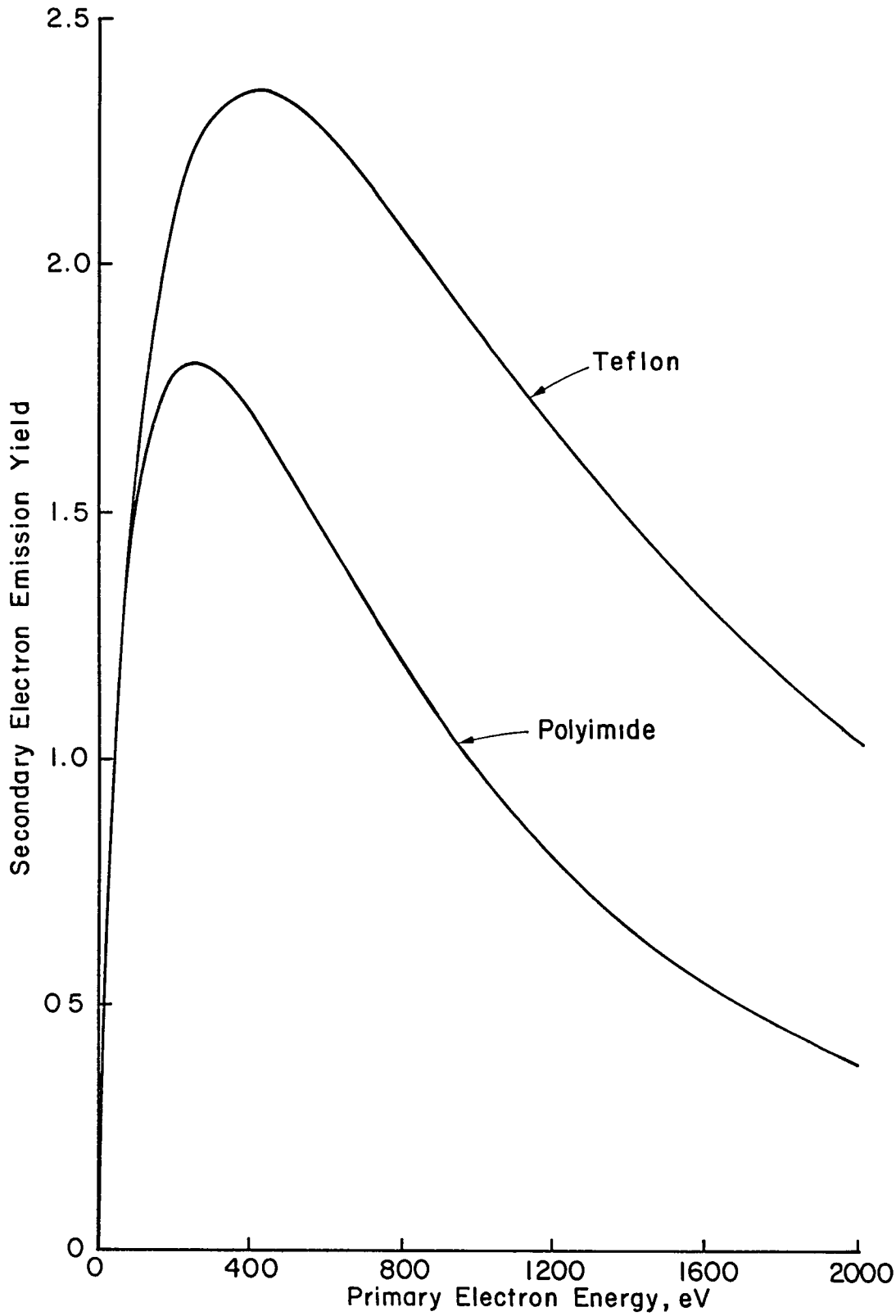

Fig. C-2. Comparison of secondary electron emission yields for polyimide[29] and teflon[14] at normal incidence.

Matskevick[14] found a temperature dependence for δ for polystyrene. The temperature dependence varied with incident energy and angle of incidence. For normal incidence, the dependence vanished at approximately 800 volts, while at 60° incidence an avarage dependence of $T^{-1/4}$ was found over a range of 2000 volts. While this data conflicts with Dekker's theory for temperature dependence, there is not sufficient data to compare with Sternglass' theory, as such, Dekker's temperature dependence will be used in the absence of any better theory.

Table C-1. Important parameters in the secondary electron emission yields for polyimide[29] and teflon.[14]

	Polyimide	Teflon
δ_m	1.8	235
E_m (eV)	250	410
β $(eV)^{-1}$	0.126	9.88×10^{-2}
E_{II}^* (eV)	1000	204
E_I^* (eV)	50	50

*E_I and E_{II} are the two cross over points, i.e., the values for E were $\delta = 1$.

REFERENCES FOR APPENDICES

APPENDIX A

1. F. F. Chen, "Electric Probes," Plasma Diagnostic Techniques (R. H. Huddlestone and S. L. Leonard, ets), Academic Press, New York, pp. 113-200, 1965.

2. G. Medicus, "Theory of Electron Collection of Spherical Probes," J. Appl. Phys. 32, pp. 2512-2520, 1961.

3. I. Langmuir and H. M. Mott-Smith, "The Theory of Collectors in Gaseous Discharges," Phys. Rev. 28, pp. 727-763, 1926. Also in The Collected Works of Irving Langmuir, Vol. 4, Electrical Discharges (C. G. Suits and H. E. Way, eds.), Pergamon Press, New York, pp. 99-132, 1961.

APPENDIX B

1. L. W. Parker and E. C. Whipple, Jr., "Theory of a Satellite Electrostatic Probe," Ann. Phys. 44, pp. 126-161, 1967.

2. L. W. Parker, "Theory of Electrostatic Planar and Spherical Probes," NASA Contr. Rep., CR-704, 1967.

3. F. F. Chen, Introduction to Plasma Physics, Plenum Press, New York, 1977.

4. J. D. Swift and M. J. R. Schwar, Electrical Probes for Plasma Diagnostics, American Elsevier Publishing Company, Inc., New York, 1969.

APPENDIX C

1. A. J. Dekker, "Secondary Electron Emission," Solid State Physics, Vol. 6 (F. Seitz and D. Turnbull, ed.), Academic Press, New York, pp. 251-311, 1958.

2. O. Hachenberg and W. Brauer, "Secondary Electron Emission from Solids," Advances in Electronics and Electron Physics, Vol. 11 (L. Marton, ed.), Academic Press, New York, pp. 413-499, 1959.

3. H. Bruining, Physics and Applications of Secondary Electron Emission, McGraw-Hill, New York, 1954.

4. R. E. Bunney, "Secondary Electron Emission," NASA Contr. Rep. CR-54366, December 1964.

5. D. J. Gibbons, "Secondary Electron Emission," Handbook of Vacuum Physics, Vol. 2, Physical Electronics (A. H. Beck, ed.) Pergammon Press, Glasgow, Scotland, pp. 301-395, 1966.

6. R. G. Lye and A. J. Dekker, "Theory of Secondary Emission," Phys. Rev. 107, pp. 977-981, 1957.

7. E. J. Sternglass, "On the Phenomenon of Secondary Electron Emission from Solids," M.S. Thesis, Cornell University, 1951.

8. J. R. Young, "Penetration of Electrons and Ions in Aluminum," J. Appl. Phys. 27, pp. 1-4, 1956.

9. J. R. Young, "Dissipation of Energy by 2.5-10 KeV Electrons in Al_2O_3," J. Appl. Phys. 28, pp. 524-525, 1957.

10. E. M. Baroody, "A Theory of Secondary Electron Emission from Metals," Phys. Rev. 78, pp. 780-787, 1950.

11. S. Gair, "Electron Backscattering and Secondary Electron Yield Measurements from Dielectric Materials," Sandia Laboratories Rep. SLL-74-5230, April 1974.

12. H. Bruining, "Secondary Electron Emission. Part II. Absorption of Secondary Electrons," Physica 5, pp. 901-912, 1938.

13. B. Javidi, "Secondary Electron Emission from a Charged Dielectric in the Presence of Normal and Oblique Electric Fields," NASA Contr. Rep. CR-168558, 1982.

14. T. L. Matskevich, "Secondary Electron Emission of Some Polymers," Fiz. Tverd, Tela., Akad. Nauk, SSSR 1, pp. 277-281, 1959, (in Russian).

15. J. B. Johnson and K. G. McKay, "Secondary Electron Emission of Crystalline MgO," Phys. Rev. 91, pp. 582-587, 1953.

16. J. B. Johnson and K. G. McKay, "Secondary Electron Emission from Germanium," Phys. Rev. 93, pp. 668-672, 1954.

17. A. J. Dekker, "Energy and Temperature Dependence of the Secondary Emission of MgO," Phys. Rev. 94, pp. 1179-1182, 1954.

18. A. J. Dekker, "On the Escape Mechanism of Secondary Electrons from Insulators," Physica 21, pp. 29-38, 1955.

19. H. Frohlick, "Theory of Electrical Breakdown in Ionic Crystals," Proc. Royal Soc. Lon., Series A 160, pp. 230-241, 1937.

20. F. Seitz, "On the Theory of Electron Multiplication in Crystal," Phys. Rev. 76, pp. 1376-1393, 1949.

21. A. R. Shulman, V. L. Makedonskiy and I. D. Yaroshetskiy, "Secondary Electron Emission from Sodium Chloride, Glass and Aluminum Oxide at Various Temperatures," NASA Tech. Memo. TM-75754, January 1980.

22. S. A. Fridrikhov and A. R. Shulman, "An Investigation of the Secondary Electron Emission by Certain Dielectrics at Low Primary Electron Energies," Soviet Physics-Solid State 1, pp. 1153-1159, 1960.

23. E. J. Sternglass, "An Experimental Investigation of Electron Backscattering and Secondary Emission from Solids," Ph.D. Thesis, Cornell University, 1953.

24. S. F. Rashkovskii, "Secondary Emission from Rough Surfaces," Radio Engng. Electron Physics 3, pp. 97-118, 1958.

25. J. L. H. Jonker, "The Angular Distribution of the Secondary Electrons of Nickel," Philips Res. Rep. 6, pp. 372-387, 1951.

26. V. A. Alekseev and V. L. Borisov, "Angular Distribution of Secondary Electrons for an Effective Emitter Consisting of an MgO Film on a CuAlMg Alloy Base," Soviet Physics-Solid State 4, pp. 191-195, 1962.

27. N. B. Gornyi, "Investigation of the Angular and Energy Distributions of Secondary Electrons from Cuprous Oxide," Soviet Physics JETP 4, pp. 346-350, 1957.

28. R. Kollath, "On the Energy Distribution of Secondary Electrons," Ann. Phys. Lpz. 39, pp. 59-80, 1941.

29. M. S. Leung, M. B. Tueling and E. R. Schnauss, "Effects of Secondary Electron Emission on Charging," Spacecraft Charging Technology Conference, Colorado Springs, Colorado, Nov. 12-14, 1980, NASA Conf. Publ. 2182.

30. R. F. Willis and D. K. Skinner, "Secondary Electron Emission Yield Behavior of Polymers," Solid State Communications 13, pp. 685-688, 1973.

31. J. A. Wall, E. A. Burke and A. R. Frederickson, "Results of Literature Search on Dielectric Properties and Electron Interaction Phenomena Related to Spacecraft Charging," Proceedings of Spacecraft Charging Technology Conference, Colorado Springs, Colorado, October 27-29, 1976, NASA TMX-73537.

End of Document